Shear Strength of Concrete Beams Prestressed with CFRP Cables

by

Mirpayam Nabipaylashgari

A Thesis submitted to the Faculty of Graduate Studies of

The University of Manitoba

in partial fulfilment of the requirements of the degree of

MASTER OF SCIENCE

Department of Civil Engineering

University of Manitoba

Winnipeg

Table of Contents

Abstract

This thesis investigates the shear capacity of concrete T-beams prestressed with CFRP cables (CFCC) and contributes to the scarce research available for shear behavior of FRP prestressed concrete beams. Four beams are tested under distributed load, while twelve beams are tested under four point bending. Three different a/d ratios of 1.5, 2.5 and 3.5 are investigated. The results show that the shear capacity of the beams increases significantly when a/d is reduced below 2.5. The effect of FRP stirrups on the shear capacity of the beams is investigated and it is shown that the minimum required stirrups according to CSA-S6-10 are ineffective in deep beams with a/d = 1.5. The accuracy of current North American shear design formulas for FRP prestressed concrete beams subjected to four-point bending and distributed load is evaluated. The available strut and tie models are studied for determining the shear capacity of FRP prestressed deep beams.

Acknowledgements

I would like to acknowledge the financial contribution of the National Science and Engineering Research Council of Canada that made this project possible. I like to especially thank my advisor Dr. Dagmar Svecova who guided me throughout the process with her valuable advice and support.

I would also like to thank the staff at the McQuade Structures Lab including the lab manager (Mr. Chad Klowak) and the technicians (Mr. Grant Whiteside and Mr. Brendan Pachal). The many hours they helped me in the Structures Lab at the University of Manitoba is greatly appreciated. On the same note, I appreciate the help of undergraduate students (Miss Michelle Bakkelund, Mr. Paulo Guzzi, and Mr. Dave Reichart) who worked really hard and provided valuable assistance in the lab.

In the end, I would like to thank my family and friends for supporting me through the ups and downs and for being there for me every step of the way.

List of Tables

List of Figures

List of Symbols

a	=	shear span length between point load and the support point (mm)
A_c	=	area of concrete section (mm^2)
A_{cs}	=	cross-sectional area of the compressive strut (mm^2)
A_{ct}	=	area of concrete on the flexural tension side of the member (mm^2)
A_p	=	area of prestressed tendon (mm^2)
A_s	=	area of non-prestressed longitudinal reinforcement (mm^2)
A_v	=	area of transverse reinforcement (mm^2)
b	=	the width of the member where stresses are calculated (mm)
b_w	=	minimum effective web width (mm)
c	=	the depth of neutral axis for a cracked transformed section (mm)
d	=	effective depth of reinforcement (mm)
d_s	=	diameter of a stirrup (mm)
d_v	=	effective shear depth (mm)
E_{cexp}	=	experimental modulus of elasticity of concrete (MPa)
$E_{ctheory}$	=	theoretical modulus of elasticity of concrete according to CPCI handbook (MPa)
E_f	=	modulus of elasticity of FRP longitudinal reinforcement (MPa)
E_p	=	modulus of Elasticity of prestressing tendon(MPa)
E_s	=	modulus of elasticity of steel longitudinal reinforcement (MPa)
E_{vFRP}	=	modulus of elasticity of FRP transverse reinforcement (MPa)
f'_c	=	compressive strength of concrete determined from tests (MPa)
f'_{ci}	=	compressive strength of concrete at time of prestressing transfer (MPa)
F_c	=	compressive force in the diagonal strut (kN)
f_{ce}	=	effective compressive strength of the strut according to ACI-318-05 (MPa)
f_{cr}	=	cracking strength of concrete according to CSA-S6-10 (MPa)
f_{ct}	=	tensile strength of concrete (MPa)
f_{cu}	=	ultimate compressive strength of diagonal strut (MPa)
$f_{FRPbend}$	=	specified tensile strength of the straight portion of a bent FRP stirrup (MPa)
F_{ns}	=	strength of the compressive strut according to ACI-318-05 (MPa)
F_{nt}	=	strength of the tension tie according to ACI-318-05 (MPa)
f_{po}	=	stress in prestressing steel when the stress in the adjacent concrete is zero (MPa)
f_{pu}	=	ultimate tensile strength of the prestressing tendon (MPa)

F_{pe} = effective prestressing force in concrete after losses (MPa)

F_{pi} = initial prestressing force applied to the concrete (MPa)

F_{ps} = actual prestressing force in the tendon at ultimate (MPa)

F_{pu} = ultimate load capacity of the prestressing tendon (kN)

f_{py} = yield strength of prestressing reinforcement (MPa)

f_{rexp} = tensile strength of concrete determined from splitting tensile test (MPa)

$f_{rtheory}$ = tensile strength of concrete determined according to CSA-S6-10 (MPa)

f_{se} = effective stress in prestressing steel after losses (ACI-318-05) (kN)

f_t = combined tensile strength of concrete and steel (MPa)

f_y = yield strength of longitudinal steel reinforcement

f_1 = average principal tensile stress (MPa)

f_2 = average principal compressive stress (MPs)

f_{2max} = maximum average principal compressive stress that section can resist (MPa)

I = moment of Inertia (mm^4)

k = accounts for the non-uniform nature of tensile stress f_1

k_a = factor accounting for the effect of arch action of shear strength of the member

k_m = factor accounting for effect of moment at a section of the member on its shear strength

k_r = factor accounting for longitudinal reinforcement rigidity on member shear strength

k_s = factor accounting for effect of member size on its shear strength

M = applied bending moment (kN.m)

M_{dc} = decompression moment equal to moment required to remove initial camber (kN.m)

M_f = factored applied bending moment (kN.m)

N_f = factored applied axial force (kN)

N_u = calculated axial compression force in the strut due to factored loads according to CSA-S6-10 (kN)

$P_{crflexure}$ = flexural cracking load (kN)

$P_{crshear}$ = shear cracking load (kN)

P_{exp} = experimental load capacity of the beams (kN)

$P_{theoretical}$ = theoretical load capacity of the beams (kN)

Q = first moment of area (mm^3)

r = radius of curvature of the bend of an FRP stirrup (mm)

s	=	spacing of transverse shear reinforcements (mm)
S_f	=	flexural crack spacing (mm)
S_{favg}	=	average flexural crack spacing (mm)
S_d	=	diagonal crack spacing (mm)
S_{davg}	=	average diagonal crack spacing (mm)
s_z	=	crack spacing considering spacing of longitudinal reinforcement (for beams) (mm)
s_{ze}	=	effective crack spacing considering aggregate size effects (mm)
T	=	tension force in the longitudinal reinforcement (kN)
T_s	=	tension force through the stirrup
T_u	=	maximum capacity of the tension tie according to CSA-S6-10 (kN)
V	=	applied shear force (kN)
V_a	=	contribution of aggregate interlock to shear strength of concrete beams (kN)
V_c	=	concrete contribution to shear strength (kN)
V_{cz}	=	the shear in the compression zone of concrete (kN)
V_d	=	contribution of dowel action of longitudinal reinforcement (kN)
V_f	=	factored applied shear force (kN)
V_{FRP}	=	FRP stirrups contribution to shear resistance (kN)
V_n	=	estimated nominal shear capacity (kN)
V_p	=	vertical component of the prestressing force (kN)
V_s	=	steel stirrups contribution to shear resistance (kN)
α_1	=	concrete reduction factor according to CSA-S6-10 strut and tie model
β	=	factor accounting for aggregate interlock in concrete sections
β_s	=	factor accounting for influence of cracking and confining reinforcement on the effective compressive strength of the concrete strut (ACI-318-05)
γ_{xy}	=	shear strain
Δf_p	=	increase in stress in prestressing steel due to factored loads (ACI-318-05) (kN)
ε_{cr}	=	the strain in concrete at cracking taken as 0.00008
ε_s	=	average tensile strain in the tension tie
ε_v	=	strain in FRP stirrup
ε_x	=	longitudinal strain at mid-depth of the section (beams)
ε_y	=	transverse strain, tension positive
ε_1	=	average principal tensile strain

ε_2	=	average principal compressive strain in the web, negative.
ν =		shear stress on an element of a homogeneous, elastic, uncracked beam
θ	=	angle of inclination of principal diagonal compressive stresses with respect to the longitudinal axis (Degrees)
ρ_f	=	longitudinal FRP reinforcement ratio (%)
σ_v	=	stress calculated according to CSA-S6-10 Clause 16.8.7
ϕ_{bend}	=	factor accounting for the reduction in the strength of the FRP stirrup at the bend
ϕ_c	=	resistance factor for concrete
ϕ_{FRP}	=	resistance factor for FRP
ϕ_s	=	resistance factor for reinforcing steel bars
ϕ_p	=	resistance factor for prestressing steel tendons

List of Abbreviations

ACI	=	American Concrete Institute
AFRP	=	Aramid Fiber Reinforced Polymer
CFCC	=	Carbon Fiber Composite Cables
CFRP	=	Carbon Fiber Reinforced Polymer
CPCI	=	Canadian Precast/ Prestressed Concrete Institute
CSA	=	Canadian Standards Association
FRP	=	Fiber Reinforced Polymer
GFRP	=	Glass Fiber Reinforced Polymer
LVDT	=	Linear Variable Displacement Transducer

1. Introduction

1.1 General

The many advantages of Fiber Reinforced Polymers (FRP) including their resistance to corrosion have intrigued researchers to investigate FRP as an alternative to steel reinforcement in concrete structures. However, since FRP is a relatively newer material, many uncertainties still remain regarding its application in concrete structures. One of the areas that still requires extensive research is the shear behaviour of FRP prestressed concrete beams.

FRP has different properties compared to steel such as lower modulus of elasticity that can result in wider shear cracks and lower shear capacity in concrete beams reinforced with FRP as opposed to steel. As a result, most current shear design codes and guidelines that were originally developed for steel reinforced concrete beams take a conservative approach towards the design of FRP reinforced beams. One way to improve the shear capacity of FRP reinforced concrete beams is through prestressing. However, lack of sufficient research on the behaviour of FRP prestressed concrete beams has resulted in often highly conservative shear formulas that overlook the benefit of prestressing.

This thesis will examine the effect of shear span to depth ratio (a/d) and the contribution of FRP transverse reinforcement to shear capacity of FRP prestressed concrete beams. The experimental results are compared to theoretical values obtained from various North American design codes and guidelines. The performance of the current shear formulas in North America are compared for FRP reinforced concrete beams as opposed to FRP prestressed beams using the results from this research as well as data from literature. Also, the thesis will check the suitability of the current North American shear design codes for design of beams exposed to distributed load as opposed to four point bending. The latter has been a common loading scheme for shear testing and has been used extensively to formulate or evaluate the current shear formulas (Razaqpur et al. 2004, Yonekura et al. 1993). In this chapter the background of the thesis is discussed along with an overview of the objectives and scope of the project.

1.2 Background

Unlike the flexural behaviour of concrete beams, shear behaviour is very complex. Shear stresses develop in regions of the beam where the bending moment varies. In beams without stirrups,

shear stresses are carried primarily through aggregate interlock at the cracks, dowel action of the longitudinal reinforcement and compression zone of concrete. This mechanism of shear transfer is known as “beam action”. Various models were developed in the past 100 years to model the shear behaviour of reinforced concrete beams after cracking. The most popular of these models include 45 degrees truss model, compression field theory and modified compression field theory. The latter is the foundation for many shear design formulas today including the Canadian highway bridge design code (CSA-S6-10).

There are many factors that are known to affect the shear behaviour of reinforced concrete beams including but not limited to axial load, a/d ratio and size of the beam. Compressive axial loads such as prestressing in concrete beams are known to enhance the shear capacity of the beams by delaying the onset of flexural cracking in the beam (MacGregor 2000).

Beams tested in this project showed significant increase in shear strength when a/d was reduced below 2.5 due to contribution of “arch action”. In these beams that are known as “deep beams” shear is carried primarily through diagonal compressive struts that connect the load points to the supports and are anchored by longitudinal tension reinforcement. The behaviour of these beams is usually evaluated using strut and tie models. In recent years, several strut and tie models have been developed for analysis of steel prestressed concrete deep beams (Tan et al 2001, Wang et al. 2008).

One of the ways to improve the shear behaviour of concrete beams is by including stirrups in the beam. The stirrups enhance shear resistance by better confining the concrete and limiting the opening of diagonal cracks. In case of deep beams, research has shown low strains in the stirrups meaning the stirrups did not have a significant contribution to shear resistance. These findings will be discussed in more detail in section 2.6.

Extensive research has been conducted on shear behavior of FRP reinforced concrete beams and has resulted in the development of reasonably conservative shear design formulas for these beams. However, the amount of past research regarding the shear behaviour of FRP prestressed concrete is scarce (Yonekura et al. 1993, Nishikawa et al. 1993, Park et al. 1999, Wang et al. 2011, Whitehead et al. 2005). Therefore, the shear design formulas are often highly conservative for FRP prestressed concrete beams which makes the design economically impractical. ACI 440.4R-04 provides no provisions to improve the theoretical shear capacity of concrete beams

prestressed with FRP due to lack of sufficient research. The code recommends using the minimum shear resistance formula for steel reinforced concrete beams because of wider cracks that are expected in FRP reinforced concrete beams as opposed to steel reinforced beams. Although CSA codes provide more reasonable estimates compared to ACI, the results as shown later remain conservative.

1.3 Objective and Scope

This project contributes to the small available experimental database for shear behaviour of FRP prestressed concrete beams. The concrete strength and prestressing level were maintained constant for all specimens. All the beams were designed to be shear deficient and the a/d ratio was the only factor that was varied in the study. The objectives of this study are listed below:

- Study the effect of a/d ratio and arch action on shear behaviour of FRP prestressed concrete beams by changing the length of the shear span of the beams to produce a/d of 1.5, 2.5, and 3.5.
- Study the contribution of minimum required FRP stirrups according to CSA-S6-10 (2010) to shear capacity of FRP prestressed concrete beams.
- Evaluate the performance of current shear design equations in North American design codes and guidelines for FRP prestressed concrete beams.
- Compare the behaviour of FRP prestressed concrete beams subjected to distributed load with similar beams tested under four point bending.
- Examine the accuracy of the shear design code formulas for predicting the capacity of beams subjected to distributed load.
- Evaluate the available strut and tie models for behaviour of prestressed deep beams with a/d = 1.5.

2. Literature Review

2.1 FRP Reinforcement for Concrete Structures

Fiber Reinforced Polymer (FRP) reinforcements are recommended as a suitable replacement for steel in reinforced concrete structures. Some of the advantages of FRP materials include light weight, high strength and resistance to corrosion which is a common problem with steel reinforcements. However, the properties of FRP are different from steel and there is still a lot of ongoing research to assess the suitability of FRP as an alternative to steel in concrete structures.

2.1.1 Properties of FRP

FRP reinforcements are usually made of Carbon, Glass or Aramid fibers held together by an epoxy resin matrix. The overall properties of the FRP reinforcement depend on the characteristics of the fiber and resin as well as the manufacturing process. The reinforcements can come in form of fabrics, grids, plates, bars and tendons. FRP tendons can be classified as bars, rods or strands. FRP composites are heterogeneous and anisotropic and although FRP reinforcements are fairly strong in longitudinal direction, they are weak in transverse direction. Also unlike steel that can yield, FRP reinforcements essentially behave in a linear manner all the way to failure and have a lower modulus of elasticity. The highest elasticity modulus among FRP materials belongs to Carbon Fibers.

A steel prestressed concrete beam behaves elastically until cracking and after cracking, the beam will deflect faster as the steel yields and failure will happen by concrete crushing or steel tendon rupturing. However, in case of concrete beams prestressed with FRP, the behaviour is elastic before cracking and continues approximately linear until the concrete crushes or FRP tendon ruptures. The post-cracking stiffness of FRP prestressed concrete beam will be lower due to lower modulus of elasticity of FRP compared to steel (El-Hacha 2004).

2.2 Shear Strength of FRP Reinforced Concrete Beams

While mechanisms of shear resistance in FRP reinforced concrete beams is similar to steel reinforce beams, the contribution of each shear resisting parameter varies.

The axial stiffness of FRP reinforced concrete beams is less than conventional steel reinforced beams due to lower modulus of elasticity of the FRP bars. As a result, crack widths in FRP reinforced structures will be wider and the uncracked compression zone will be smaller compared to beams reinforced with steel tendons. Therefore, the contribution from the uncracked concrete as well as aggregate interlock and the mechanism of residual tensile stresses between cracks are expected to be smaller. Also, due to the low strength and modulus of FRP reinforcement in transverse direction, transfer of shear through dowel action of longitudinal reinforcement will be insignificant.

Khuntia et al. (2001) proposed a simplified shear design formula based on tests conducted on steel reinforced concrete beams without transverse reinforcement. The authors confirmed that the shear resistance of the beams was a function of longitudinal reinforcement stiffness, a/d ratio and the concrete compressive strength. Razaqpur et al. (2004) conducted a similar study on FRP reinforced concrete beams. The results showed that the same factors identified by Khuntia et al (2001) for steel reinforced concrete beams also affect the concrete shear resistance V_c for FRP reinforced concrete beams.

Razaqpur et al. (2004) argued that V_c for slender beams changes almost linearly with the cubic root of longitudinal reinforcement stiffness, a/d and concrete compressive strength. The authors noted that due to variable elastic modulus of FRP materials, the axial rigidity of the reinforcement should be expressed as a product of $E_f\rho_f$ rather than ρ_f alone. The study showed that raising the axial stiffness of the longitudinal reinforcement to power of 1/3 provides better approximation than assuming a linear relation. El-Sayed et al (2011) also confirmed that raising the axial stiffness of the longitudinal reinforcement to 1/3 in the V_c formula improves the approximation of shear capacity of FRP reinforced concrete beams.

2.3 Shear Behaviour of Deep Beams

Behaviour of deep beams cannot be modelled using the conventional beam theory due to the development of arch action in these beams. Therefore, shear design formulas in the codes that are based on beam behaviour cannot be used to predict the behaviour of deep beams. Most design codes propose strut and tie models for analysing deep beams (CSA-S6-10, ACI-318-05).

Razaqpur et al. (2004) argued that the shear strength of deep beams is governed by the compressive resistance of concrete (f'_c) in direction of the diagonal struts. Oh et al. (2001) also

noticed with steel reinforced concrete deep beams that before yielding of the longitudinal steel, the ultimate shear capacity of the beams seemed proportional to f'_c. While, the failure mode of deep beams did not change between normal and high strength concrete, f'_c had a significant effect on ultimate shear strength of the beams. The authors also found that the ultimate strength of the beams was governed by the a/d ratio. The strut and tie models for steel reinforced concrete beams are appropriate for FRP reinforced concrete beams as long as the failure is caused by crushing of concrete rather than rupture of FRP (Razaqpur et al. 2004). Razaqpur et al. (2006) proposed a factor to account for arch action for the V_c formula in the CSA-S806-12 design code. The factor proposed by the authors was adopted from a formula based on study of steel reinforced concrete beams (Zsutty 1968).

The strut and tie model in the Canadian codes (CSA-A23.3-04 and CSA-S6-10) is based on the modified compression field theory. The formula considers the principal tensile strain as a contribution of both the concrete and longitudinal reinforcement to calculate the ultimate compressive strength of the strut (f_{cu}) as shown in Eq.3-2.

$$f_{cu} = \frac{f_c'}{0.8 + 170\varepsilon_1} \qquad \textbf{Eq.2- 1}$$

In Eq.2-1 shown above, f'_c is the compressive strength of concrete and ε_1 is the principal tensile strain calculated by taking in to account the strains in the concrete and the reinforcement around the strut.

Tan et al. (2001) proposed a simple strut and tie model for the analysis of prestressed deep beams. The authors believed that for regions of the beam with high prestressing, the formula for ε_1 could return a negative value which could then make the formula for f_{cu} invalid. The model is based on linear interaction between the principal compressive and tensile stresses at the bottom node and is valid for both pre- and post- tensioned beams.

2.4 Shear Resistance of FRP Prestressed Concrete Beams

Research has shown that presence of prestressing can significantly enhance the shear capacity of FRP reinforced concrete beams and as the level of prestressing increases so does the shear capacity of the concrete beams (Whitehead et al. 2005, Park et al. 1999, Yonekura et al. 1993, Nishikawa et al. 1993). Park et al. (1999) compared an FRP prestressed concrete beam with an effective prestress level of 40% with a similar FRP reinforced concrete beam. While both beams

showed a shear tension failure, the ultimate capacity of the beam with no prestressing was about 40% of the capacity of the prestressed beam. Also, the angle of the shear failure plane changed from 35 degrees to 45 degrees when the beam was prestressed. Prestressing the beams was found to increase the ultimate shear strength of the beams considerably, as well as their stiffness. The ultimate deflection of prestressed beams was 60% less than the similar FRP reinforced concrete beam.

Yonekura et al. (1993) also noticed that at any given load, the deflection of an FRP prestressed concrete beam decreased as the prestressing force was increased. Nishikawa et al. (1993) analyzed the shear capacity of rectangular concrete beams prestressed with FRP rods and strands. The test parameters consisted of type of tendon (CFRP, AFRP, and Steel) and prestressing ratio of 0, 30 and 60%. The test results showed that in prestressed concrete beams, the ultimate load capacity increased when higher prestressing ratio was applied.

The shear capacity of FRP prestressed concrete beams has also been found to be a function of the shear span to depth (a/d) ratio (Park et al. 1999, Wang et al. 2011). Park et al. (1999) tested CFCC prestressed concrete beams with a/d ratio of 2.5 except for two beams that were designed with a/d ratios of 1.5 and 3.5. The results from the experiment showed that increasing the a/d ratio reduced the shear resistance, while increasing the shear ductility (displacement) of the beams. Wang et al. (2011) tested five CFRP prestressed concrete beams without transverse reinforcement under four point bending with different a/d ratios of 0.71, 1.43, 2.14, and 2.86. The study showed that the shear capacity of the beams increased by 72% as the a/d was reduced below 2.14, while the increase in capacity was only 2.6% when the a/d was reduced from 2.86 to 2.14.

Park et al. (1999) also tested CFRP prestressed concrete beams with the same level of prestressing but different ratios of steel web reinforcement. Beam C5 was reinforced with minimum allowable steel stirrups at maximum allowable spacing according to ACI-318 (1995). Beam (C7) was reinforced with required amount of steel stirrups to avoid shear failure according to ACI-318 (1995). Increasing the amount of stirrups increased the ultimate shear capacity of the beams by 12%. The failure mode of the beams changed from diagonal tension failure for beam C5 to diagonal tension with rupture of longitudinal FRP reinforcement for beam C7. Also, beam C7 had slightly higher post-cracking stiffness and showed 25% larger deflection at ultimate. The

crack width for beam C7 at the failure plane was about one-third of the corresponding crack width for beam C5.

Yonekura et al. (1993) noticed in their study than the contribution of steel stirrups in steel prestressed concrete beams was far more significant that FRP spirals in FRP prestressed beams. The rate of increase of shear strength with increase in ratio of web reinforcement was much more significant for steel prestressed concrete beams with steel stirrups rather than FRP prestressed beams with FRP spirals as web reinforcement.

2.5 Overview of the Behaviour of FRP Stirrups

High strength and low elastic modulus of FRP, allows for high strains at ultimate around 0.012 to 0.03 for FRP stirrups compared to steel stirrups that are restricted by the yield strain of steel which is around 0.002. Therefore, design codes limit the strain allowed in FRP stirrups and do not allow the full capacity of the FRP stirrups to be utilised (El-Sayed et al. 2011). This is to avoid excessive shear cracking in the concrete which can affect the contribution of aggregate interlock in resisting the shear stresses.

It is common to bend shear stirrups to provide them with enough anchorage. However, in case of FRP stirrups, research has shown that bending the bars will result in reduced tensile capacity at the bent portion. The reduction of capacity at the bent portion is the result of localised stress development due to curvature and the inherent weakness of FRP in transverse direction (Shehata et al. 2000). Therefore, the strength of FRP stirrups is restricted by the minimum of their bend capacity or the strain limit (El-Sayed et al. 2011).

Shehata et al. (2000) conducted experiments on concrete beams reinforced with various types of FRP stirrups. The results showed that the strength of the stirrup can be reduced by as much as 60% due to the weakness of the bend. The paper stipulates that the strength of the FRP stirrups is a function of bend radius and the tail length that is critical for avoiding slip at the bend. For factored loads of CSA A23.3 (2004), a limit of 40% of the tensile capacity of the straight portion of the stirrups was proposed in calculating the contribution of the stirrups to shear resistance.

2.6 Behaviour of Stirrups in Deep Beams

As it was discussed earlier, deep beams transfer shear through continuous compressive struts that connect load points to the supports and are anchored by the tension tie. Therefore, the function of

the stirrups is not expected to be the same as for the case of slender beams which resist shear through mechanisms of beam action.

Guadagnini et al. (2006) tested beams reinforced with GFRP and steel longitudinal reinforcements with different span to depth ratios. In the second phase of testing, CFRP and GFRP stirrups in form of external links were provided. The authors expected longer debonding length in external links resulting in larger shear cracks which would in turn increase the demand on the transverse reinforcements. In other words, the external links were expected to attract higher stresses compared to internal stirrups. The results showed that the shear reinforcements of beams with a/d = 1.1 which failed in flexural compression, recorded relatively lower strain values compared to beams with a/d = 3.3, and 2.2. The findings were true for both steel and FRP reinforced concrete beams. The authors stated that this is due to the fact that in beams with a/d = 1.1, shear is mostly carried through compressive struts.

Cucchiara et al. (2002) tested beams with different ratios and combinations of steel fibers and stirrups. The test consisted of two series of beams with a/d ratios of 2.8 and 2.0. For the case of deep beams with a/d = 2, containing only steel stirrups, the authors noticed that the stirrups were less effective compared to beams with a/d = 2.8. The authors argued that deformations due to arch action did not allow the truss action associated with the stirrups to fully utilise.

Oh et al. (2001) noticed with reinforced high strength concrete deep beams that the ultimate shear strength of the beams only increased slightly with the addition of web reinforcement. The a/d ratio was varied from 0.5 to 2.0 and the concrete strength of 23 to 74 MPa. Also, different ratios of transverse and horizontal reinforcement were tested. While at a/d ratios of 0.5-0.85, the failure was sudden despite the web reinforcement, at higher a/d ratios of 1.25 and 2.0, web reinforcement controlled the sudden failure. In deep beams with higher a/d, increasing transverse reinforcement ratio from 0.12 to 0.34%, only slightly increased the ultimate shear strength. At lower a/d ratios of 0.5, the web reinforcement ratio had no effect on the ultimate capacity of the beams. Tan et al. (2003) believed that transverse steel reinforcement especially when inclined can have beneficial effect on ultimate shear strength of deep beams. Based on previous experiments, the authors mentioned that the tensile force in the longitudinal steel is reduced when transverse reinforcement is provided in deep beams.

2.7 Research on Beams Subjected to Uniform Loading

Kani (1966) showed that a uniformly distributed load best matches the case of two point loads applied at quarter spans of the beam. In other words, the shear span for a uniformly loaded beam can be taken as a = l/4; l being the span length of the beam. Kani (1966) argued that if two point loads on a beam applied at quarter lengths are replaced with a uniformly distributed load, the resultant forces from the distributed load remain at quarter-lengths. Later, Russo et al. (2005) proposed a model for shear analysis of steel reinforced concrete beams without web reinforcement loaded under four point bending. The model was used to analyse 56 beams tested under uniform loading from other researchers using Kani's analogy. The proposed model was found to be applicable to beams tested under uniform loading by assuming a/d = l/4d. The model even performed better than ACI code and AASHTO. The applicability of the model to uniformly loaded beams using Kani's relationship further validated Kani's findings.

2.8 Summary

In this chapter it was shown that the lower modulus of elasticity of FRP compared to steel and its weakness in transverse direction results in lower shear capacity in FRP reinforced concrete structures. The weakness of FRP in transverse direction is also the reason the performance of FRP stirrups is governed by their capacity around the bend which could be 40% of the tensile capacity of the straight portion of the stirrup (Shehata et al. 2000).

Also, past research on the effect of the level of prestressing and shear span to depth ratio (a/d) on shear capacity of FRP prestressed concrete beams was outlined. It was shown that arch action can significantly improve the shear capacity of concrete deep beams. The strut and tie models for steel reinforced concrete beams are appropriate for FRP reinforced concrete beams as long as the failure is caused by concrete crushing and not rupture of FRP longitudinal reinforcement (Razaqpur 2004). Also, research has shown that stirrups are not as effective in deep beams as they are in slender beams since the behaviour of deep beams is governed by arch action (Cucchiara et al. 2002, Guadagnini et al. (2006), Oh et al. 2001).

Also, Kani's (1966) analogy regarding the suitability of four point bending test with point loads at quarter lengths as a model for distributed loading was outlined.

3. Shear Behaviour of Concrete Beams

3.1 General

In this chapter the shear behaviour of concrete beams and the underlying factors are discussed. The applicable theoretical models and design procedures and their backgrounds are reviewed as well as various strut and tie models for the analysis of deep beams.

3.2 Behaviour of Reinforced Concrete Beams

A reinforced concrete beam under load is subjected to flexural and shear stresses. The shear forces exist in locations along the beam where the moment varies. Figure 3-1 demonstrates the shear and flexural stresses acting on an element inside a homogenous uncracked concrete beam. As it can be seen from the Figure, equal shearing stresses act on the element in both the vertical and horizontal planes while the flexural forces only result in normal stresses applied in the horizontal plane (MacGregor 2000).

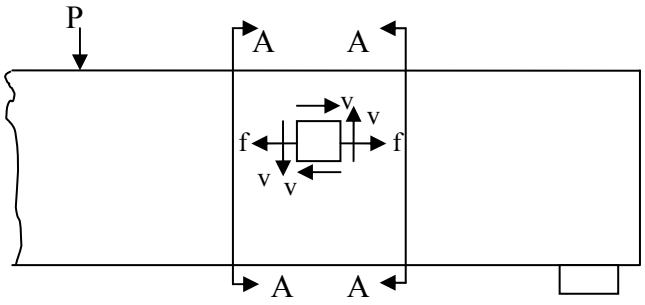

Figure 3- 1: Flexural and shear stresses within the shear span (MacGregor 2000)

The combination of flexural and shearing stresses on the element in top portion of the beam shown in Figure 3-1, result in normal stresses acting on a rotated element within the beam (Figure 3-2). The maximum and minimum normal stresses acting on the element are referred to as principal stresses (MacGregor 2000).

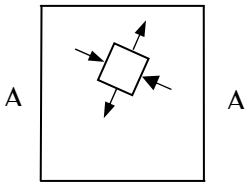

Figure 3- 2: Principal stresses acting on the element (MacGregor 2000)

In a homogeneous, elastic, uncracked beam the shear stresses on an element in the beam can be calculated from Eq. 3-1:

$$\upsilon = \frac{VQ}{Ib} \qquad \textbf{Eq.3- 1}$$

V = shear force on the cross section

I = Moment of inertia of the cross section

Q = first moment of area

b = the width of the member where the stresses are being calculated

The principal tensile stresses in the uncracked beam act perpendicular to principal compressive stress trajectories (Figure 3-3). Cracks occur perpendicular to the direction of the principal tensile stresses where these stresses exceed the tensile resistance of the concrete (MacGregor 2000).

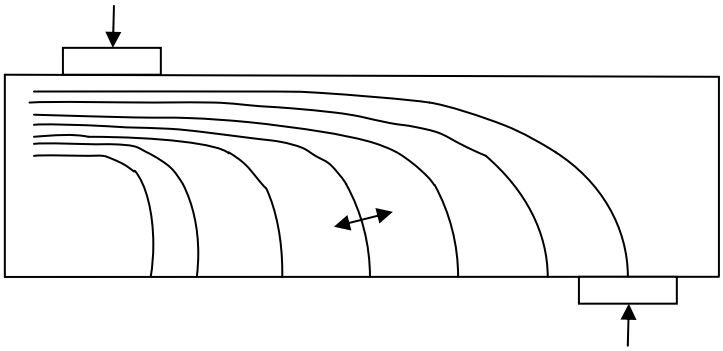

Figure 3- 3: Principle compressive stress lines in the shear span of an uncracked beam

3.2.1 Beam Action and Arch Action

For balance of moment at the section shown in Figure 3-4 the following general equation can be derived which shows a relationship between the force ΔT and the horizontal shear force on top of the element:

$$V = \frac{dM}{dx} = \frac{d}{dx}(Tjd) = jd\frac{dT}{dx} + T\frac{d(jd)}{dx} \qquad \textbf{Eq.3- 2}$$

For normal elastic beam theory to apply, the lever arm in Eq.3-2 has to remain constant resulting in the equation being reduced to:

$$V = jd\frac{dT}{dx}$$ **Eq.3- 3**

dT/dx is the rate of change of the internal shear force across any horizontal plane between the longitudinal reinforcement and the compression zone of the concrete. The existence of this shear flow is essential for development of beam action. However, if the shear flow is lost beam action will not develop and Eq.3-2 will be:

$$V = T\frac{d(jd)}{dx}$$ **Eq.3- 4**

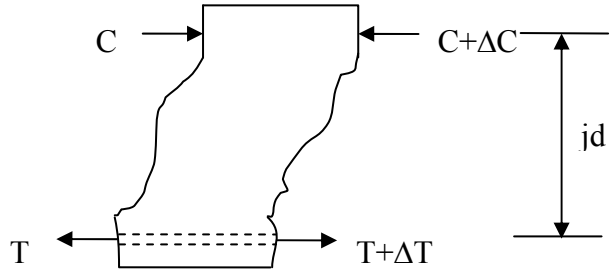

Figure 3- 4: Average shear stress in between diagonal cracks (MacGregor 2000)

The loss of bond between the reinforcement and the concrete can occur due to unbonding of the reinforcement or diagonal cracks that extend from load point to the supports. In this case, the external shear forces are resisted by inclined internal compression struts. This mode of shear resistance in the beam is known as arch action (MacGregor 2000).

3.2.2 Shear Resistance of Beams without Web Reinforcement

Figure 3-5 demonstrates the forces carrying the shear stresses across the diagonal crack in concrete beams without web reinforcement.

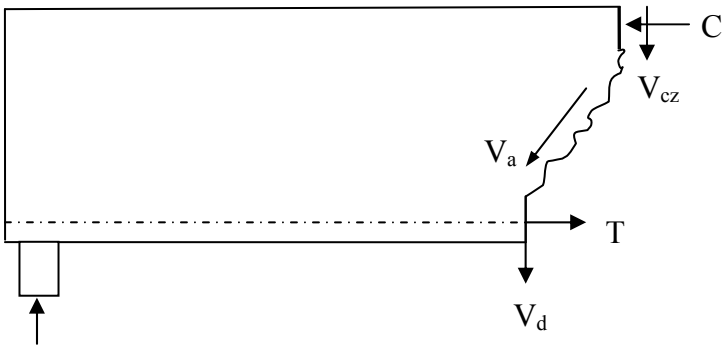

Figure 3- 5: Internal forces at a diagonal crack for beams without stirrup (MacGregor 2000)

The shear is carried by aggregate interlock (V_a), dowel action of the longitudinal reinforcement (V_d), and shear in the compression zone (V_{cz}) (MacGregor 2000).

3.3 Factors Affecting the Shear Strength of Concrete Beams

The concrete contribution to shear resistance of reinforced concrete beams without transverse reinforcement has been found to vary with the following parameters (MacGregor 2000):

1. Concrete tensile strength
2. axial forces
3. Size of the beam
4. Shear span to depth ratio (a/d or M/Vd)
5. Longitudinal reinforcement ratio

3.3.1 Variability of the Shear Strength of concrete beams with the a/d ratio

Shear spans of concrete beams can be divided in to two general categories of "slender" and "deep" beams. The a/d ratio is an indication of the category the beam falls in to. Beams with a/d ratio less than 2 in simply supported beams are classified as deep beams (Park and Paulay1975).

Arch action is more efficient at smaller a/d ratios (less than 2). Beams with a/d ratio between 0 and 1, develop inclined cracks extending from the supports to the load points. These cracks disrupt horizontal shear flow from longitudinal reinforcement to the compression zone of concrete and result in arch behaviour. Anchorage failure is common with these beams as the arch action relies on proper anchorage of the longitudinal reinforcement at the supports. Beams with a/d ratio between 1 and 2.5, develop diagonal cracks and after the redistribution of the internal stresses in the beam due to cracking, carry additional shear through arch action. Slender beams with a/d ratio from roughly 2.5 to 6 are governed by beam action. In very slender beams diagonal cracks disrupt the balance of the stresses to the point where the beam fails at the inclined cracking load (MacGregor 2000).

3.3.2 Effect of Axial Loads on Shear Strength of Concrete beams

Unlike axial tensile forces, axial compressive forces tend to increase the flexural cracking load in concrete beams. The higher the axial compressive force, the later flexural cracks will appear in the beam, and a larger shear force will be needed for the principal tensile stresses to reach the

concrete's tensile capacity. However, once the flexural cracks appear the cracks will be just as deep as for a regular reinforced concrete beam (MacGregor 2000).

3.4 Transversally Reinforced Concrete Beams

The purpose of transverse reinforcements in concrete beams is to enhance the shear resistance of the concrete. In reinforced concrete beams without web reinforcement, sections between diagonal cracks act as concrete cantilevers that contribute to shear resistance of the beam. In transversally reinforced concrete beams, these cantilevers are tied and behave like diagonal compression members in a truss as shown in Figure 3-6. Reinforced concrete beams with transverse reinforcement are able to carry an additional bond force ΔT' (Park and Paulay 1975). Prior to inclined cracking, the strain in the stirrups is the same as the strain in the concrete at the location of the stirrup. Therefore, the stirrups do not prevent inclined cracking and only become active when they are crossed by an inclined crack (MacGregor 2000). As Figure 3-6 shows, once the inclined crack is formed, portion of the shear is carried by tension force T_s through the stirrup.

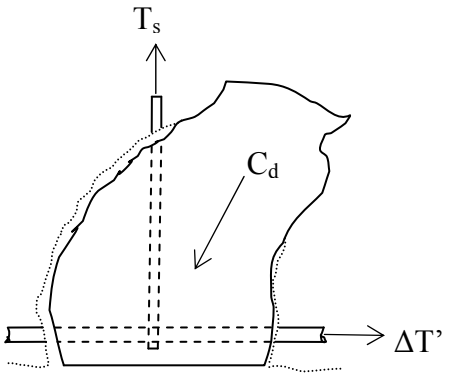

Figure 3- 6: Forces between diagonal cracks (beams with stirrups) (Park and Paulay 1975)

The stirrups can improve the shear resistance of the concrete beam by (Park and Paulay 1975):

1. Confining the concrete when adequately spaced stirrups are provided, improving the compressive strength of local regions mainly affected by arch action
2. Sufficient amount of stirrups can prevent bond failures and resulting splitting cracks in the concrete due to loss of bond in anchorage zones or dowel forces.
3. Enhancing dowel action by providing support to the longitudinal reinforcement that is being crossed by a flexural shear crack near the stirrup.

4. Overcoming the flexural tensile stresses in the cantilever blocks between diagonal cracks through the diagonal compression force C_d resulting from truss action (Figure 3-6)
5. Improving and sustaining shear resistance through aggregate interlock by restricting the opening of diagonal cracking within the elastic range.

3.5 Shear Design Analytical Models

Unlike the flexural behaviour of concrete beams, the shear behaviour is very complex. Below are various theoretical models that have been used to analyze the shear behaviour of concrete beams. The Modified Compression Field Theory is the latest model that is the foundation for the shear design formulas in the CSA A23.3 (2004) and CSA-S6-10 (2010) design codes.

3.5.1 The 45° Truss Model

Ritter (1899) proposed a truss model to describe the flow of forces in a reinforced concrete beam after cracking. In Ritter's model, the diagonal compressive stresses in the concrete provide the diagonal compression members of the truss and the stirrups act as vertical tension members. The longitudinal reinforcement in the concrete acts as the bottom chord of the truss. Mörsch (1902) clarified that the compression members in the truss model are a continuous field of diagonal compression rather than distinct diagonal compressive struts. However, both Ritter (1899) and Mörsch (1902) ignored the tensile stresses in the cracked concrete and assumed the angel of diagonal compression stresses (θ) will remain at 45 degrees after cracking. Later on, Mörsch's model was made more accurate in "variable-angle truss model" by providing a range of values for angle θ and accepting the fact that θ is usually less than 45 degrees. However, since concrete shear failures are brittle, it was necessary to impose limits on θ (ex. $\theta > 30$ or the diagonal compressive stresses ($f < 0.6f'_c$) to ensure safe design (Collins and Mitchell 1997, Bentz et al. 2006).

3.5.2 Compression Field Theory

The compression field theory provided a more sensible approach towards modelling the shear behaviour of reinforced concrete beams. Unlike the older models, the compression field theory used the state of strains in the web after cracking to determine the angle of inclination (θ).

Wagner (1929) argued that in thin webbed metal girders, after bucking the web cannot resist compression anymore and the shear resistance will be provided through a field of diagonal tension. To determine the angle of diagonal tension in the web, Wagner assumed that the angle would match the inclination angle of the principal tensile strains. Wagner's approach came to be known as the tension field theory. Wagner's theory was applied to analysis of shear in reinforced concrete beams by assuming that concrete cannot carry tension after cracking and the shear is resisted through a field of diagonal compression. This approach provides the foundation for the compression field theory and resulted in the following formula for determining the angle (θ) of diagonal compression (Collins and Mitchell 1997):

$$\tan^2\theta = \frac{\varepsilon_x - \varepsilon_2}{\varepsilon_y - \varepsilon_2} \qquad \textbf{Eq.3- 5}$$

In Eq.3-5, ε_x = longitudinal strain of the web, tension positive; ε_y transverse strain, tension positive; ε_2 = principal compressive strain, negative; ε_1 = principal tensile strain, positive

The direction of the strains is shown in Figure 3-7. Since ε_x is usually much smaller than ε_y, the angle θ will end up being much less than 45 degrees which results in less conservative prediction for the shear strength of the web (Collins and Mitchell 1997).

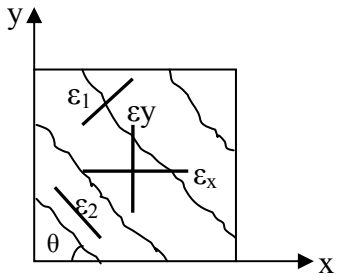

Figure 3- 7: Average strains in cracked member (Collins and Mitchell 1997)

3.5.3 Modified Compression Field Theory

Before diagonal cracking, equal principal tensile and compressive stresses acting at 45 degrees resist the shear in the web. After diagonal cracks are formed, the tensile stresses in concrete significantly reduce. Compression field theory assumes the principal tensile stresses go to zero after diagonal cracking. However, the modified compression field theory accounts for the contribution of the tensile stresses in areas between diagonal cracks. The tensile stresses in

diagonally cracked concrete vary from 0 at crack location to maximum value in between the cracks. These residual tensile stresses enhance the ability of the cracked concrete to carry shear in between diagonal cracks (Collins and Mitchell 1997, Bentz et al. 2006). Experiments on reinforced concrete elements under biaxial stresses have shown that even after extensive diagonal cracking, tensile stresses still exist between cracks (Vecchio et al. 1982).

3.6 Analysis of Deep Beams

As it was discussed earlier, behaviour of deep beams cannot be modelled using the conventional beam theory. Therefore most shear design formulas cannot be used to estimate the capacity of deep beams and instead strut and tie models are recommended.

While the elastic analysis is useful to predict the stresses in the beams prior to cracking, it cannot be used to model the flow of stresses in the beam after cracking. A cracked reinforced concrete beam resists load through compressive stresses in the concrete and tension in the longitudinal reinforcement. The compressive stress trajectories approach a straight line after extensive cracking and can therefore be modelled by straight compressive struts. The distribution of internal stresses in a deep beam can be modelled using compressive struts, longitudinal reinforcement as tension tie and nodes that connect the struts with the tie (Collins and Mitchell 1997).

The strut and tie models are set up by first drawing the flow of forces in the beam based on the location of the loading points and support bearings and determining the size of the nodal regions. The nodes have to be made sufficiently large to make sure the allowable stresses at the nodes are not exceeded. According to the CSA A23.3 (2004), stresses at CCC nodes (enclosed by compressive struts and bearing areas) should not surpass $0.85\phi_c f'_c$. The maximum stress limit for CCT nodes (anchored by a tension tie from one side) is $0.75\phi_c f'_c$ and for nodes bounded by tension tie in more than one direction the limit is reduced to $0.6\phi_c f'_c$. Figure 3-8 illustrates the detailing of a strut and tie model for a deep beam subjected to four point bending.

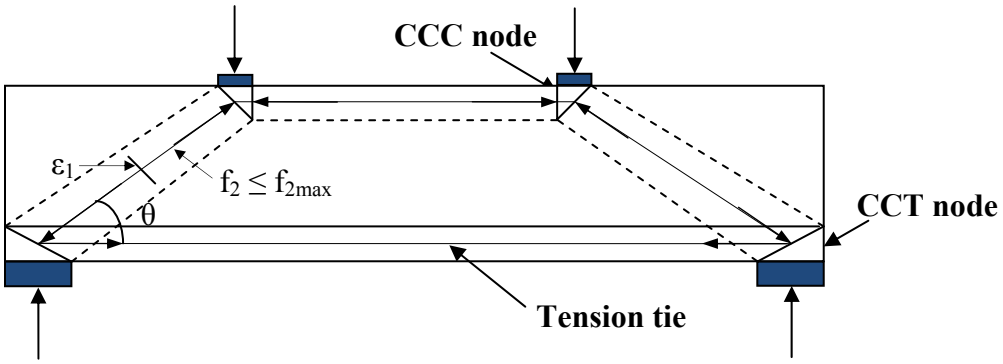

Figure 3- 8: Strut and tie model (Collins and Mitchell 1997)

The stress limits at the nodal regions in CSA S6-10 (2010) code are $\alpha_1\phi_c f'c$ for CCC nodes and $0.88\alpha_1\phi_c f'c$ for CCT nodes and $0.76\alpha_1\phi_c f'c$ for nodes anchored by a tie in more than one direction. α_1 is calculated from the formula below:

$$\alpha_1 = 0.85 - 0.0015 f_c^{'} \qquad \textbf{Eq.3- 6}$$

The concrete resistance ϕ_c is equal to 0.75 for design purposes. The resistance factors are not used in research related analysis.

The maximum capacity of the tie is found from Eq.3-7:

$$T_u = \phi_s f_y A_s + \phi_p f_{py} A_p \qquad \textbf{Eq.3- 7}$$

In Eq.3-7, f_y and A_s are the yield strength and cross sectional area of reinforcing bars; f_{py} and A_p are the yield strength and cross sectional area of prestressing tendons; ϕ_s and ϕ_p are respectively resistance factors for reinforcing bars and prestressing tendons.

The compressive strut must be large enough to make sure the stresses in the strut due to loading do not exceed the crushing strength of concrete.

$$N_u \le \phi_c A_{cs} f_{2\max} \qquad \textbf{Eq.3- 8}$$

N_u is the calculated axial compression force in the strut due to factored loads. A_{cs} is the effective cross sectional area of the strut and f_{2max} is the crushing strength of cracked concrete calculated from Eq.3-9:

$$f_{2\max} = \frac{f_c^{'}}{0.8 + 170\varepsilon_1} \le \alpha_1 f_c^{'} \qquad \textbf{Eq.3- 9}$$

Where the compressive strut is anchored by a tension tie, the resulting tensile straining will decrease the ability of the concrete to resist compressive stresses. The principal tensile strain is therefore calculated as follows:

$$\varepsilon_1 = \varepsilon_s + (\varepsilon_s + 0.002)\cot^2\theta \qquad \textbf{Eq.3- 10}$$

In Eq.3-10, the principal compressive strain in the strut at ultimate is assumed to be 0.002; θ is the smallest angle between the compressive strut and the tension tie and ε_s is the average tensile strain in the tie calculated from the formula below:

$$\varepsilon_s = \frac{T}{A_s E_s} \qquad \textbf{Eq.3- 11}$$

T is the tension force in the tie. A_s and E_s are respectively the cross sectional area and modulus of elasticity of the tension tie reinforcing bars. The force in the tension tie reinforcements is still developing in the area where the ties cross the strut which means the strain in the ties varies from 0 to ε_s over the development length. Therefore, an average value of ε_s at the centre of the strut is used for calculating the principal tensile strain ε_1 equal to half the value calculated from Eq.3-11 (Collins and Mitchell 1997).

ACI 318-05 (2005) limits the angle of the compressive strut with the tension tie to 25 degrees. The strength of a compressive strut without longitudinal reinforcement parallel to the axis of the strut is found from Eq.3-12 (ACI 318-05 Appendix A):

$$F_{ns} = f_{ce} A_{cs} \qquad \textbf{Eq.3- 12}$$

$$f_{ce} = 0.85\beta_s f_c^{'} \qquad \textbf{Eq.3- 13}$$

F_{ns} is the strength of the compressive strut; A_{cs} is the cross-sectional area of the strut calculated based on the minimum width of the strut at the ends in the direction perpendicular to its axis; f_{ce} is the effective compressive strength of the strut; β_s is a reduction factor which is 1.0 for a strut with uniform cross-sectional area. For this project the case of $\beta_s = 0.6$ applied, both because the cross-section of the struts was non uniform and diagonal parallel cracks developed in the web.

The strength of the tie is found from Eq.3-14:

$$F_{nt} = A_s f_y + A_p (f_{se} + \Delta f_p) \qquad \textbf{Eq.3- 14}$$

$(f_{se}+\Delta f_p)$ shall not exceed the yield stress of the steel flexural reinforcements (f_{py}).

Tan et al. (2001) developed an alternative strut and tie model for the analysis of prestressed deep beams. The authors believed that the CSA code approach could lead to negative values for ε_1 if the prestressing force is too high and the formula may not be usable. The authors developed a new model to account for both pre- and post- tensioned beams as well as different configurations of web reinforcement. Figure 3-9 outlines the model proposed by the authors and shows the interaction between the compressive strut and the tension tie at the bottom node.

The proposed model is set up based on a linear interaction between the principal compressive and tensile stresses at the bottom node shown as shown in Eq.3-15:

$$\frac{f_1}{f_t} + \frac{f_2}{f_c'} = 1.0 \qquad \textbf{Eq.3- 15}$$

The authors used Eq.3-15 as a different way to address the detrimental effect of the tensile stresses in the tie on the capacity of the compressive strut to carry compression. In Eq.3-15, f'_c is the actual compressive strength of concrete determined from cylinder tests along the f_2 direction; f_t represents the ultimate tensile capacity in the f_1 direction and considers the contribution of both the concrete and the reinforcement to tensile capacity. In this model, compressive stress f_2 should not go beyond the compressive strength of concrete ($f_2 \leq f'_c$).

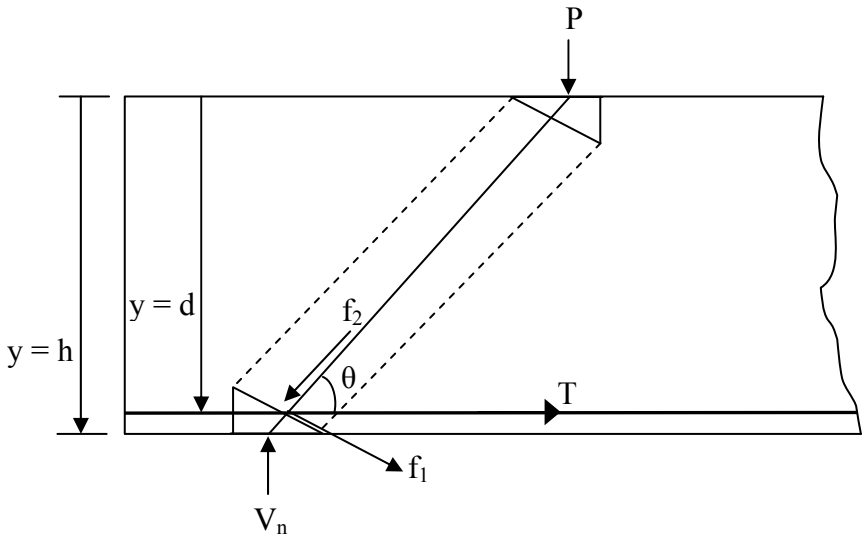

Figure 3- 9: Tan et al. (2001) strut and tie model

$$f_1 = \frac{kT\sin\theta}{A_c/\sin\theta} - \frac{kF_{pe}\sin\theta}{A_c/\sin\theta} \qquad \textbf{Eq.3- 16}$$

$$f_2 = \frac{V_n}{\sin\theta A_{cs}}$$ **Eq.3- 17**

$$f_t = \frac{2(F_{pu} - F_{pe})\sin\theta}{A_c / \sin\theta} + f_{ct}$$ **Eq.3- 18**

In the above equations, the original formula for f_t proposed by Tan et al. (2001) has been simplified for prestressed concrete deep beams with straight tendons and no non-prestressed reinforcement. A_c is the cross sectional area of concrete section; F_{pu} and F_{pe} are respectively the ultimate and effective prestressing force of the prestressing tendon; V_n is the estimated nominal shear capacity; A_{cs} is the cross sectional area of the compressive strut; k is a factor that accounts for the non-uniform nature of tensile stress f_1 that acts perpendicular to the diagonal strut and is taken as 2.0, and f_{ct} is the tensile capacity of concrete. Also, the authors used experimental values from split cylinder tension tests for f_{ct} but also proposed $0.5\sqrt{f'_c}$ to be used in lack of experimental data.

Zhang and Tan (2007) proposed a number of changes to the original model for analysing deep reinforced concrete beams. First, derivation of k factor was modified to satisfy moment equilibrium as well as force equilibrium resulting in k = 4 at the bottom node. Also, the authors argued that close to failure, due to extensive cracking the concrete tensile strength is severely reduced and it is therefore non conservative to use the full tensile strength of concrete. A formula by Belarbi et al. (1994) for tensile strength of cracked concrete was used instead:

$$f_{ct} = 0.31\sqrt{f'_c}\left(\frac{\varepsilon_{cr}}{\varepsilon_1}\right)^{0.4}$$ **Eq.3- 19**

ε_{cr} is the strain in concrete at cracking taken as 0.00008, adopted from Belarbi et al. (1994) research; and ε_1 is calculated exactly the same as Eq.3-10.

Also, the authors included the component of the bottom reinforcement force (Tcosθ) along the diagonal compressive strut that was originally ignored. The authors thought that this force can be significant for higher a/d ratios where angle θ is small. Below is the modified formula for calculating f_2:

$$f_2 = \frac{F_c - T\cos\theta}{A_{cs}}$$ **Eq.3- 20**

Wang et al. (2008) developed a similar model to Tan et al. (2001) model for analysis of prestressed concrete deep beams. The model was developed to work for any shape of draped tendon including parabolic.

The stress distribution factors are the same as the one adopted by Zhang et al. (2007) in their modified model for reinforced concrete deep beams. Also, the component of the force in the bottom longitudinal reinforcement in direction of the diagonal strut is ignored similar to Tan et al. (2001) model. Wang et al. (2008) believed that whether a/d is very small or comparably high, the term Tcosθ can be ignored because it won't be the governing factor. However, they also acknowledged that omitting the term Tcosθ in calculating f_2 could be the reason for the model's conservative predictions.

To account for the concrete softening effect at the bottom node, the authors utilised the Kupfer et al. (1973) formula shown below:

$$\frac{f_1}{f_t} + 0.8\frac{f_2}{f_c^{'}} = 1 \qquad \textbf{Eq.3- 21}$$

For the case of prestressed deep beams with straight tendons and no non-prestressed reinforcement, the formula for f_t is similar to Eq.3-18, except F_{ps} is used in the formula instead of F_{pu}. F_{ps} is the actual prestressing force in the tendon at ultimate. The authors acknowledged that the value of F_{ps} cannot be easily determined and noted that the value should be slightly less than F_{pu} for bonded tendons so F_{pu} could be used. The value of f_{ct} however, is determined from the formula below which is adopted from National Standards of People's Republic of China code fore design of concrete structures (2002):

$$f_{ct} = 0.27 f_c^{'2/3} \qquad \textbf{Eq.3- 22}$$

The proposed model was evaluated against experimental results from literature and compared to Tan et al. (2001) model for prestressed concrete beams. The authors argued that their proposed model better matched the test results in terms of precision and reliability. However, the average ratios of experimental results to predictions from each model were almost the same, with Tan et al. (2001) model having a slightly higher coefficient of variation.

3.7 Background of the CSA A23.3 Shear Design Code

Over 100 years ago, Ritter's 45 degrees truss model became the foundation for many building codes in North America and worldwide. As mentioned earlier, the truss model assumed that diagonally cracked concrete cannot sustain tension. For the case of stirrups at 90 degrees angle to the longitudinal reinforcement, the following familiar formula known as "steel contribution" was derived: (Khaldoun et al. (1999)

$$V_s = \frac{A_v f_{yv} d_v}{s} \qquad \textbf{Eq.3- 23}$$

A_v and f_{yv} are respectively the area and yield strength of transverse reinforcement; s is the spacing between transverse shear reinforcements and d_v is the effective shear depth. The above formula also assumes that the diagonal compressive stresses always act at 45 degrees.

Later research proved that the angle θ is not always 45 degrees and can vary which led to the development of the Compression Field Theory. The Compression Field Theory allowed for a sensible method to determine the angle θ but still ignored the tensile stresses in concrete after diagonal cracking. The Compression Field Theory was the foundation for the shear design general formula in the 1984 edition of CSA design code. Since the Compression Field Theory ignored the tensile stresses in the concrete after cracking, it was unable to model the shear behaviour of members without transverse reinforcement. In 1994, the CSA shear design general formula was modified according to the Modified Compression Field Theory to account for the average tensile stresses between diagonal cracks. In the 1994 CSA design code, the term V_c was added to the formula for shear resistance to account for the concrete contribution after diagonal cracking. The contribution of stirrups is accounted for by V_s and V_p is a measure of the vertical component of the prestressing force (Khaldoun et al. 1999).

$$V_r = V_c + V_s + V_p \qquad \textbf{Eq.3- 24}$$

The concrete contribution through aggregate interlock at the crack location was determined from Eqn. 3-25 (CSA-A23.3-04 Clause 11.3.4). The parameter $\sqrt{f'_c}$ accounts for the tensile resistance of concrete. Also the factor β relies on the ability of the concrete to transfer the tensile stresses. In other words β is a measure of aggregate interlock at the crack. In 1994 fixed values for θ were provided in separate tables for beams with and without stirrups rather than allowing θ to vary

over a range of 15-75 degrees. Overall, lower values of θ correspond to designs that use less transverse reinforcement and more longitudinal reinforcement.

$$V_c = \beta\sqrt{f_c'}\,b_w d_v \qquad \textbf{Eq.3- 25}$$

It should be noted that in the Modified Compression Field Theory and subsequently the CSA code, the dowel action of the flexural reinforcement is ignored and not included in the shear resistance formula (Bentz et al. 2006).

The V_s formula is similar to Ritter's formula except for the fact that it allows for variable angle θ. The stirrups contribution which depends on the number of stirrup legs intercepting the diagonal crack was calculated from Eq. 3-26 (CSA A23.3-04 Clause 11.3.5.1) shown below:

$$V_s = \frac{A_v f_{yv} d_v}{s}\cot\theta \qquad \textbf{Eq.3- 26}$$

The formulas outlined so far are part of the general method for shear design provided in the CSA 1994 code. However, same as in the 1984 design code, there is a separate simplified method derived from the empirical techniques of the ACI-318-05 (2005) code. Due to complexities of the general method, engineers were more prone to using the simplified method which could result in conservative and less economical structures. Also, a certain design could be safe according to the rational general method but deemed on safe by the more conservative empirical simplified method, causing incompatibilities (Bentz et al. 2006).

Therefore, in 2004 the new CSA design code provided simple equations for calculating β and θ, replacing the tables in the 1994 edition of the code making design with the general method easier. The simplified method in 2004 version of the CSA code is derived from the general method with the longitudinal strain assumed for yielding of 400 MPa steel. The factor β in the 2004 version of the CSA general method is determined by the following formula (Bentz et al. 2006):

$$\beta = \frac{0.4}{1+1500\varepsilon_x}\left(\frac{1300}{1000+s_{ze}}\right) \qquad \textbf{Eq.3- 27}$$

In above formula, ε_x is the average tensile strain at mid-depth of the section; s_{ze} is the equivalent value of crack spacing parameter s_z and it considers the effect of aggregate size on shear strength of reinforced concrete beams.

The angle θ in the 2004 CSA A23.3 code is calculated based on the value of ε_x and the allowable range for θ:

$$\theta = 29 + 7000\varepsilon_x \qquad \textbf{Eq.3- 28}$$

The above equation is conservative for large members without transverse reinforcement and therefore the following adjustment is recommended for these members:

$$\theta = (29 + 7000\varepsilon_x) \times (0.88 + \frac{s_{ze}}{2500}) \qquad \textbf{Eq.3- 29}$$

All the above equations are only valid if the beam has enough flexural strength to have a shear failure before a flexural failure.

3.7.1 Significance of the Longitudinal Strain (ε_x)

The shear resistance of concrete beams is affected by several factors related to geometric and loading conditions of the beam. The average longitudinal strain at a certain depth (ε_x) is a single parameter that is used to account for all the various factors that influence the shear resistance of the beam. The idea is that the higher the value of ε_x, the wider the diagonal cracks in the beam which means less aggregate interlock and lower contribution from the concrete to shear resistance (Bentz et al. 2006).

CSA-A23.3 (2004) suggests measuring ε_x at mid-depth of the section. The code assumes the magnitude of ε_x at mid-depth to be approximately half the strain at the centroid of the flexural tension reinforcement (Eq. 3-30), which is more conservative (Bentz et al. 2006):

$$\varepsilon_x = \frac{\frac{M_f}{d_v} + V_f + 0.5N_f - V_p - A_p f_{po}}{E_s A_s + E_p A_p} \qquad \textbf{Eq.3- 30}$$

A_s and E_s are the area and modulus of elasticity of the non-prestressed reinforcement; A_p and E_p are the area and modulus of elasticity of the prestressed reinforcement; N_f is the factored applied axial force (positive for tension); f_{po} is the stress in the prestressing steel when the stress in the adjacent concrete is zero; M_f is the factored bending moment and V_f is the factored applied shear force.

Figure 3-10 shows a model of the behaviour of the beam and the relationship between different stresses at a particular section of the beam used to derive Eq.3-30. Taking moment about the

external compressive force (C) acting on top of the section, the flexural tension force (T) in the reinforcement can be obtained as $0.5V_f\cot\theta$. The 2004 CSA code conservatively assumes $0.5\cot\theta$ is equal to one and thereby eliminates the need for iteration. The force in the flexural tension reinforcement is then converted to strain using the relationship outlined in Figure 3-10. $A_{ct}E_c$ in the figure accounts for the stiffness of concrete, where A_{ct} is the concrete area on the flexural tension side of the member and E_c is the concrete's uncracked elastic modulus. The effect of prestressing is considered in the graph by off-setting the cracking force at which point the stiffness of concrete no longer has an impact on strain (Bentz et al. 2006).

In reinforced concrete beams with large axial compressive load such as highly prestressed beams, the value of ε_x could be negative. Negative values for ε_x means the crack widths will be much smaller and the shear strength will be considerably larger (Bentz et al. 2006). The CSA-S6-10 (2010) suggests using 0 for ε_x if the parameter is calculated to be negative.

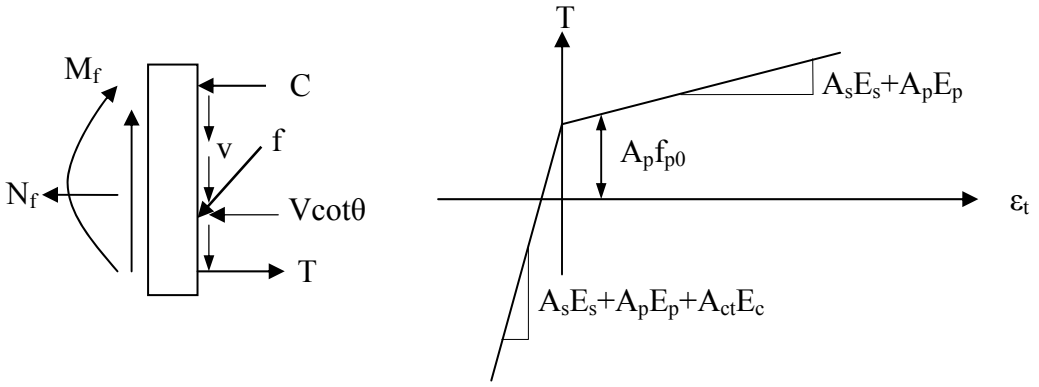

Figure 3- 10: Development of ε_x parameter (Bentz et al. 2006)

3.8 Summary

The shear behaviour of concrete beams and the relevant analytical models were outlined in this chapter. It was shown that concrete beams crack where principal tensile stresses exceed the tensile strength of the concrete. The shear behaviour of concrete beams with and without stirrups was discussed. Concrete beams without stirrups resist shear through aggregate interlock at the diagonal crack, dowel action of the longitudinal reinforcement and contribution of the uncracked compression zone of concrete. In transversally reinforced concrete beams, portion of the shear is

carried through tension in the stirrup where the stirrup is crossed by a diagonal crack and shear strength of the member is enhanced. Different factors that can affect the shear strength of the concrete beams were discussed with special focus on the effect of prestressing and a/d on the shear behaviour of concrete beams. Axial compressive forces such as prestressing were shown to delay flexural cracking and subsequently the diagonal cracking in the beam and enhance the ultimate shear strength of the concrete beams.

Also, the development of various analytical models for shear behaviour of reinforced concrete beams was discussed. It was shown that modified compression field theory improved the modelling of the shear behaviour of concrete beams by accounting for residual tensile stresses between diagonal cracks. Modified compression field theory is the foundation for the CSA general method for shear design. Also, different strut and tie models for analysis of concrete deep beams were outlined including the models in North American design codes as well as available models in literature for analysis of prestressed concrete deep beams.

4. Experimental Work

4.1 General

This research investigates the shear capacity of concrete T-beams prestressed with CFRP cables (CFCC). Four different groups of beams were studied. Each beam group consisted of two beams without transverse reinforcement (Series 1) and two beams with transverse reinforcement (Series2). The first three beam groups were tested under four point bending and had different span to depth ratios of 1.5, 2.5 and 3.5, and the last group were tested under distributed load. Table 4.1 outlines the specifications of each beam group. The goal of the research was to evaluate the effect of the shear span to depth ratio on the shear resistance of FRP reinforced concrete beams. Also, the effect of distributing the load over the span length of the beams as opposed to applying the load as two equal point loads was investigated.

Table 4- 1: Design specifications of beam specimens

Beam ID	Stirrups	No. Samples	Length (mm)	Loading type	Initial prestressing [%]	f'_c [MPa]
PR-1.5-NS*	-	2	1716	Four point bending	53	47
PR-1.5-S	Ø6mm GFRP	2				
PR-2.5-NS	-	2	1994		51	47
PR-2.5-S	Ø6mm GFRP	2				
PR-3.5-NS	-	2	2370		53	48
PR-3.5-S	Ø6mm GFRP	2				
PR-U-NS	-	2	1900	Distributed loading	53	49
PR-U-S	Ø6mm GFRP	2				

* PR refers to prestressed beams; the following numerical values refer to a/d ratio and U refers to distributed loading; S and NS refer to beams with and without stirrups respectively

The load deflection behaviour, crack pattern, angle of cracks, strain in the longitudinal reinforcement and concrete as well as ultimate load capacity of each specimen were studied. The plain concrete contribution to shear resistance was analysed using results from beams in Series 1. Also, the contribution of the stirrups was studied using beams in Series 2.

4.2 Design of Test Specimens

All the specimens were designed as T-beams with a 150mm wide web and a cross sectional area of 80500 mm^2. The longitudinal reinforcement consisted of four prestressed CFCC cables (Ø12.5 mm) provided in two levels. The beams were designed to have a flexural capacity significantly larger than their shear capacity to ensure shear failure. The end zones of all the beams were reinforced with GFRP stirrups and steel coils around the cables to avoid cracking in the anchorage zones resulting from transfer of prestressing to concrete (Figure 4-1).

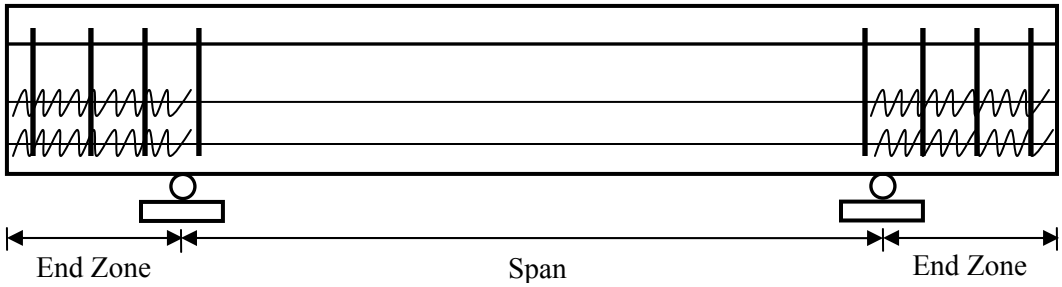

Figure 4- 1: Reinforcement details in the end zones

The steel coils and the stirrups were provided over 300 mm from the ends of the beams to cover the transfer length and confine the high bursting stresses in this zone at the time of transfer of prestressing force to concrete. The beam overhangs were designed to contain the end zone reinforcements. The length of the over hangs was also governed by the development length of the beams. For PR-1.5 beams the overhangs were 50 mm longer than 300 mm provided for other beams to compensate for the very short shear span of these beams.

4.2.1 Design Specifications for Series 1 Beams

Four prestressed CFCC cables (Ø12.5 mm) were provided in the web. The spacing between the cables and the cover were selected to minimise the width of the web as much as possible within the allowable limits specified by the CSA-S6-10 guidelines. Also GFRP grid reinforcement was used in the flange to overcome the tensile stresses in top of the beams from transfer of prestressing and the shrinkage stresses after casting. The grid reinforcement was also used to anchor the GFRP stirrups in the top flange.

For the Series 1 beams no stirrups were provided in the shear spans. The reason for that was to capture the contribution of concrete to the shear resistance of the beams. Figure 4-2 illustrates the cross-section of Series 1 beams.

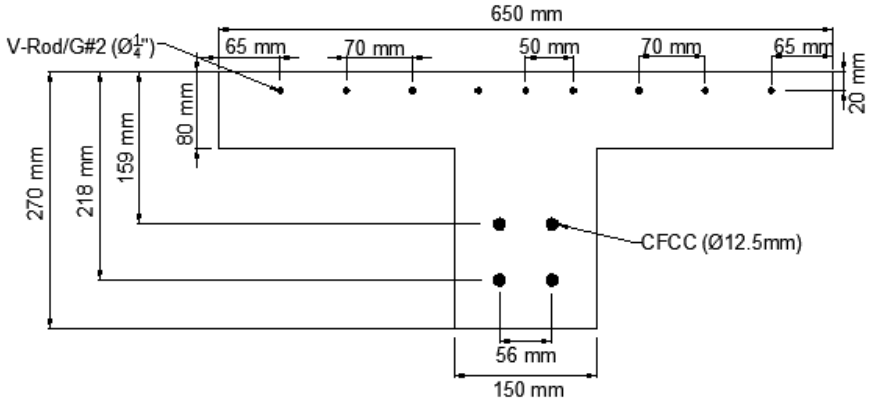

Figure 4- 2: Cross-section of the beam specimens in Series1

A total of eight beams were cast and tested with the Series 1 configuration. The first six beams were tested under four point bending with varying span to depth ratio and the last two were subjected to distributed load. The span to depth ratio for the first three beam groups was varied by changing the length of the shear span as shown in Figure 4-3.

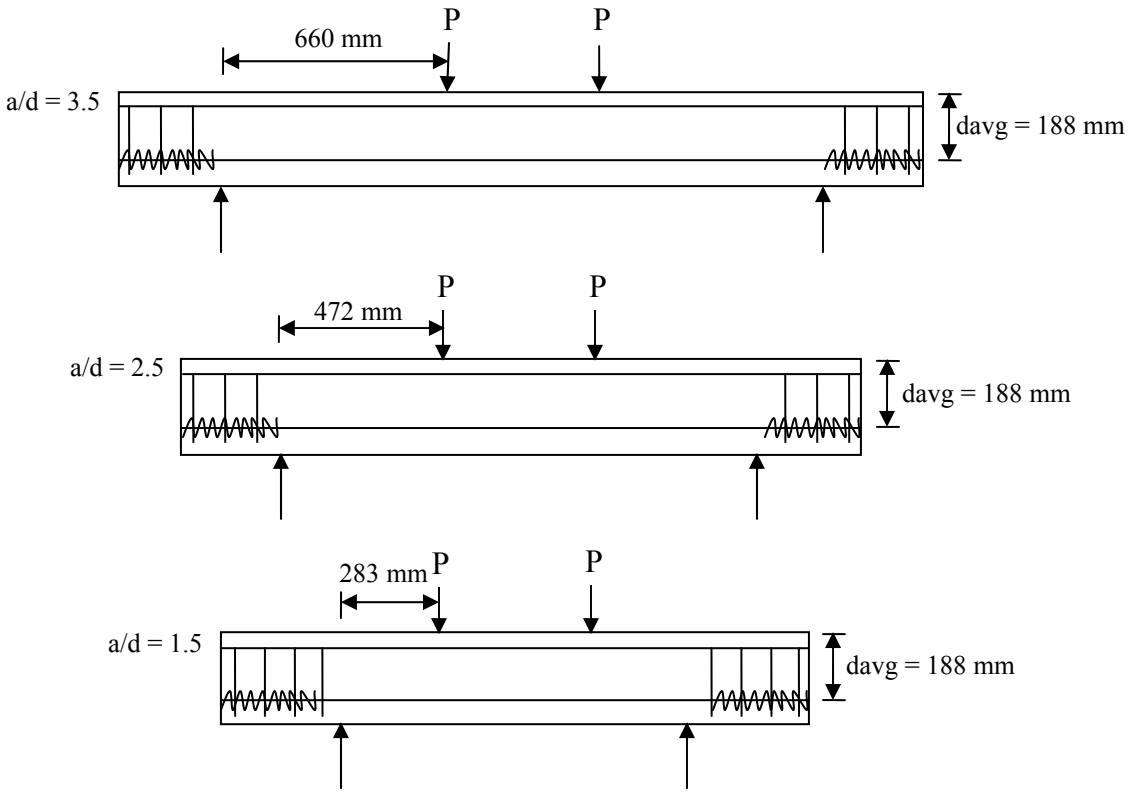

Figure 4- 3: Variation of a/d and reinforcement layout for Series 1 beams

Figure 4-3 also shows the reinforcement layout in Series 1 beams. The end zone reinforcement for Series 1 PR-U beams was the same as for PR-2.5 beams.

4.2.2 Design Specifications for Series 2 Beams

The Series 2 beams differed from Series 1 in the fact that they included stirrups within their shear spans. Figure 4-4 shows a typical cross-section of Series 2 beam.

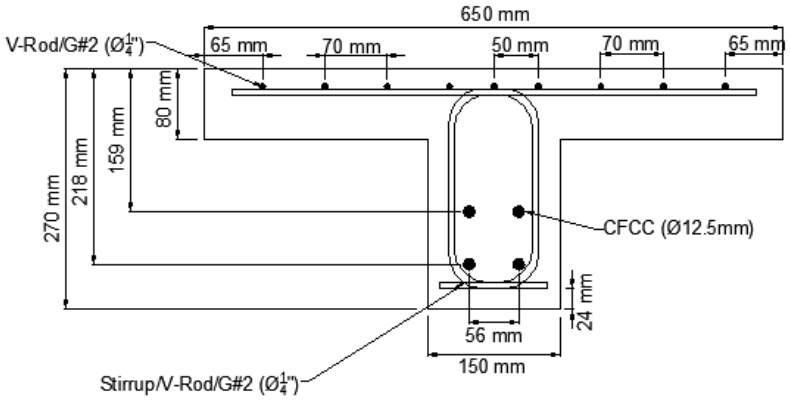

Figure 4- 4: Cross-section of the beam specimens in Series 2

The stirrups wrapped around the CFCC cables and were anchored with zip ties to the grid reinforcement in the flange to make them stiff and make sure they remain vertical at 90^{o} after casting.

The stirrups in the shear span of all the beams tested under four point bending were spaced at 204 mm which is approximately the maximum recommended by CSA-S6-10 (2010) design code. The spacing of the stirrups was reduced to 178 mm for beams tested under distributed load to ensure even spacing of the stirrups along the span. The angle of the stirrups was set at 90 degrees to the horizontal. The end zone reinforcements as well as the tension and flange reinforcements remained the same as for the Series 1 beams. The reinforcement layout for Series 2 beams is shown in Figure 4-5.

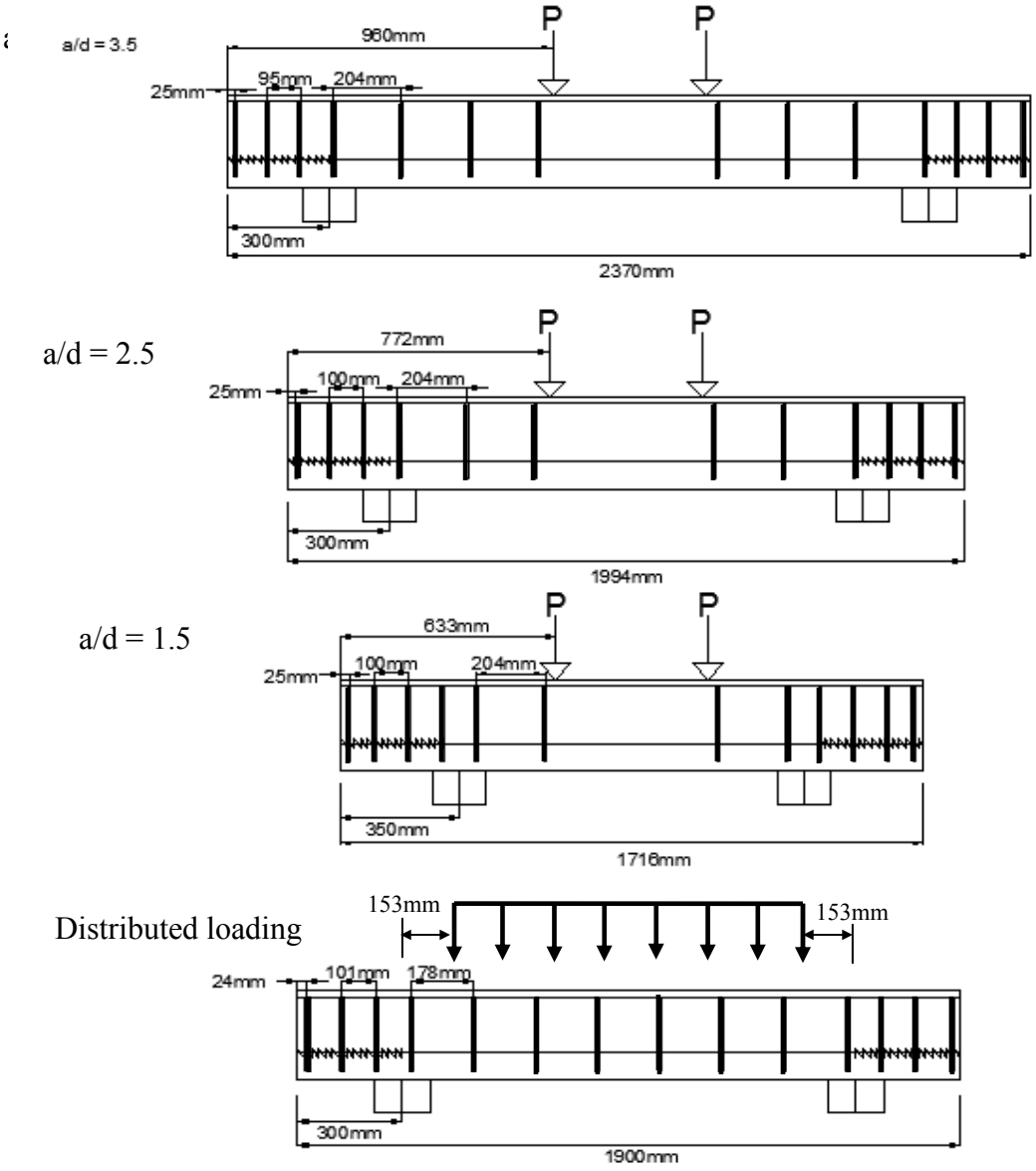

Figure 4- 5: Profile view of the Series 2 beam specimens

4.3 Properties of Longitudinal Reinforcement

CFRP cables (CFCC) manufactured by Tokyo Rope were used as flexural reinforcement for all the beam specimens. Tensile properties of the CFCC cables reported by the manufacturer were verified based on tension tests conducted in the lab.

4.3.1 Properties of Flange Reinforcement

The grid reinforcement in the flange was made from GFRP rebars manufactured by Pultrall under the trade name V-Rod. Longer longitudinal bars were tied to shorter 584 mm rebars and the stirrups. The longitudinal bars were cut to the span length of the beams minus 10 mm cover on each side from the end of the formwork. The reinforcement that was used in the flange had the same properties as the rebars that were bent to make the stirrups. Properties of longitudinal and transverse reinforcement are listed in Table 4-2.

Table 4- 2: Properties of longitudinal and transverse reinforcements

Reinforcement	Material	Type	Diameter [mm]	Cross-section [mm^2]	f_{pu} [MPa]	E_p [GPa]
Flexural	CFRP	cables	12.5	76	2100	136
Grid/stirrups	GFRP	rebars	6	31.67	827	40.8

4.4 Properties of Transverse Reinforcement

Two legged stirrups were used to confine the end zones of all the beams as well as reinforce the shear span of the Series 2 beams. Size 6 mm stirrups were custom made by Pultrall with a bend radius of 38 mm. In designing the bend radius of the stirrups, requirements of the CSA-S6-10 code regarding minimum bend radius of FRP bars were considered as well as the manufacturer's capabilities. The bend radius for FRP bars is usually determined based on four times the bar diameter. However, in case of the No.2 bars that were used in this project, the manufacturer could only bend the bars to a radius that corresponded to No.3 bars. Figure 4-7 illustrates a sketch of the stirrups showing all the dimensions.

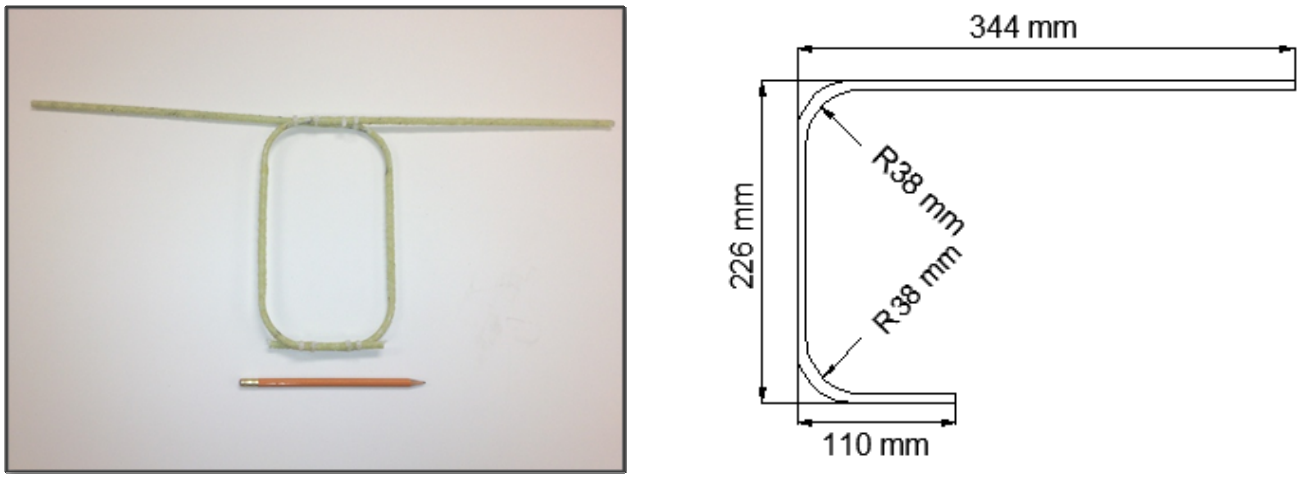

Figure 4- 6: GFRP stirrups specifications

4.5 Reinforcing Coils for the End Zones

Steel coils were placed around each stand in the end zones of the beams. Details of the reinforcing coil can be seen in Figure 4-8. The purpose of the coils was to confine the bursting stresses when the prestressing force in the cables was transferred to the concrete. The coils were manufactured by Western Spring and Wire in Winnipeg and were 280 mm long with a 20 mm diameter pitch. Steel coils were used because of smaller diameter and pitch that was possible with steel compared to FRP.

Figure 4- 7: End zone reinforcing coils specifications

4.5.1 Tension Tests on CFCC Cables

Five CFCC cable specimens (Ø12.5 mm) were tested in tension to verify their ultimate capacity and elastic modulus. The length of the specimens as well as their anchorage mechanism was designed according to CSA-S806-12 Annex B (2012). Each specimen was cut to 1500 mm

length and 500 mm steel pipes were casted on each end of the cables using expansive grout. All specimens were tested in a 1000 kN MTS machine. The dimensions of the steel anchors as well as the test setup are shown in Figure 4-6.

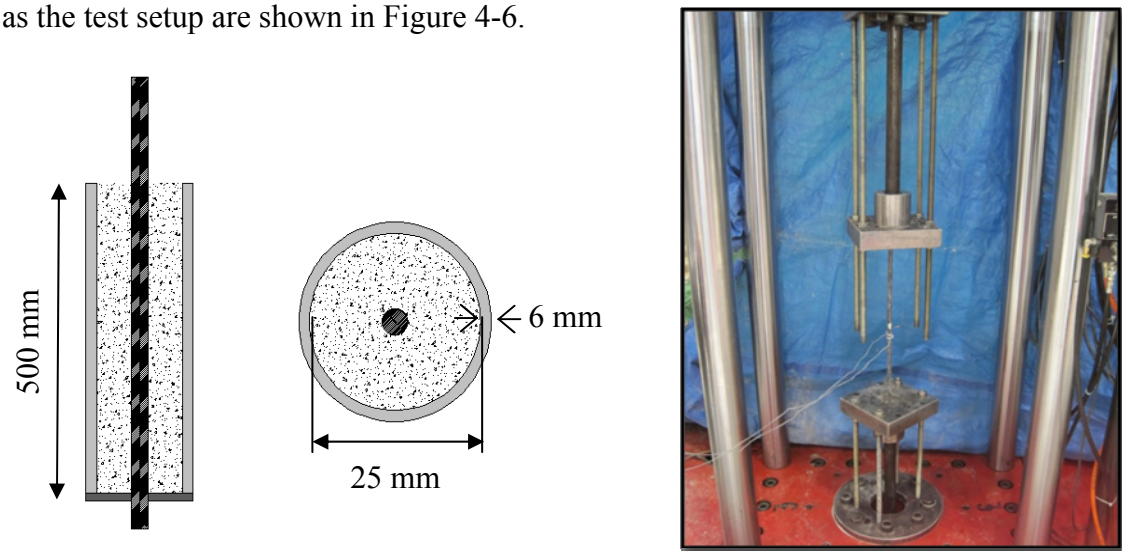

Figure 4- 8: Tension test specifications and test setup

4.6 Concrete

The concrete for all the beams was ordered from Lafarge in Winnipeg and was designed for 30 MPa strength at release and approximately 46 MPa at the time of testing. Normal Portland cement was used with half inch aggregates. A total of 45 small concrete cylinders (102 mm diameter and 202 mm high) were casted with every set of beams. Cylinders were tested in compression after 3 days and then every 7 days until testing to monitor the strength of the concrete. Also, splitting tensile test was conducted before releasing the stress and testing the beams.

The modulus of elasticity of the concrete was also obtained by using a special jig with mounted dial gauge that could measure displacement to 0.00254 mm. Displacement measurements were taken at 22 kN intervals over the elastic range of concrete. The results were plotted in form of load- strain and the slope was measured as the elastic modulus of concrete (Figure 4-9).

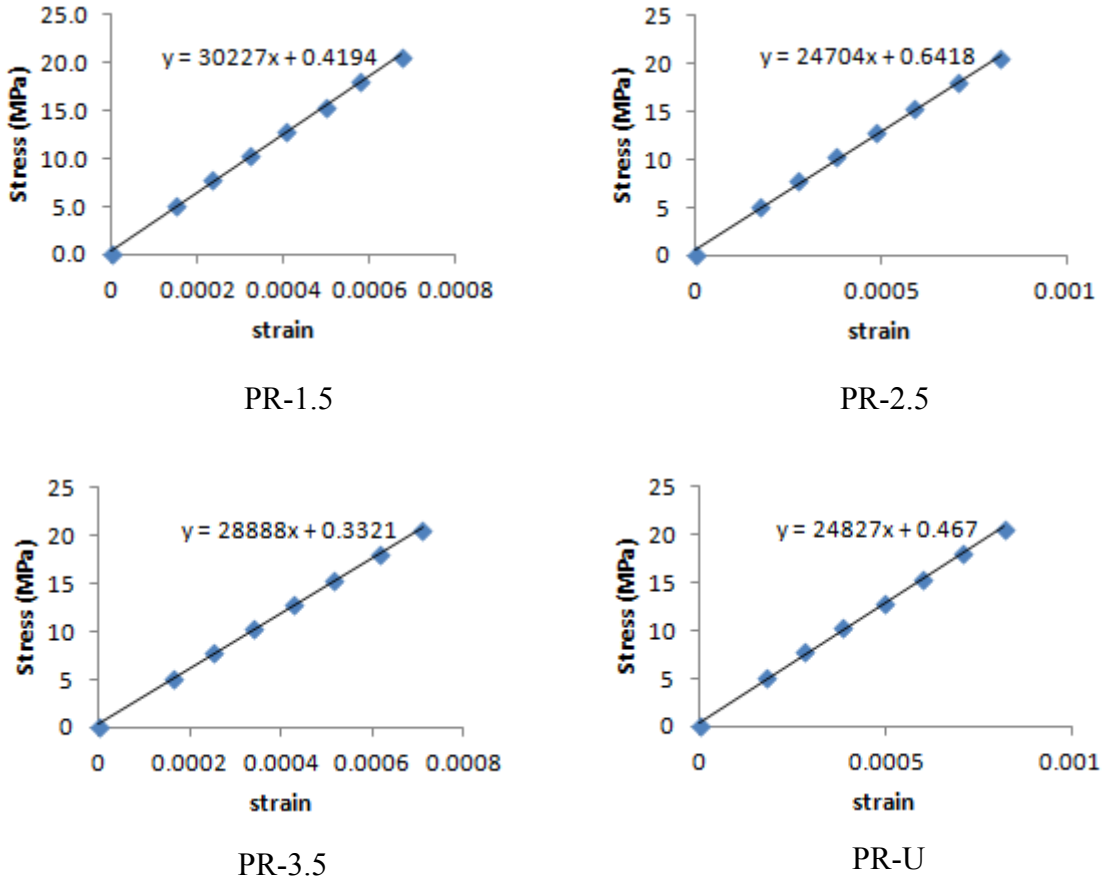

Figure 4- 9: Calculation of Ec from experiment

4.7 Fabrication of the Beams

The formwork was designed to fit the shape and size of the beams. Four forms were fabricated to allow for casting four beams at a time, two beams from Series 1 and two from Series 2 (Figure 4-10). The form was built out of plywood with adjustable end pieces to accommodate different length beams and was supported underneath with 38 mm steel struts. Small bolts were welded inside the struts to hold threaded rods that were bolted down to the concrete floor. The threaded rods were used to adjust the height of the formwork to match the bulkheads and ensure the CFRP cables are levelled and at the right height in the beams.

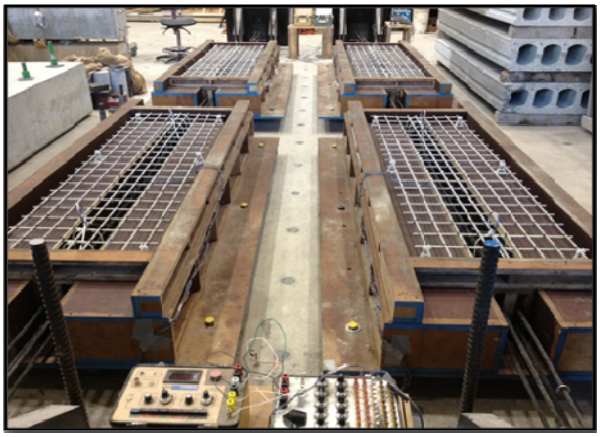

Figure 4- 10: Formwork for casting the beams

4.8 Prestressing the CFCC Cables

The steel bulkheads were stressed down to the concrete floor using high strength dywidag bars to prevent slipping of the bulkheads under the prestressing load. The strands were stressed individually using a hydraulic jack. Due to the weakness of FRP in transverse direction, it is not possible to directly grip the bars during prestressing as it is done with steel bars, unless a special gripping system is used. No such system was found for CFCC cables and therefore, it was decided to follow common practice and pull the CFCC cables using steel strands that connected with FRP through couplers.

A new coupler system was designed for this project that could work with the close spacing between the strands and had enough capacity to sustain the prestressing load. The same anchors that were used for the tension tests were incorporated in the coupler system. Figure 4-11 illustrates the couplers that were used in this research.

An anchor was cast on each end of the CFCC cables; while for steel strands only one end was casted. On the dead end the CFCC cables passed through the bulkheads and the anchors on their ends rested against the back plate of the bulkheads.

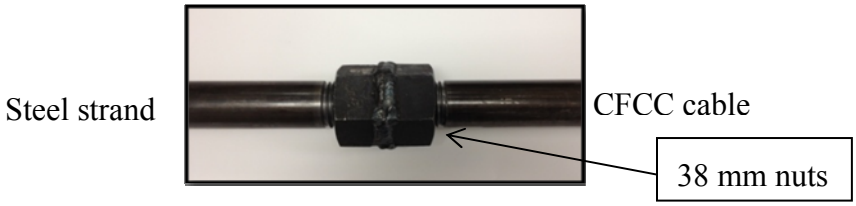

Figure 4- 11: Coupler used for prestressing the CFCC cables

On the live end, the anchors on CFCC cables were threaded and connected to anchors on steel strands with two nuts that were welded together (Figure 4-11). The anchors twisted in to the nuts and connected the steel with FRP but not all the way to allow them to turn freely if necessary when the strands are pulled to avoid rupture of the CFCC cables.

The coupler system was tested under tension and was able to sustain a load 50% beyond the required prestressing load without the steel yielding or the welds on the nuts breaking off. The test was done in a 300 kN INSTRON machine and the strain in the steel anchors was monitored using a strain gauge to make sure the anchors did not yield. The result from the tension test on the couplers is shown in Figure 4-12.

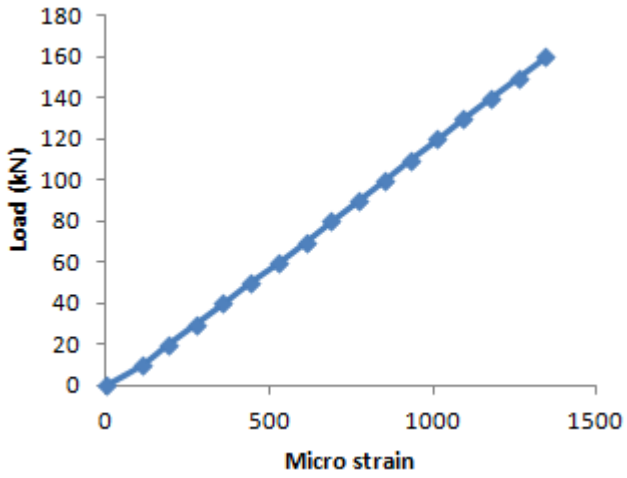

Figure 4- 12: Results from tension test on the couplers

4.8.1 Prestressing Process

A schematic of the prestressing setup is shown in Figure 4-13. The couplers were staggered as the figure shows to allow for the close spacing between the cables. The steel strand passed through the bulkhead on the live end and was gripped using steel chucks.

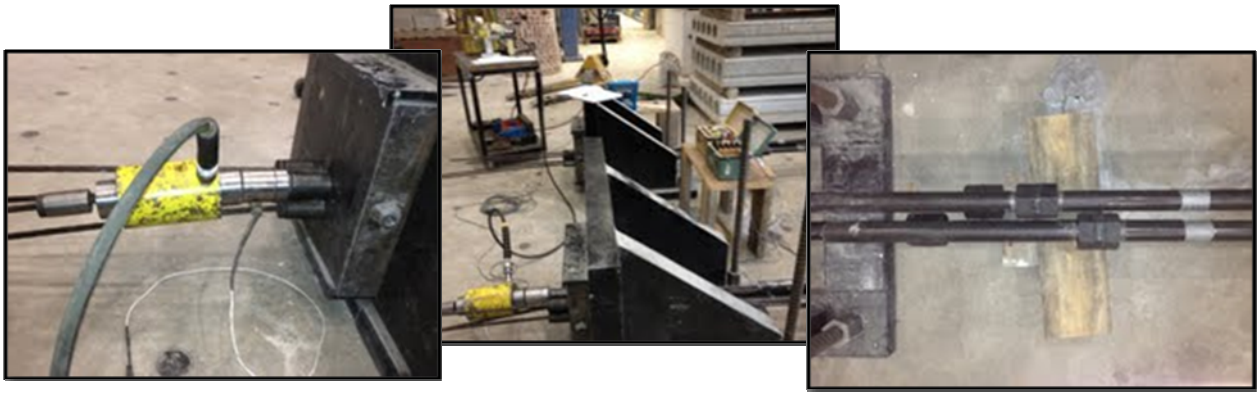

Figure 4- 13: Prestressing setup on the live end

A load cell was placed right behind the steel chuck to measure the load during stressing and the strands were pulled using a hydraulic jack with 60 kips (267 kN) capacity. The strain in the FRP cables was monitored by an extensometer that was placed on each cable between the form-works as well as strain gauges on the cables. Two strain gauges were placed on each cable (one for each beam) which made a total of four strain gauges per beam. The strain gauges were placed so that they would be in the mid-span of the beams after the cables were prestressed. After the jack was released, the ultimate elongation of the cables was measured against a pre-specified mark. The measurement was used to check the available stress in the cables after the losses from releasing the jack.

4.8.2 Releasing the Stress

The stress in the CFRP cables was released by cutting the steel strands on the live end one by one starting with the two strands in the bottom. A blow torch was used to cut the steel strands. The FRP in between the formwork as well as the FRP anchored in to the bulkheads on the dead end was cut using a diamond grinder. It should be noted that all the end and side pieces of the formwork were removed prior to releasing the stress to allow for the beams to shorten as a result

of the stress transferring into the concrete. Figure 4-14 shows the cutting of the steel strands to release the stress using a flame cutter.

Figure 4- 14: Releasing the prestressing force

4.9 Instrumentation of the Specimens

Different instruments were used to monitor strains and loads in the specimens during preliminary tests, prestressing and testing the beams. These instruments included strain-gauges, Pi-gauges, extensometers, LVDTs and load cells. It should be noted that demec points were also used initially in addition to Pi-gauges for beams with a/d = 2.5. However, due to the shorter depth of the web, it proved difficult to capture accurate readings. Also, due to brittle nature of the failure in these beams, it was not feasible to take readings all the way to failure for safety reasons. Therefore, the demec points were not used for any other specimens.

4.9.1 Electrical Strain Gauges

Strain gauges were installed on longitudinal reinforcements as well as in the middle of the flange for beams tested under distributed load. Strain gauges with 2 mm gauge length were placed on the longitudinal reinforcements at a location that would correspond to mid-span of the beams after the cables were prestressed. The strain gauges had a resistance of 120 ohms and were manufactured by Tokyo Sokki Kenkyujo CO., Ltd, Japan. The strain gauges were used to monitor jacking stress during prestressing, subsequent stress losses and the strain in the cables during the test.

To install the strain gauges, the coating on top of the fibres was first removed to expose the longitudinal fibres at the location where the strain gauges were to be installed. The protective

layer was removed using a sharp blade and the surface was carefully evened using sand paper and was cleaned using methanol. Next, the bond-side was wetted with Catalyst-C and few drops of M-Bond 200 adhesive. The gauges were then placed on the reinforcement using a tape, uniform pressure was applied for at least 3 minutes and the tape was slowly peeled back. Later, the gauges and the exposed wires were coated with M-Coat B Nitrite Rubber Coating and covered with Teflon tape. The gauges were also covered with butyl rubber and wrapped using linerless rubber splicing tape for extra protection.

The concrete strain gauges placed on the flange of beams tested under distributed load, had a gauge length of 50 mm. The gauge length was in excess of double the size of the aggregate used in the concrete mix which is a standard for choosing the length of concrete gauges. Before installing the concrete gauge, the surface of the concrete was ground over the specified gauge length until the surface was smooth. The surface was then cleaned and all the voids were filled with epoxy before placing the gauge.

Strain gauges were also installed at the mid-height of the stirrups within the shear span of beams tested under four point bending and throughout the span for beams subjected to distributed load. However, the results obtained from these strain gauges were not consistent and large gaps existed in the data due to malfunction of the strain gauge channels that the stirrups were hooked up to. Also, the readings from the strain gauges can only be meaningful if the strain gauge is placed in a location that it would be hit by all the diagonal cracks that cross the stirrup which is difficult to do.

4.9.2 Linear Variable Displacement Transducers (LVDTs)

Small range high accuracy LVDTs were modified to measure crack width and were installed in vertical direction within the shear spans as part of rosette stations that also included diagonal and longitudinal Pi-gauges (Figure 4-15). The measurement from the LVDTs was later converted to strain by dividing the measured value by the gauge length of the LVDTs. To use the LVDTs for measuring crack width, a small threaded shaft was attached to the top of the LVDTs. As the shear cracks widened in transverse direction, the LVDT measured the deformation as the shaft extended out. The LVDTs were held on the web over 100 mm gauge length, using a small aluminium jig that was attached to the web using epoxy.

Figure 4- 15: Small LVDT in a rosette station within the shear span

Figure 4-17 and 4-19 show the instrumentation setup on top of the flange. Three LVDTs were used on all the beams to monitor mid-span as well as quarter-span deflections. For PR-2.5 and PR-3.5 beams the shear spans were long enough to place the LVDTs on top of the flange. However, for the other beams due to limited space, the LVDTs were placed underneath the flange at the same location as for beams with a/d = 2.5, 3.5. The LVDTs were placed 150 mm from the edge of the flange.

4.9.3 Electrical Pi-Gauges

Pi-gauges with gauge length of 100 mm and 200 mm were used to measure strain in the concrete at several locations on the beam. Figure 4-16 and 4-18 show typical instrumentation setup on the web of the beam specimens during testing. For PR-2.5 and PR-3.5 beams the rosette stations placed in the shear spans consisted of Pi-gauges in longitudinal and diagonal direction plus a small range high accuracy LVDT in vertical direction. For PR-U beams, the rosette stations consisted of Pi-gauges in all three directions. The rosette stations were placed so that they would be approximately centred on a stirrup within the shear span that was most likely to capture all the diagonal cracks.

For PR-1.5 beams; due to very short shear span, only diagonal Pi-gauges were used at the location of the stirrup near the support. The rosette stations were not possible since the longitudinal gauge would either extend passed the support or in the constant bending region

depending on where the rosette station was placed. The ideal location for the diagonal gauge was close to the support where it would best capture the diagonal cracks extending from the load points to the supports. Therefore, the diagonal Pi-gauge was placed at 75 mm from the centreline of the supports which corresponded to the first stirrup from the support.

For beams NS2 and S2 tested with a/d = 2.5, the rosette stations were placed at 230 mm from centre line of the supports which corresponded to the stirrup in the middle of the shear span. For beams tested with a/d = 3.5, the rosette stations were placed at 420 mm from the centre line of the supports which corresponded to the second stirrup from the load point. For PR-U beams the centre of the rosette station was at 40 mm offset from the third stirrup from the centre line of the supports. The rosette stations were placed at the same distance from the support as for PR-3.5 beams. The purpose of that was to see how the strains in the concrete will change when the load is distributed as opposed to point loads.

As it can be seen in Figure 4-17 and 4-19, a 100 mm Pi-gauge was used at the centre of the flange to measure compressive strain in all the beams tested under four point bending. Another two Pi-gauges with 200 mm gauge length were used at mid-span of the web in all the beam specimens to record strains in the constant moment zone. These two Pi-gauges were placed at 54 and 100 mm vertical distance from the extreme tension fibre. The Pi-gauge at 54 mm height was placed at the same level as the bottom reinforcement layer.

4.9.4 Data Acquisition and Monitoring

The strain in the strain gauges mounted on the strands and extensometer as well as the load cell that measured the jacking load, were monitored using a strain indicator box during prestressing. The same indicator box was used to monitor prestressing losses until testing. During the test, all the instrumentation was hooked up to a data acquisition system to store and view the data. Results from the mid-span and quarter-span LVDTs, the diagonal Pi-gauges, strain gauges on longitudinal reinforcements and the top Pi-gauge were plotted during the test to monitor the performance of the instruments.

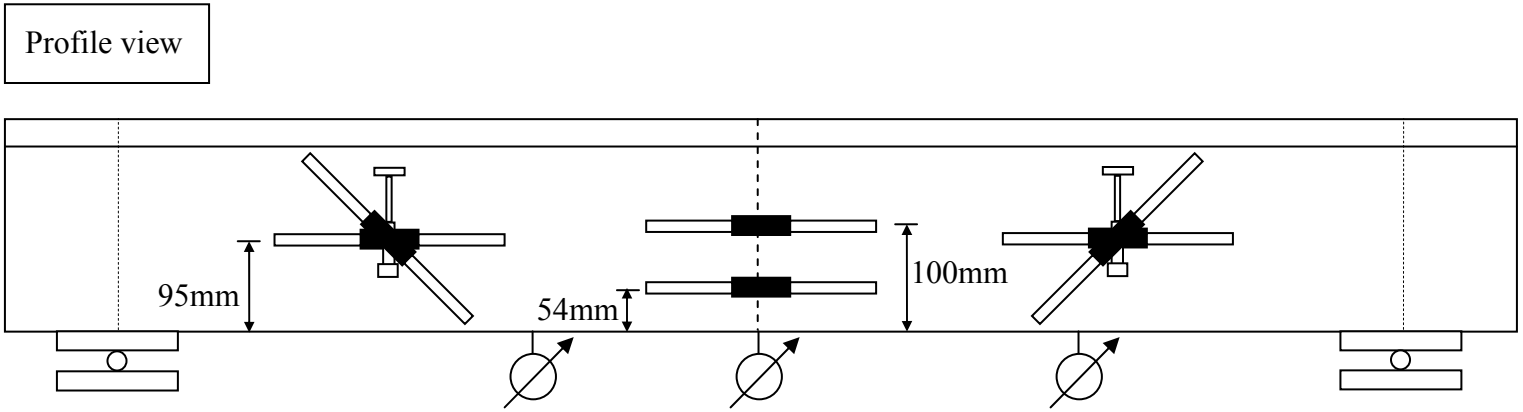

Figure 4- 16: Instrumentation setup on the web for (PR-2.5, 3.5, U)

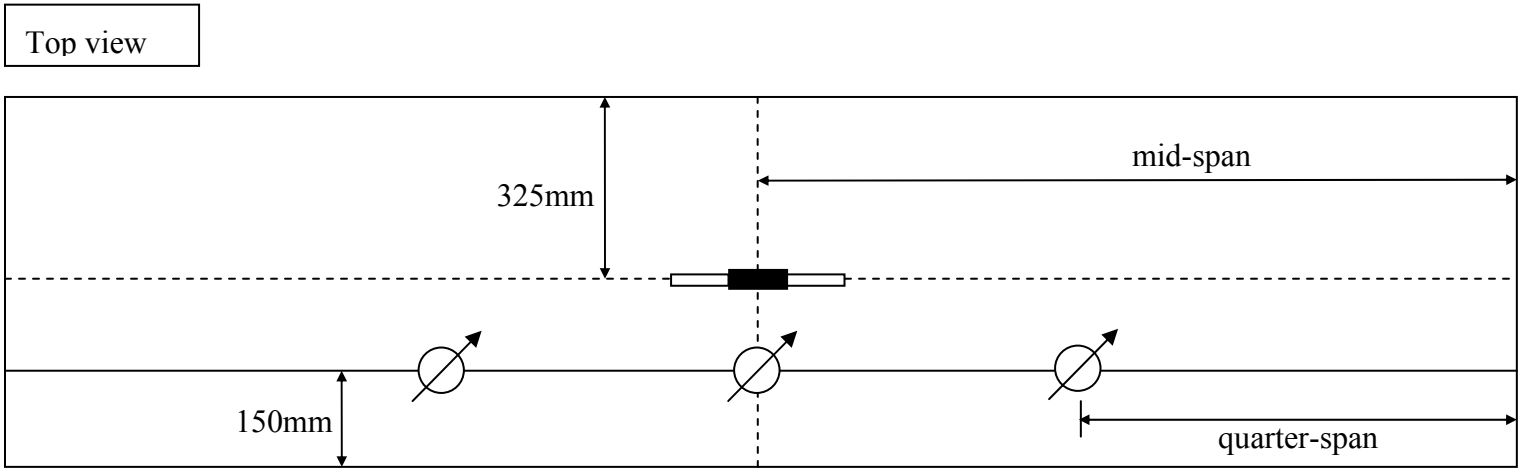

Figure 4- 17: Instrumentation setup on the flange (PR-2.5, 3.5)

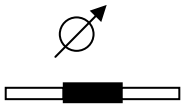

LVDT

PI-Gauge

Profile view

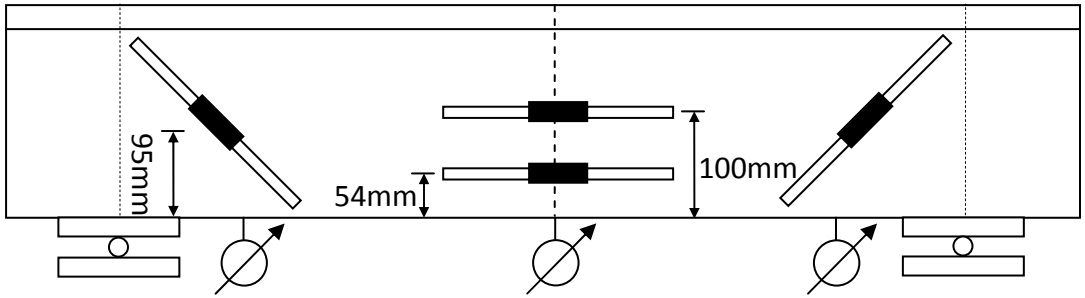

Figure 4- 18: Instrumentation setup on the web (PR-1.5)

Top view

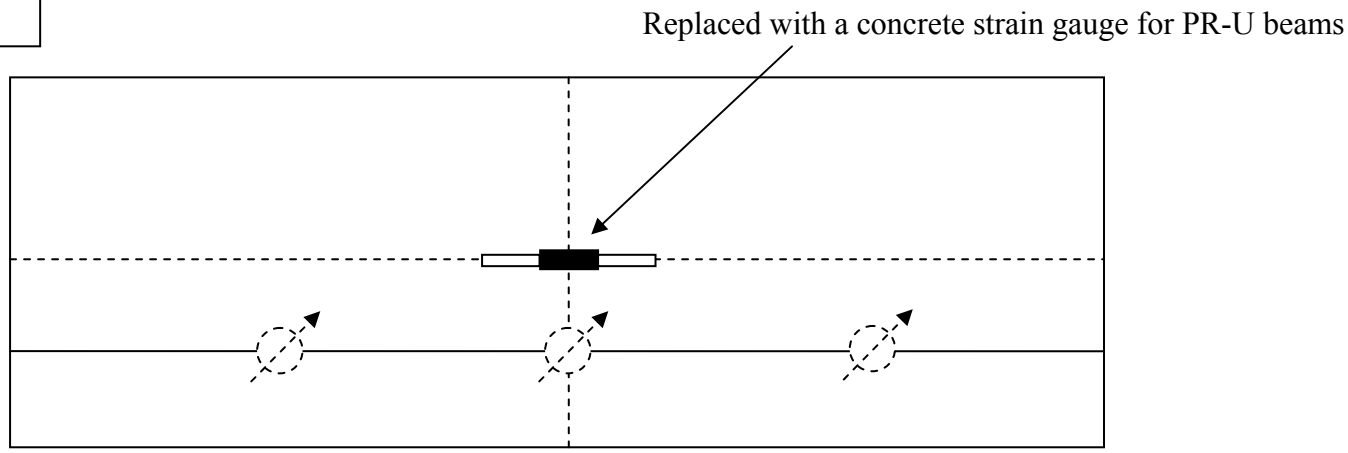

Figure 4- 19: Instrumentation setup on the flange (PR-1.5, U)

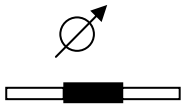

LVDT

PI-Gauge

4.10 Test Setup

All beam specimens were simply supported on steel rollers welded to heavy concrete blocks that had a steel cover on top. The roller support consisted of two steel plates with a steel roller in between that allowed the top plate to pivot from side to side. Twelve beams were tested under four point bending arrangement and four beams were subjected to distributed load.

4.10.1 Test Setup for Beams with Variable a/d ratio

All the beams were tested in a 1000 kN MTS machine under stroke control. The load was applied by the actuator through a spreader beam with two load points. Figure 4-20 illustrates the test setup. The two smaller spreader beams extended over the width of the flange and were connected to the larger spreader beam through a hinged connection to allow them to pivot freely. The smaller spreader beams that applied load to the beams were spaced exactly at 450 mm centre to centre and were spaced equally apart from the centre of the beams. Three inch wide rubber pads were placed under the spreader beams. All specimens were properly aligned with respect to the centre of the MTS machine.

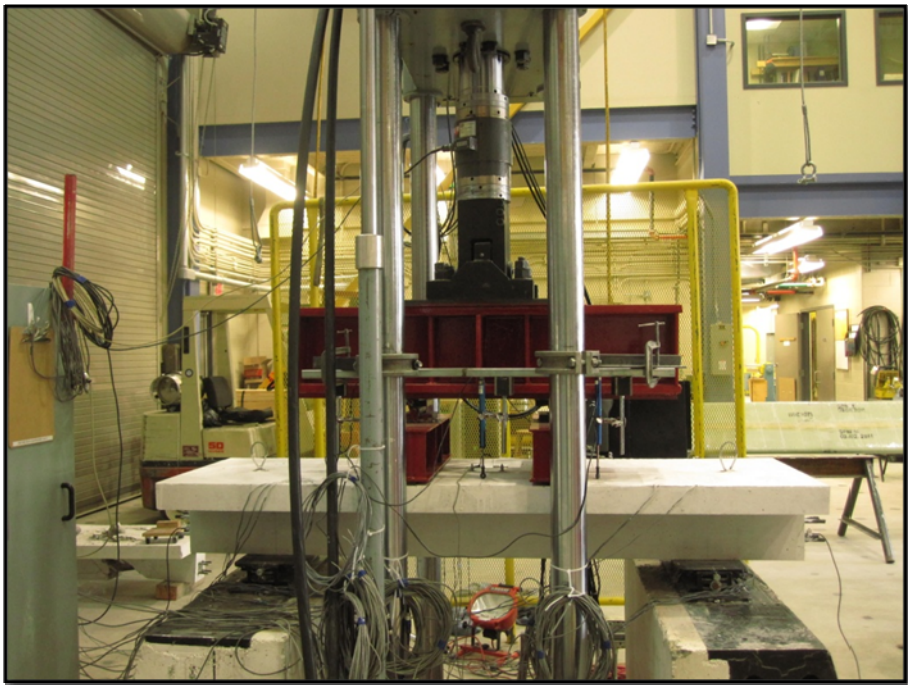

Figure 4- 20: Test setup for beams subjected to four point bending

4.10.2 Test Setup for Beams Tested Under Distributed Load

The beam specimens tested under distributed load were 1900 mm long with a span of 1300 mm as shown in Figure 4-5. Two 55 ton actuators with 156 mm stroke were used to apply load to the beams. Each actuator loaded half the beams on each side of the mid-span. This loading arrangement allowed more freedom for the spreader beams to maintain contact with the beam as it deflected during testing. Rubber pads were placed underneath the 8 spreader beams that pushed down on the beams. The load setup was fabricated in the structures lab and a load frame was set up to hold the actuators in place.

The actuators were manually operated using hydraulic pumps and a load cell encased in a custom made jig that was held in place under each actuator to monitor the load during testing. Figure 4-21 illustrates the test setup for beams that were subjected to distributed load. The connection between each layer of spreader beams was designed to be interchangeable between hinged and roller connections. Each top spreader beam was connected to two smaller middle beams, one with roller and one with hinged connection to provide the setup with flexibility to have movement without de-stabilising the top spreader beams.

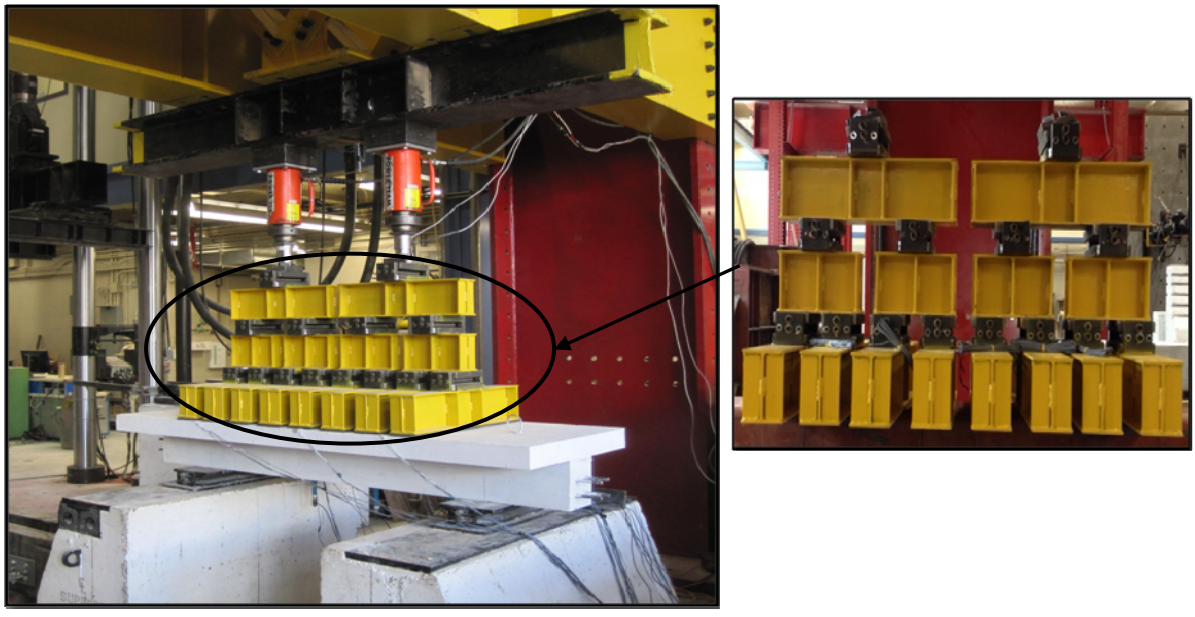

Figure 4- 21: Test setup for beams tested under distributed load

An experiment was conducted using the test setup on a steel HSS section to make sure the eight steel I-beams loading the beam received equal share of the load. Strain gauges with 6 mm gauge

length were installed on the extreme top and bottom of the HSS section at mid-span to record the tensile and compressive strains during the test. The height of the HSS section was 254 mm which was about the same height as the concrete beam specimens. Each actuator was used to apply a load of around 200 kN. Later, theoretical strains at the same locations were estimated for the given load arrangement assuming equal load distribution between the eight spreader beams and the results were compared. The experimental and theoretical results matched perfectly as shown in Figure 4-22 which proves the setup allowed equal load distribution between the bottom spreader beams. The results are plotted on the same graph for each actuator and compared to the theoretical values. The letters N and S in brackets within the legend refer to north and south actuators. The test was repeated twice for accuracy and the same results were obtained each time.

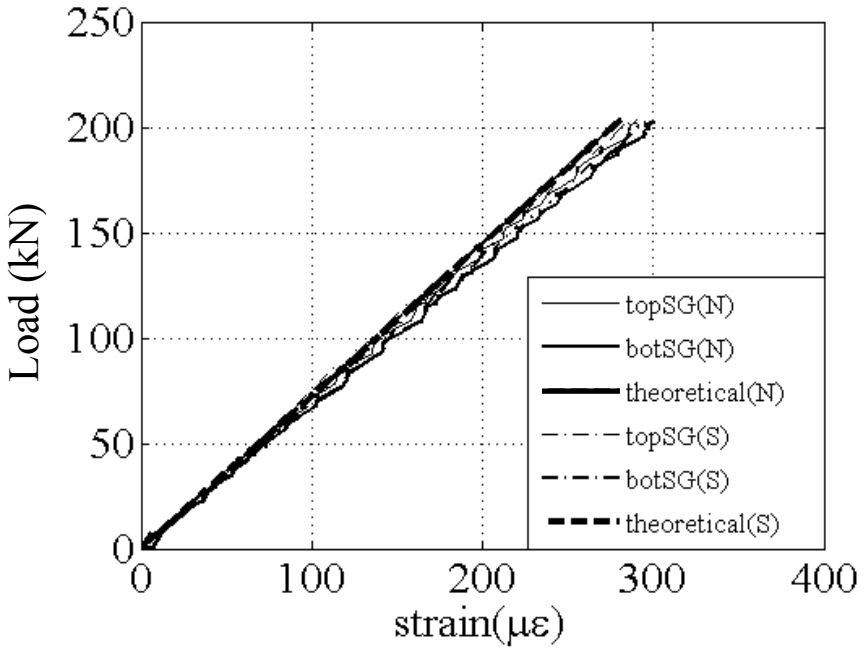

Figure 4- 22: Results from testing the HSS under distributed load

4.11 Preparations for Testing

All the beams received a wash of white paint before testing to better identify cracks on the beams. The calibration of all instruments was checked before each test to make sure everything was working properly. The beams were marked to illustrate the location of all the instruments. After the beams were aligned in the test machines, the screws for Pi-gauges were glued on to the beams using five minutes epoxy. A steel bar clamped to the columns on the MTS machine held

the LVTDs in place at mid-span and quarter-spans for beams with a/d ratios of 2.5 and 3.5. For beams tested under distributed load or a/d = 1.5 arrangement, the LVDTs measured deflection from underneath the flanges and were held in place using a steel bar welded to the concrete blocks.

4.12 Testing

All the beams with variable a/d ratio were tested under stroke control mode at a rate of 1mm/min. The load rate was reduced to 0.5 mm/min after the appearance of the first flexural crack at mid-span. The beams were loaded in increments to allow for marking the cracks on the beams at each load stage. The loads corresponding to first flexural crack and shear diagonal crack were recorded.

For the case of beams tested under distributed load, the load was applied manually using two hydraulic pumps each connected to one of the hydraulic jacks. The loading was stopped at 25 kN increments to inspect the beam and mark the cracks. One technician was in charge of both pumps for consistency. The load was kept at the same level between the two hydraulic jacks and verified by the quarter-span deflection curves that were monitored during testing.

4.13 Summary

Details of the experimental program that was carried out at the University of Manitoba as part of this study were outlined in this chapter. Twelve beams were tested under four point bending with a/d = 1.5, 2.5, 3.5 and four beams were tested under distributed load. In each beam group, two beams were reinforced with approximately the minimum required GFRP stirrups according to CSA-S6-10 (2010) to study the effect of the stirrups on shear behaviour of the beams. The fabrication process, prestressing method, instrumentation and the design of test setups were outlined.

5. Experimental Data and Results

5.1 General

All the experimental data and observations from the tests conducted during the course of this project are presented in this chapter. These include results relating to material properties of reinforcements and concrete as well as the behaviour and deformation characteristics of the beams.

The behaviour of different beam groups is compared and the effect of a/d ratio is discussed and the role of the stirrups in enhancing the shear resistance of the beams in each group is analysed. Also, the effect of distributed load on the behaviour of the beams compared to four point bending is evaluated.

The following section outlines the results from the tension tests conducted on CFCC cables as well as the properties of concrete used to build the beams.

5.1.1 Properties of CFCC Cables

Five tension specimens were tested. Details of the tension specimen's design and test procedure are outlined in section 4.5.1. Results of the tests including strength and modulus of elasticity of the CFCC cables are provided in Table 5-1.

Table 5- 1: Results from tension tests on CFCC cables

Specimens	Bar 1	Bar 2	Bar 3	Bar 4	Bar 5	average	Manufacturer's report
F_{pu} [kN]	161	160	162	155	140	155.6	161
f_{pu} [MPa]	2118	2105	2132	2039	1842	2047.2	2118
E_f [GPa]	132	134	139	138	135	135.6	137

In all the specimens the failure occurred by rupture of the CFCC cables as they unwound close to the middle and away from the anchors. The results from the tests were consistent except for Bar 5 that had a sudden premature failure and therefore was discarded. The average values of strength and modulus of elasticity of the first four specimens were used for design purpose. These include strength of 2047 MPa and a modulus of elasticity of 136 GPa.

5.1.2 Concrete Properties

The concrete strength was specified as 46 MPa after 28 days with 100 mm slump and half inch aggregates. Table 5- 2 shows the concrete properties for each set of beams that were tested including compressive strength, tensile strength and elastic modulus at transfer and testing. The modulus of elasticity of the beams was determined from experiment and also obtained from theory as specified in the CPCI design manual (2007). The tensile strength of concrete was determined from splitting tensile test and theoretically according to CSA-A23.3 (2004). The inconsistencies between theoretical and experimental E_c are due to difficulty in manually maintaining a consistent load rate between tests. In all the relevant calculations, using f_r from experiment or theory did not make a significant difference.

Table 5- 2: Concrete properties for the beam specimens

Beam Groups	Loading Type	f'_c [MPa]		f_r [MPa]		E_c [MPa]	
		f'_{ci}	f'_c	f_{rexp}	$f_{rtheory}$	E_{cexp}	$E_{ctheory}$
PR-1.5	four point bending (a/d = 1.5)	33	47	3.34	4.1	30227	31470
PR-2.5	four point bending (a/d = 2.5)	39	47	3.6	4.1	24704	31470
PR-3.5	four point bending (a/d = 3.5)	31	48	3.2	4.1	28888	31725
PR-U	distributed	32	49	3.14	4.2	24827	31978

5.2 Prestressing Load in the Beams

As shown in Table 5-3, the PR-2.5 beams were initially prestressed to 51% of the tensile capacity of the CFCC cables and after losses showed an effective prestressing of 245 kN which was 39.3% of the tensile capacity of the cables. In order to better compensate for the prestressing losses and maintain effective prestressing equal to 40% of the tensile strength of the bars, the initial prestressing load was increased by 2% for all the other beam groups. The average prestressing loss for all the samples was 22% of the initial jacking force (Table 5-3).

Table 5- 3: Prestressing loads in the beams

Beam Groups	F_{pi} [kN]	$\%F_{pu}$	F_{pe} [kN]	Loss [%]
PR-2.5	320	51	245	23.4
PR-3.5	330	53	267	19
PR-1.5	330	53	255	22.7
PR-U	330	53	255	22.7

As mentioned in Chapter 4, the anchorage zones of all the beams were reinforced with GFRP stirrups and steel coils to prevent splitting cracks resulting from bursting stresses in the transfer region. This reinforcing technique proved successful as these cracks were not visible on the surface of concrete except for few cases that splitting cracks were visible around individual cables at the end of the beams(Figure 5- 1). The occurrence of these cracks could be due to the steel coil around a particular cable moving away from the end of the beams during casting and not confining the critical stress region at transfer.

Figure 5- 1: Bursting cracks around the cables for beam S1-2.5

5.3 Strength and Behaviour of the Beam Specimens under Load

In this section the overall behaviour of the beam specimens along with observations recorded during the test are presented. Table 5- 4 outlines the flexural and diagonal shear cracking loads, ultimate capacity and the failure modes for all the tested samples. The loads in the table refer to the total machine load applied to the beams. The flexural cracking load is the load at which the first flexural crack was noticed in the mid-span of the beams. The diagonal cracking load refers to the load at which the first diagonal shear crack was observed in the web of the beams.

Table 5- 4: Summary of the test results for the beam specimens

Beam ID	$P_{crflexure}$ [kN]	$P_{crshear}$ [kN]	$P_{ultimate}$ [kN]	Mode of failure
PR-3.5 Beams				
NS1-3.5	166	233	298	Diagonal tension
NS2-3.5	162	240	293	Diagonal tension
S1-3.5	156	239	324	Diagonal tension
S2-3.5	158	248	317	Diagonal tension
PR-2.5 Beams				
NS1-2.5	200	284	372	Diagonal tension
NS2-2.5	202	294	364	Diagonal tension
S1-2.5	200	280	406	Diagonal tension
S2-2.5	210	304	397	Diagonal tension
PR-1.5 Beams				
NS1-1.5	316	406	655	Shear compression failure
NS2-1.5	330	422	666	Shear compression failure
S1-1.5	340	420	639	Shear compression failure
S2-1.5	318	396	613	Flexural compression failure
PR-U Beams				
NS1-U	245	400	598	Diagonal tension
NS2-U	225	420	601	Diagonal tension
S1-U	250	400	647	Flexural tension failure
S2-U	225	400	637	Flexural tension failure

5.3.1 Contribution of the Stirrups to Shear Resistance

The Series 2 beams clearly showed a higher capacity compared to Series 1 beams for all the beam groups except for PR-1.5 beams. The increase in the capacity of the beams was not very large due to the fact that approximately minimum amount of stirrups as specified by CSA-S6-10 (2010) were provided.

However, in case of PR-1.5 beams no increase in capacity was observed between Series 1 and Series 2 beams. In fact, S1and S2-1.5 beams showed less capacity compared to NS1 and NS2-1.5 beams. The stirrups did not contribute to the load carrying capacity of these beams as the behaviour of these beams was governed by arch action. The lower capacity of the Series 2 PR-1.5 beams compared to Series 1 is believed to be due to variability in the concrete properties between the beams. The capacity of these beams is governed by the strength and properties of the concrete as they rely on the concrete compressive struts to transfer the load from the load

points to the supports. While the concrete strength was the same among all the specimens in each group, the properties could vary for example due to different compaction or vibration of the concrete.

Another evidence of the stirrups not playing a major role in the shear behaviour of the PR-1.5 beams is the fact that the stirrups did not rupture as it was the case for stirrups in PR-2.5 and PR-3.5 beams. For both Series 2 beams in PR-2.5 group, the stirrup near the support ruptured around the bottom bend. Figure 5- 2 shows failure of the stirrups near the support for these beams. For S1-3.5, two stirrups within the failure region ruptured, one near the load and another near the support. In beam S2-3.5, the stirrup near the load ruptured. Only for beam S1-1.5, the stirrup near the support was slightly damaged but not ruptured even though the beam reached a much higher load compared to PR-2.5 and PR-3.5 beams.

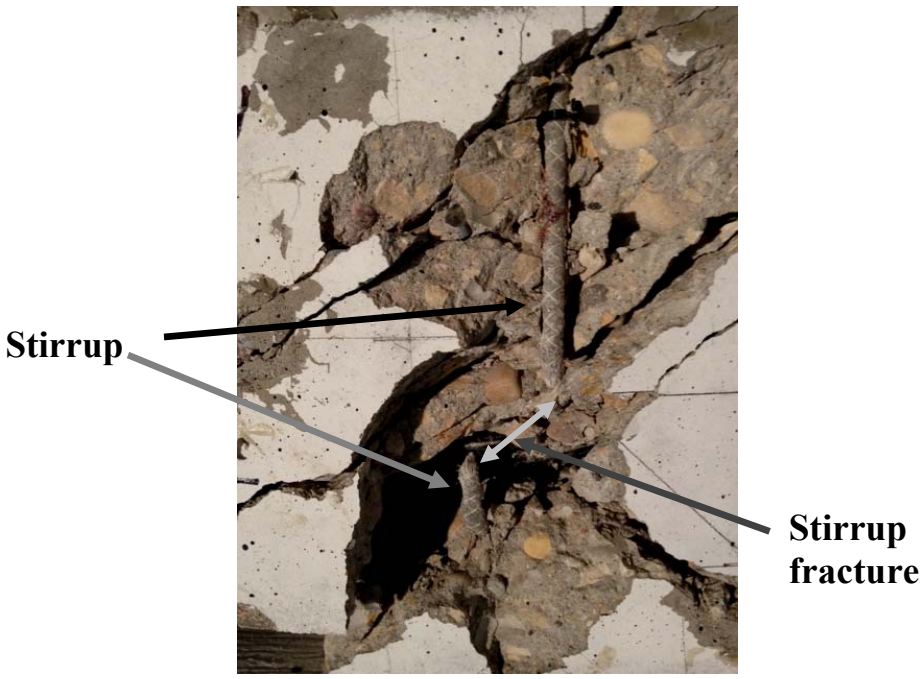

Figure 5- 2: Failed stirrup near the support for beams S2-2.5

Figure 5-3 to Figure 5-6 show the failure profiles of the beam specimens. The crack pattern was similar between Series 1 and Series 2 beams for all the beams that had similar mode of failure including PR-2.5, PR-3.5, and PR-U beams. In case of PR-1.5 beams, S2-1.5 which failed in flexural compression showed more flexural cracks with closer spacing compared to the other beams in its group which can be seen in Figure 5-5. Also, splitting cracks that can be seen in the

mid-span of the S2-1.5 beam are not seen in the other PR-1.5 beams. The effect of these cracks on the failure of these beams is discussed in more detail in Section 5.10.1. For PR-U beams the crack pattern did not change between Series 1 and Series 2 beams, even though the mode of failure changed. The shear capacity of Series 1 PR-U beams was almost as high as the flexural capacity of these beams. S1-U and S2-U beams failed in tension at approximately 40 kN higher load compared to NS1-U and NS2-U beams (Table 5-4). For Series 2 PR-U beams, the shear capacity of the beams exceeded their flexural capacity; therefore the beams failed in flexure before the full strength of the stirrups was utilised. The stirrups in Series 2 PR-U beams did not rupture which is another sign that the full strength of the stirrups was not reached.

5.3.2 Modes of Failure of the Beam Specimens

All the beams experienced shear failure except for S1-U and S2-U beams that failed in flexural tension (Table 5-4). In case of beam S2-1.5, the beam crushed in compression at mid-span which is another common arch failure, also observed by other researchers testing deep beams (Oh et al. 2001, Zararis et al. 2003). For the other PR-1.5 beams, the failure occurred by crushing of the concrete at the load point as the top node of the compressive strut failed. In case of PR-2.5 and PR-3.5 beams, the failure was loud and sudden especially for PR-3.5 beams as the beams failed shortly after diagonal cracking. Series 2 PR-U beams, failed in tension with the two bottom cables rupturing. The Series 1 PR-U beams failed in diagonal shear and did not show rupture of the bottom cables. However, the two top cables were damaged at the failure location due to the brittle nature of the failure. Both the diagonal shear failure and tension failure were loud and brittle.

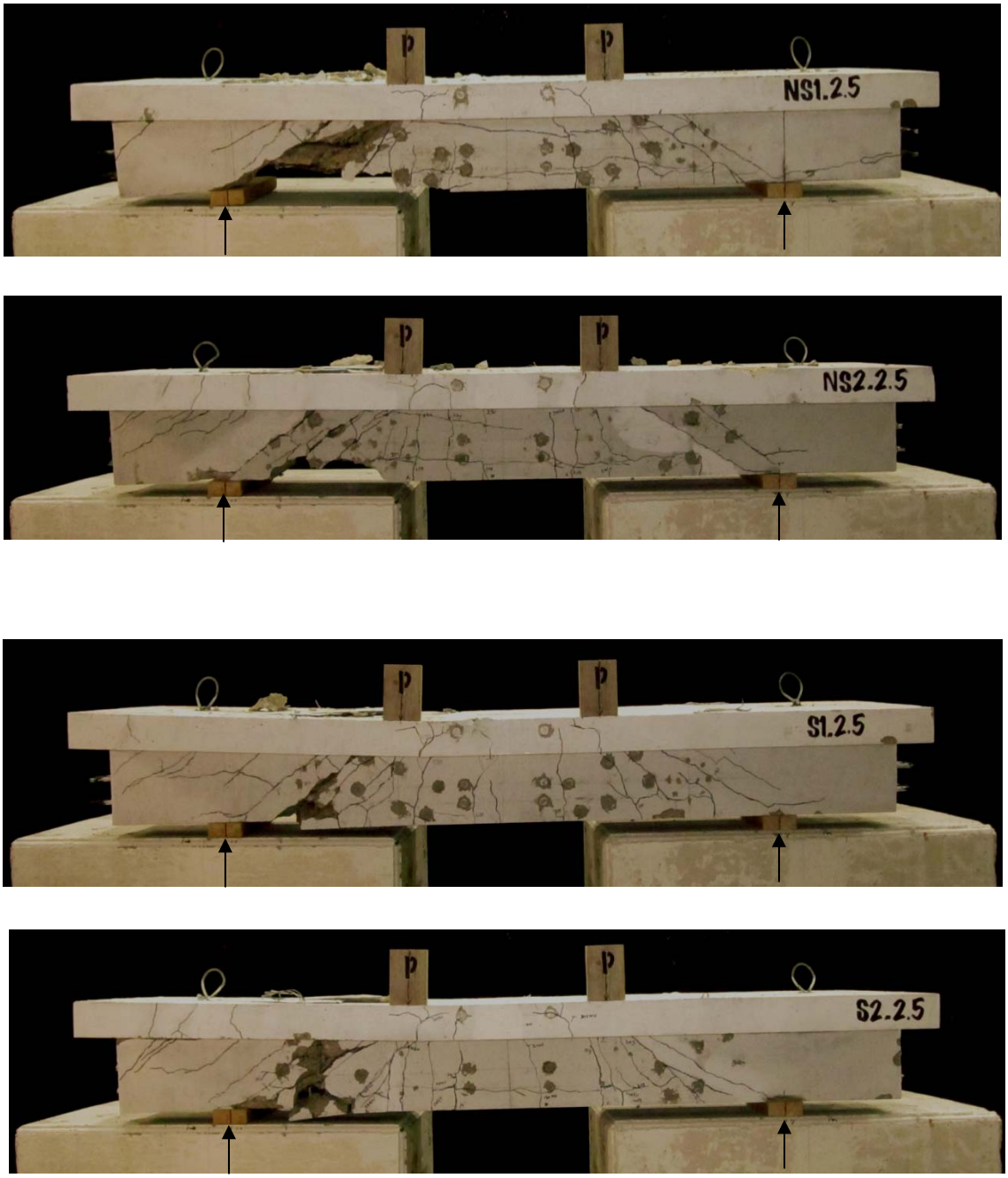

Figure 5- 3: Failure profile of PR-2.5 beams

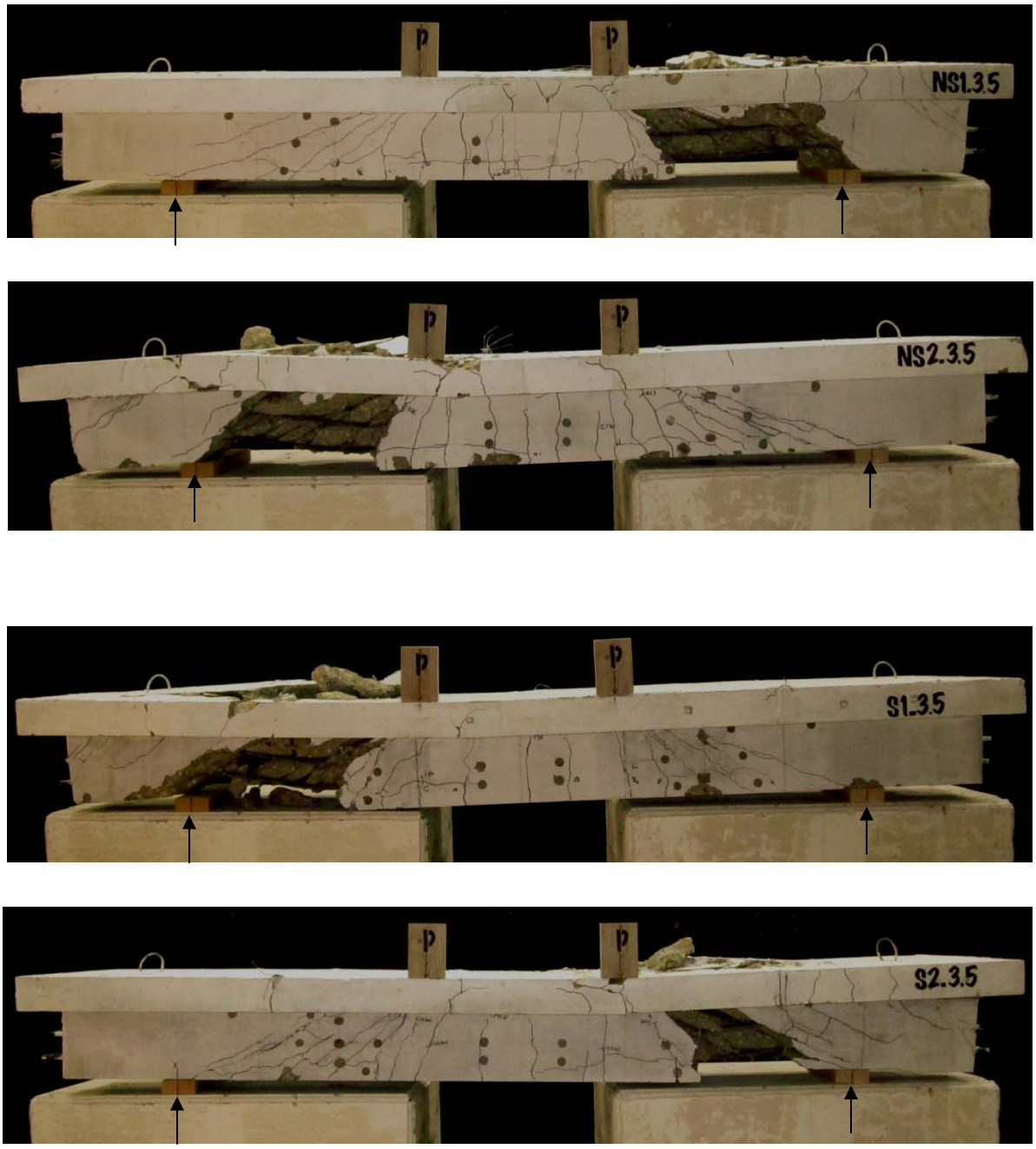

Figure 5- 4: Failure profile of PR-3.5 beams

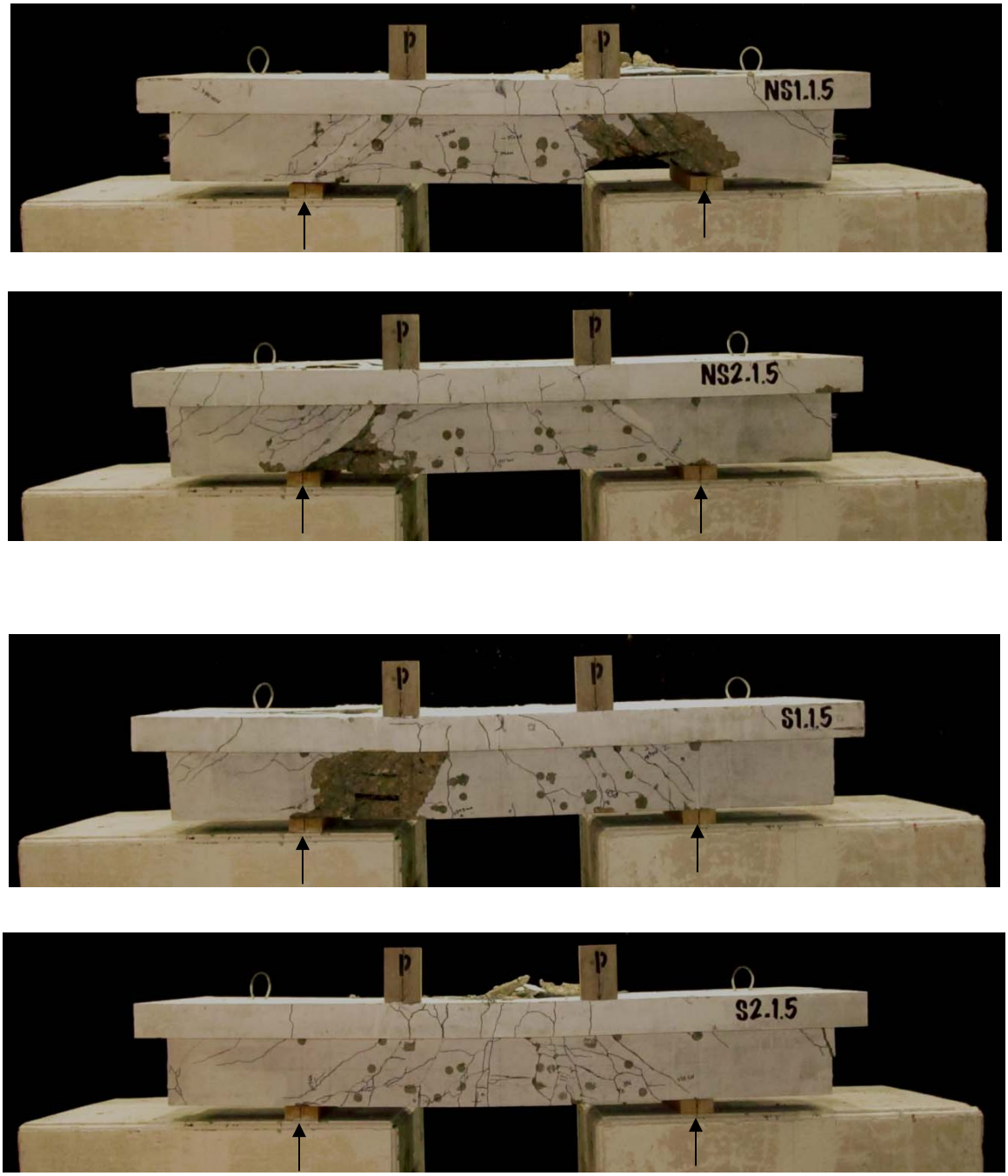

Figure 5- 5: Failure profile of PR-1.5 beams

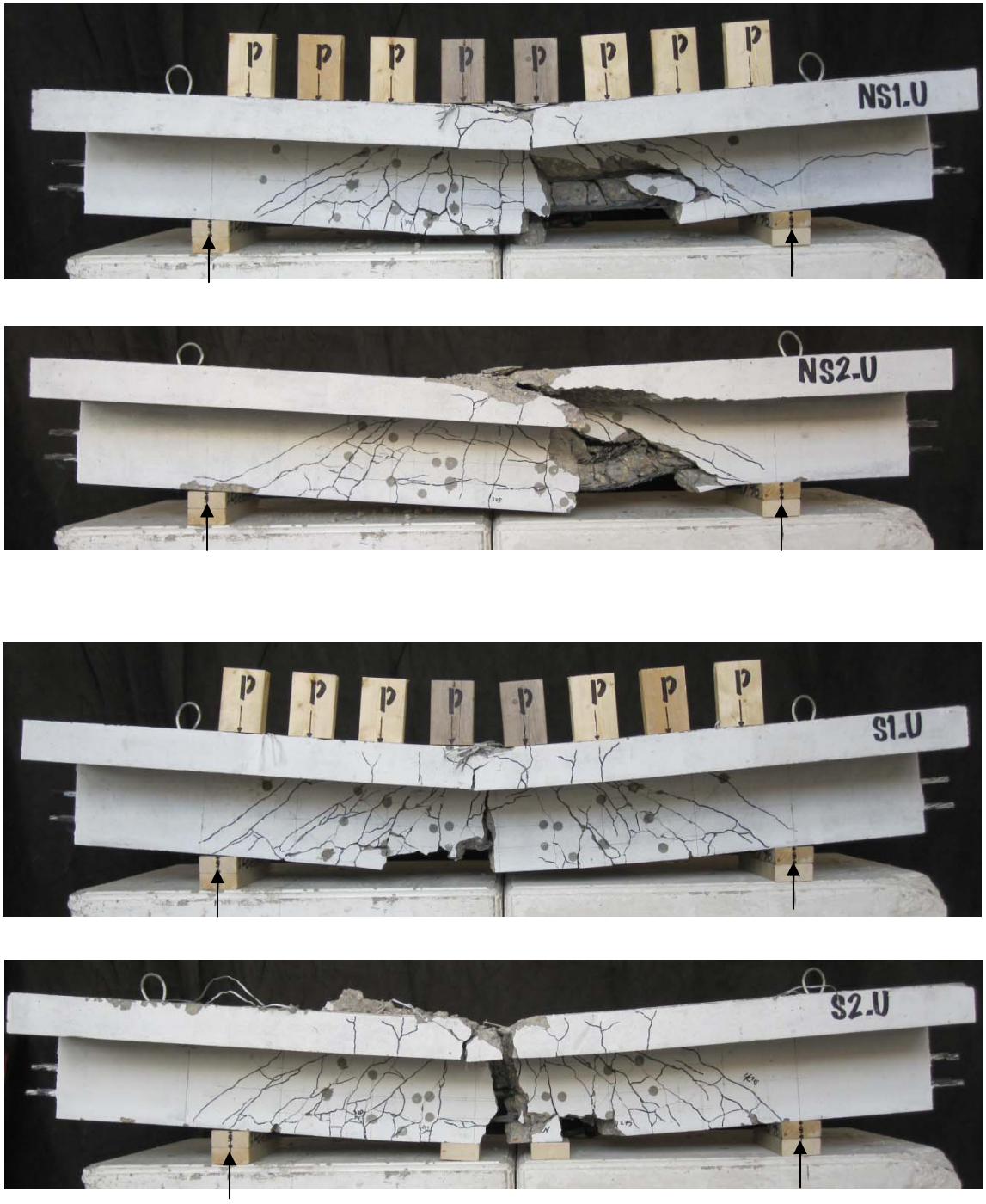

Figure 5- 6: Failure profile of PR-U beams

5.3.3 Effect of the a/d ratio on the Shear Resistance of the Beams

It can be seen from Table 5- 4, that the ultimate shear capacity of the beams increased significantly as the a/d ratio was reduced below 2.5. Shear resistance of Series 1 beams increased by almost 70% by reducing the a/d ratio from 2.5 to 1.5, while the increase in shear capacity was less than 30% when a/d was reduced from 3.5 to 2.5. The dramatic increase in the shear capacity of the PR-1.5 beams was due to the fact that these beams were able to develop and maintain significant arch action after diagonal cracking.

As a result of the arch action that developed in PR-1.5 beams, the range between web shear cracking and the ultimate failure of the beams increased significantly compared to PR-2.5 and PR-3.5 beams. As it was discussed in Chapter 3, unlike PR-1.5 beams, PR-2.5 and especially PR-3.5 beams failed shortly after diagonal cracking.

The shear cracking load also increased dramatically for PR-1.5 beams compared to PR-2.5 and PR-3.5 beams. Overall the shear cracking load seemed to increase with decrease in the a/d ratio, but the increase was most significant for PR-1.5 beams. This can be due to the shorter shear span in these beams and the fact that for any given shear force, the ratio of M (bending moment) to V (shear force) was less for these beams compared to PR-2.5 and 3.5 beams.

5.4 Crack pattern of the Beams

All the analysis in this section is based on examining the side of the beam that did not fail. The concrete spalled at the failure location which made it impossible to see the cracks. For beams with variable a/d ratio, the flexural crack spacing corresponds to flexural cracks in the constant moment region. The flexural crack spacing (S_f) was measured parallel to the bottom of the beam at approximately one inch height from the extreme tension fibre. The flexural crack spacing could not be measured for PR-U beams due to the beam being damaged at mid-span. The diagonal crack spacing (S_d) was measured as the horizontal spacing between primary diagonal web shear cracks at the mid-height of the web as shown in Figure 5- 7. The flexural and diagonal crack spacing were measured on both the front and back of the beam on the side that did not fail and were averaged between the beams from the same Series and beam group.

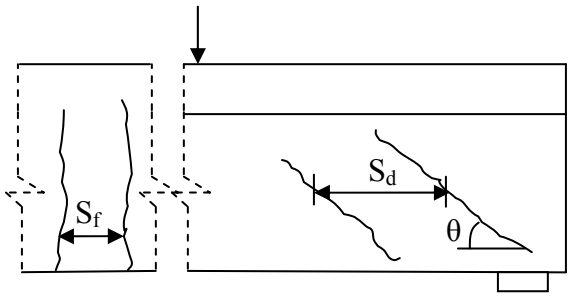

Figure 5- 7: Crack angle and spacing measurement

In Table 5-5, the crack angles refer to the angle of the diagonal shear cracks with the horizontal axis. Parallel diagonal cracks that were close to each other were averaged. Therefore, the reported values show the progression of the diagonal cracks from supports to the load points and do not necessarily correspond to individual cracks. Crack angles were also measured on both the front and back of each beam.

Table 5- 5: Crack angle and spacing for the beam specimens

Beam ID	θ (diagonal shear crack angle) [°]	S_{favg} (mm)	S_{davg} (mm)
PR-3.5 Beams			
NS1-3.5	19, 31, 42	93	92
NS2-3.5	19, 27, 33		
S1-3.5	19, 31, 36, 45	127	94
S2-3.5	22, 30, 41		
PR-2.5 Beams			
NS1-2.5	31, 40	145	101
NS2-2.5	32, 40		
S1-2.5	30, 44	138	98
S2-2.5	32, 44		
PR-1.5 Beams			
NS1-1.5	43	120	52
NS2-1.5	41		
S1-1.5	43	102	49
S2-1.5	39		
PR-U Beams			
NS1-U	32	-	76
NS2-U	29		
S1-U	34	-	69
S2-U	35		

5.4.1 Variation of Crack Pattern with a/d Ratio

Figure 5- 8 compares the crack pattern of beam specimens that failed in shear. The region with diagonally hatched pattern is where the failure occurred. In all the specimens, cracking began in form of flexural cracks in the mid-span region of the beams. More flexural cracks were formed in the shear spans upon further increase in loading and later shear cracks were formed as extension of these flexural cracks and propagated towards the compression face of the beams. Later, diagonal web shear cracks were formed near the supports and grew wider with increase in load.

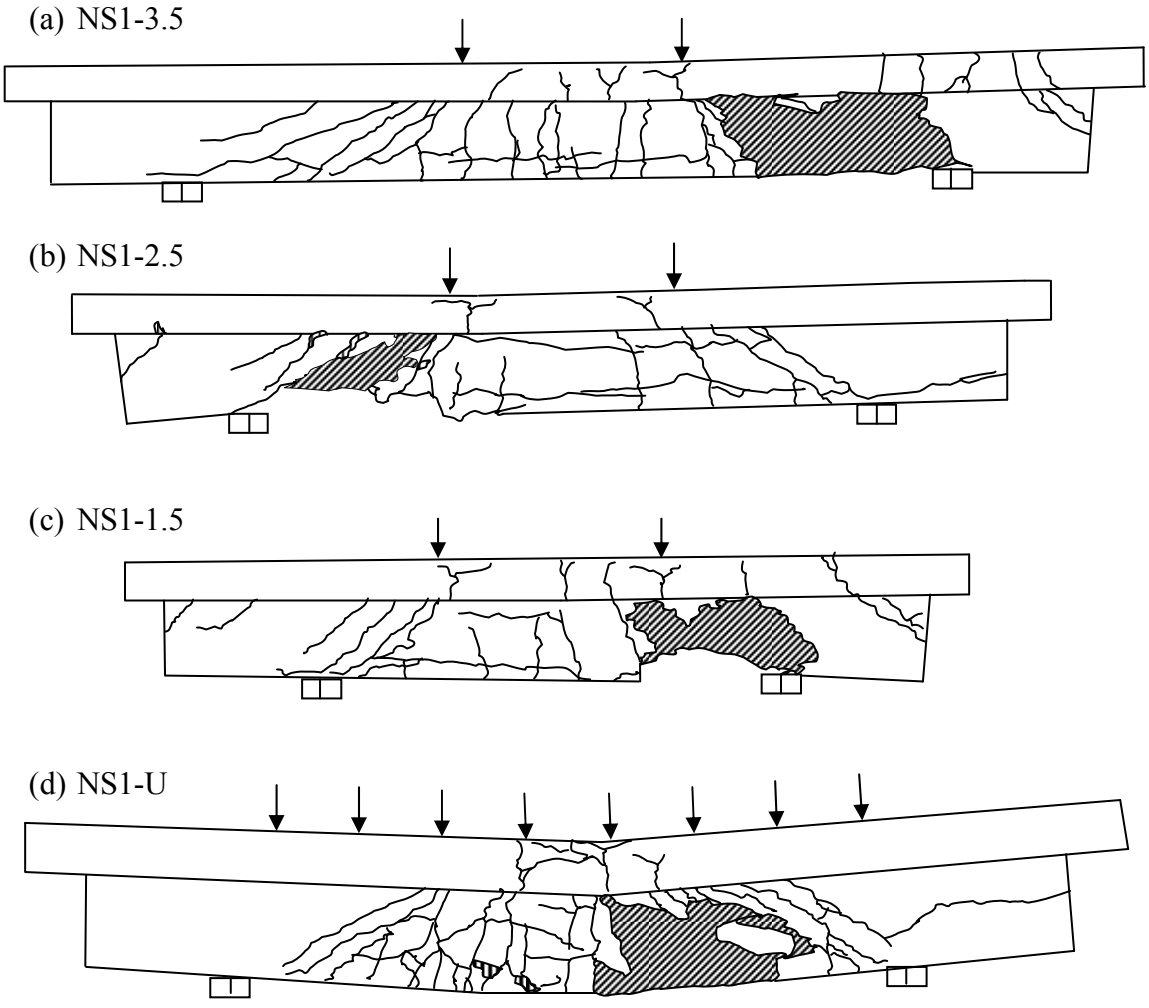

Figure 5- 8: Crack pattern of the beam specimens

In case of PR-3.5 beams the failure occurred shortly after diagonal cracking. For PR-1.5 beams, the failure occurred by the concrete crushing at the tip of the diagonal crack as the compressive strut failed at the load point after significant shear resistance post-diagonal cracking.

Overall, the PR-3.5 beams showed more extensive flexural and diagonal cracking as can be seen in Figure 5- 8. However, as shown in Table 5-5, the average diagonal crack spacing for PR-3.5 beams was larger compared to PR-1.5 beams. This is likely due to the much shorter shear span in PR-1.5 beams. The average diagonal crack spacing was similar between PR-2.5 and PR-3.5 beams.

Another form of cracks that were visible in all the beams tested under four point bending were small diagonal cracks on the beam overhangs close to where the beams failed. These cracks were in form of tension cracks that started in the flange and extended diagonally in to the web. The cracks were the result of a negative moment created when the beams were picked up from the embedded hooks and transported with the crane after failure. The reason these cracks did not occur in PR-U beams was that the failure occurred closer to mid-span, while for the other beams the failure happened near the supports and the location of the hooks in the flange.

5.4.2 Variation of Crack Angle with a/d Ratio

As the shear span was shortened the diagonal web shear cracks became steeper as expected since the path between the support and the load was reduced. The diagonal cracks in PR-1.5 beams were all angled at approximately 40 degrees and were therefore averaged together. In PR-2.5 and PR-3.5 beams, similar cracks near the supports were angled at approximately 31 and 20 degrees respectively. The angle of the diagonal shear cracks increased from the supports towards the load points and approached 45 degrees for PR-2.5 and PR-3.5 beams.

5.4.3 Effect of Distributed Load on Crack Pattern of the Beams

Series 1 PR-U beams failed in diagonal tension within a zone between the support and the mid-span of the beams. Diagonal shear cracks close to the supports did not cause the failure of the beams and the majority of the shear cracks were in form of flexural shear cracks. This was different for beams tested under four point bending which failed at the diagonal crack that extended from the support to the load point. Also, the average angle of diagonal cracks near the supports for PR-U beams was 32 degrees, similar to PR-2.5 beams.

5.5 Deflection Behaviour of the Beams

For all the beams, deflection measurements were taken at mid-span and quarter-spans using LVDTs. The LVDTs were placed on top of the flange with the exception of PR-1.5 and PR-U beams for which the LVDTs were set up underneath the flange due to space constraints. However, deflections were measured at exactly 150 mm in to the flange for all the beams.

5.5.1 Load-Deflection Curves

This section includes the load- mid-span deflection curves (Figure 5-9 to Figure 5-12) for all the tested beams. PR-3.5 beams showed the highest deformability among all the beams followed by PR-U and PR-2.5 beams. For NS1-1.5 and NS2-1.5 beams, the beams had to be reloaded after the first attempt to fail the beams was unsuccessful due to failure of the setup. The MTS machine cross head slipped close to failure of beam NS1-1.5 at approximately 600 kN. The test was repeated the next day after fixing the MTS machine. For NS2-1.5, the roller holding one of the spreader beams exploded half way through the test since it was made of cast iron. All the rollers were replaced with solid steel ones before more testing was done. For NS1-1.5, the beam was very close to failure when the test stopped which explains the large plastic deformation in the beam when it was reloaded as shown in Figure 5-11.

.

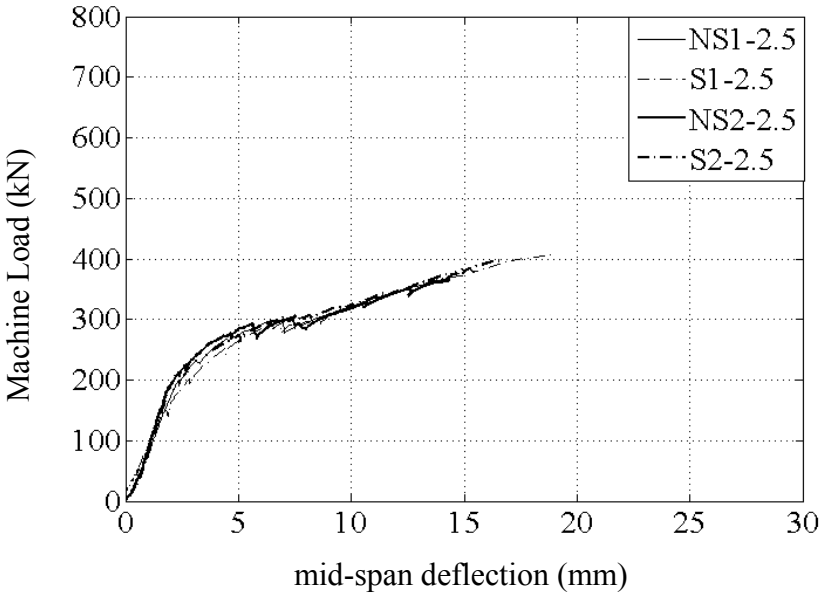

Figure 5- 9: Flexural behaviour of PR-2.5 beams

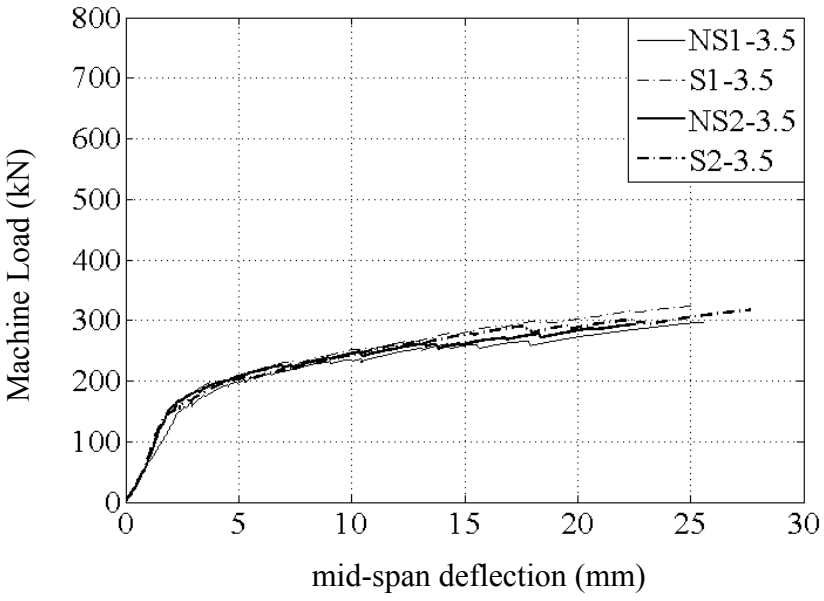

Figure 5- 10: Flexural behaviour of PR-3.5 beams

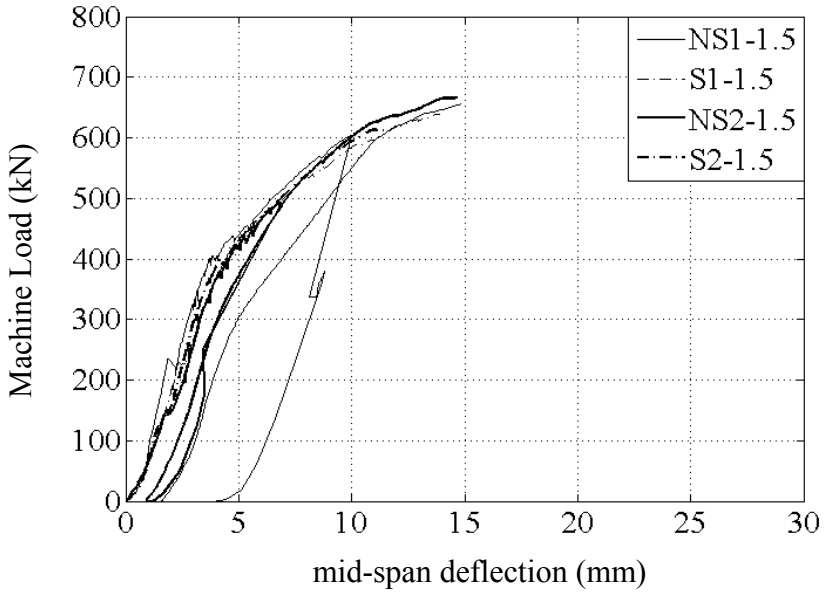

Figure 5- 11: Flexural behaviour of PR-1.5 beams

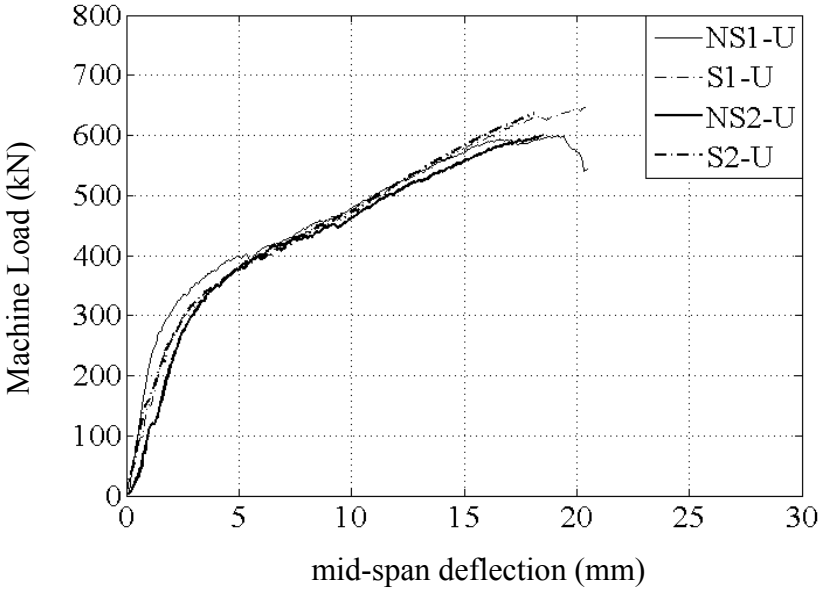

Figure 5- 12: Flexural behaviour of PR-U beams

Figure 5- 13 compares the typical deflection behaviour of the S1 beams from each group. The Load-deflection graphs have been normalised with respect to ultimate load and ultimate deflection for the sake of comparison. Similar graphs for the other beams are shown in Figure C-

2. The non-normalised load-mid-span deflection graphs that compare the behaviour of different beam groups can be found in Figure C-1. The post-cracking stiffness of the beams increased specially as a/d decreased below 2.5 due to significant arch action that developed, while deformability of the beams decreased. This is seen among all the beams in both Series 1 and Series 2. For example at load levels of 50% ultimate, PR-1.5 beams reached almost 30% of their ultimate deflection, while PR-3.5 beams reached about 10%. The normalised mid-span deflection of the PR-U beams fell between PR-2.5 and 3.5 beams but was best comparable to PR-2.5 beams.

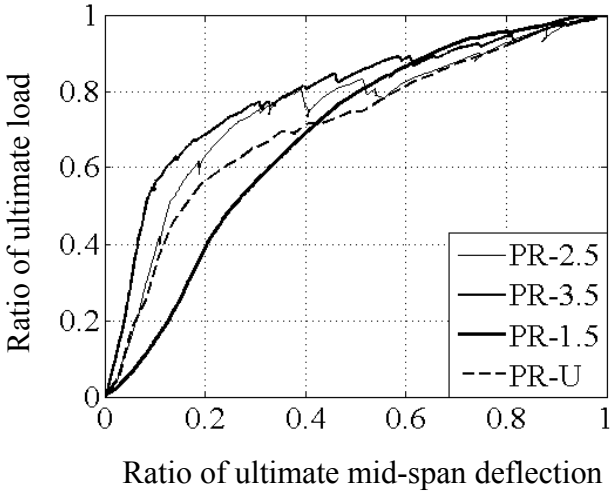

Figure 5- 13: Typical normalised load-deflection curves for beam specimens

The change in the post-cracking stiffness of the beams with a/d ratio was also observed for steel reinforced concrete beams (Fathifazl et al. 2009). Fathifazl et al. (2009) conducted a study on the shear strength of reinforced recycled concrete beams without transverse reinforcement and different a/d ratios among other variables. The authors found that as the a/d ratio increased, the post-cracking stiffness of the beams decreased. They believed that this is due to higher ratio of maximum moment to shear for beams with higher a/d ratio at any given shear load which results in lower effective moment of inertia beyond cracking.

5.6 Deflection Profiles of the Beam Specimens

In this section, data from the two LVDTs at quarter-spans and the LVDT at mid-span were used to plot the deflection profiles of the beams. The load-deflection profiles are plotted for Series 1 and Series 2 beams from each group at 50%, 70% and 100% of the ultimate load. The load is the total machine load applied to the beams. Figure 5-14 to Figure 5-17 show the deflection profiles

for some of the tested beams. For PR-1.5 beams the quarter-span LVDTs did not work very well for NS1 and S2 beams. Therefore, the results are plotted for NS2 and S1 beams. The irregular shape of the deflection profile at ultimate for NS2-1.5 is due to quarter-span LVDTs losing contact with the beam due to the screw holding the LVDTs falling off from underneath the flange. The deflection profiles for other beams can be found in Figure C-3.

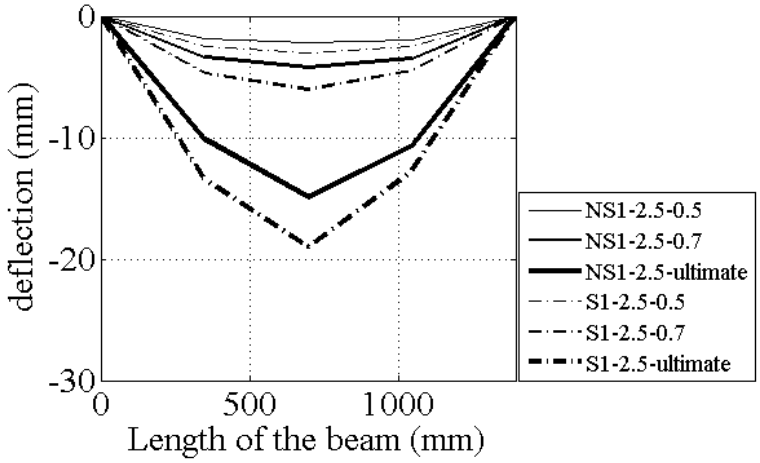

Figure 5- 14: Deflection profiles for PR-2.5 beams

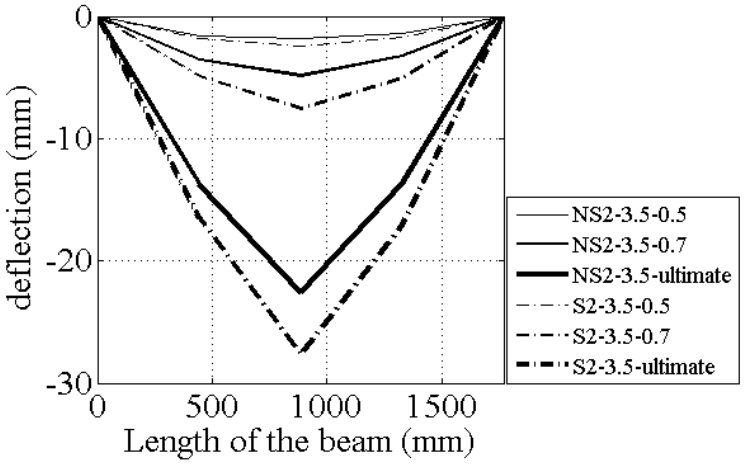

Figure 5- 15: Deflection profiles for PR-3.5 beams

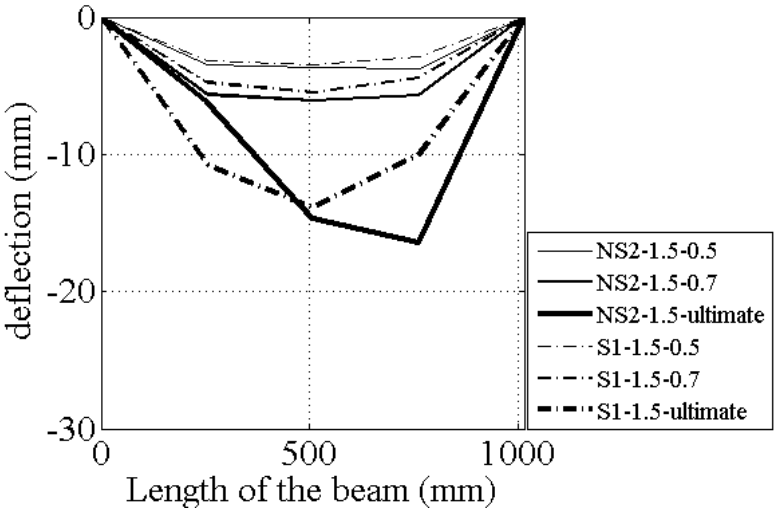

Figure 5- 16: Deflection profiles for PR-1.5 beams

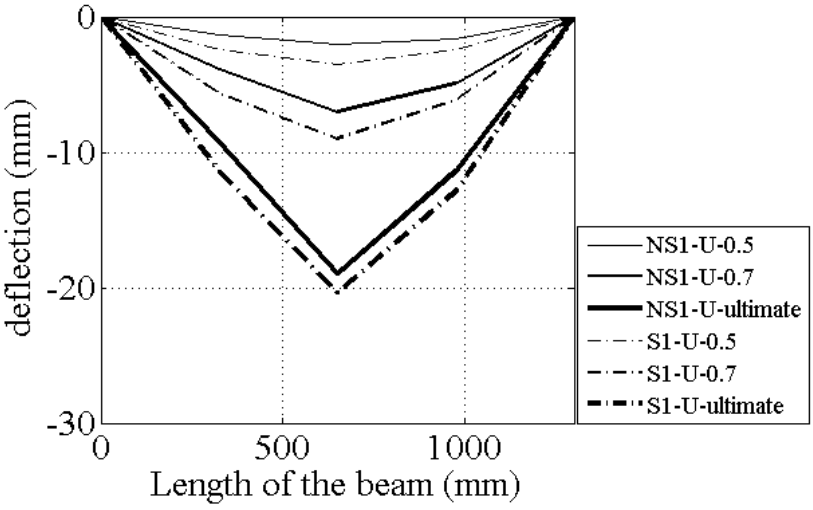

Figure 5- 17: Deflection profiles for PR-U beams

It can be seen from the deflection profiles (Figure 5-14- Figure 5-17) that PR-3.5 beams showed significantly larger deflection compared to other beam groups from 70% of the ultimate load to failure. For Series 1 beams, PR-2.5 and PR-U beams showed an average of 11 mm deflection over the specified load range. PR-3.5 and PR-1.5 beams showed 63% more and 57% less deflection respectively compared to PR-2.5 and PR-U beams from 70% to 100% of the ultimate load. The same results were obtained for Series 2 beams. It is evident that the PR-3.5 beams had the largest deformability compared to the other beam groups.

The results from the deflection profiles confirms that the post-cracking stiffness of PR-2.5 and PR-U beams were relatively similar, while PR-1.5 beams were much stiffer due to the arch behaviour in these beams. Also, the contribution from the FRP stirrups was not to the extent to produce significantly larger deflection in Series 2 beams compared to Series 1 beams.

5.7 Strain in the Flexural Reinforcement

In this section the results from the strain gauges installed on the longitudinal reinforcements at mid-span are discussed. Load-strain graphs were analysed for the bottom layer reinforcements that experienced the highest stress and were compared between different beam groups. The strain development in the prestressing cable on the right side of the beam in the bottom layer (cable 2) is plotted with respect to load for beams without stirrups (Figure 5-18 (a)). All the beams tested under four point bending are plotted in black marker and the beam tested under distributed load is plotted in light marker. The load represents the total load applied to the beams by the test machine.

The load-strain behaviour for the left cable in the bottom layer was the same as for cable 2 and is therefore not shown here. As Figure 5-18 (a) shows, the strain gauges for beams NS1-3.5 and NS1-U broke-off at some point during the test before the ultimate load was reached. It is evident that the strain gauges started to record large values of strain for small increase in load increments which is why the load-strain graphs suddenly turn in to a horizontal line. This is especially significant for the strain gauge on beam NS1-U that stopped at approximately 500 kN which is at 83% of the ultimate capacity of the beam. It seemed from Figure 5-18 (a) that strain development in the bottom reinforcement of NS1-U matched that of NS2-2.5 beam in the post-cracking stage. To clarify this, Figure 5-18 (b) was plotted over a strain range of 0 to 3000 με to compare the beams over a range where the strain gauges on all the beams were working.

For NS1-3.5, the last meaningful strain value recorded was slightly less than 3000 με. Similar graph for Series 2 beams can be found in the Appendix (Figure A-9).

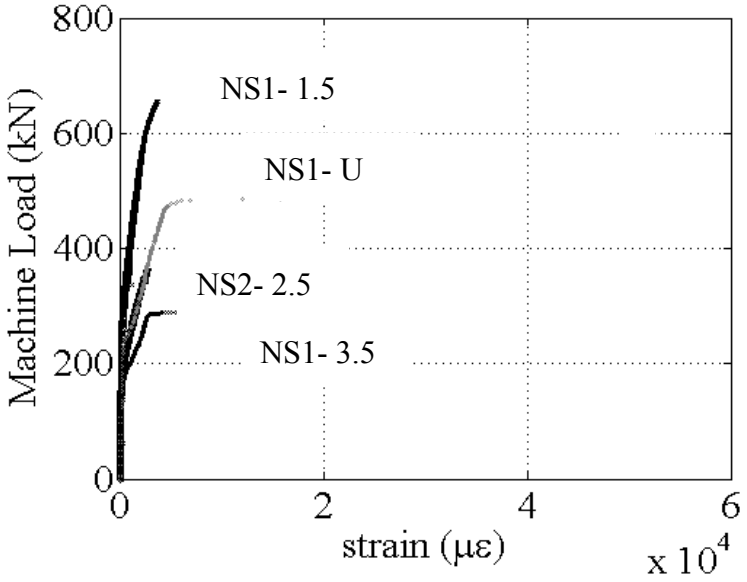

(a) Total range

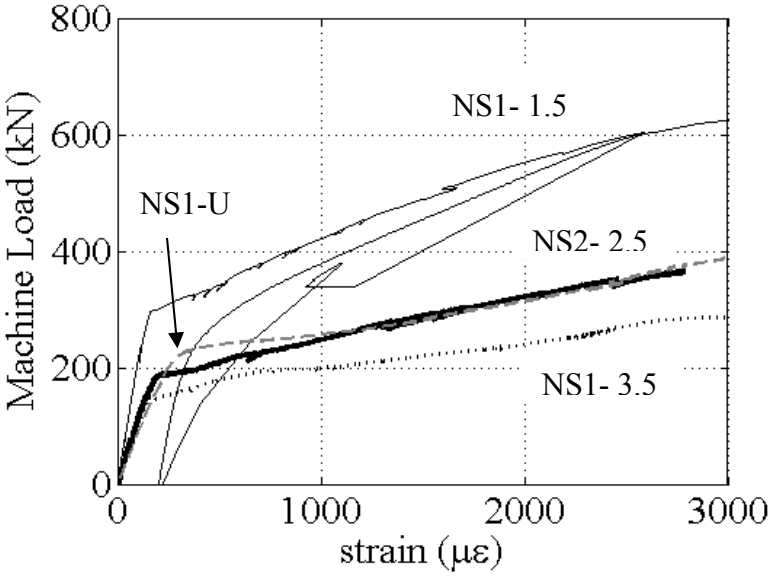

(b) Reduced range

Figure 5- 18: Load-strain behaviour of the bottom right cable (Series 1 beams)

Figure 5-18 (b) clearly shows that the load-strain behaviour in the bottom longitudinal reinforcement of NS1-U matched that of NS2-2.5 within the range shown on the graph.

However, It is evident from Figure 5-18 (a) that NS1-U beam maintained the same slope all the way to 500 kN before the strain gauge broke-off.

Also, it was observed from Figure 5-18 that the bottom longitudinal reinforcements in PR-1.5 beams reached higher strain at ultimate compared to PR-2.5 and PR-3.5 beams. This can be seen more clearly in Figure 5-19 (a) and (b) that compare the load-strain curves for bottom longitudinal reinforcements in Series 1 and 2 of the beams tested under four point bending. The figure shows that S1-1.5 beam reached approximately 40% higher strain at ultimate compared to S1-2.5 and S1-3.5 beams.

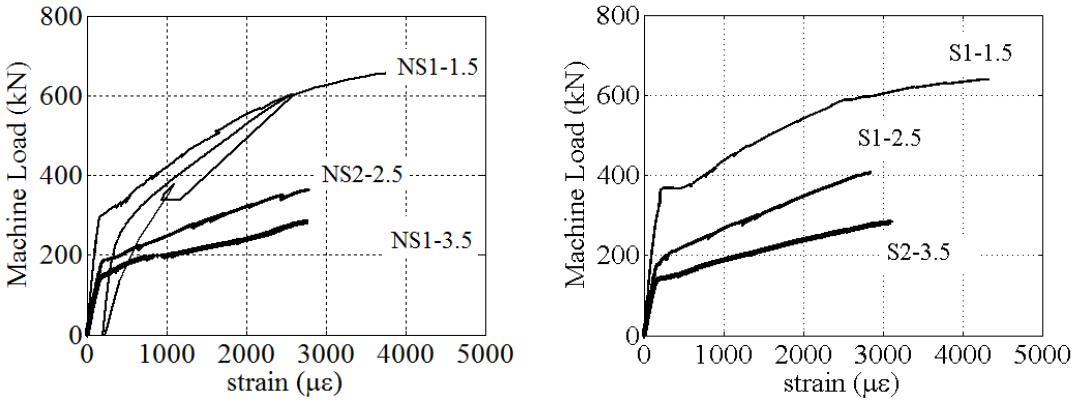

(a) Series 1 **(b) Series 2**

Figure 5- 19: Load-strain curves for the bottom right cable

For beams NS1-3.5 and S1-3.5, the strain gauge broke-off close to failure of the beams which was 285 kN for beam NS1-3.5; therefore, the portion of the curve beyond this point was removed. However, the strain in the cable was not expected to develop much higher because the beam was only 13 kN from failure. Also, the ultimate strain in the longitudinal reinforcement for PR-3.5 beams is not expected to be more than that of PR-2.5 beams since the PR-3.5 had approximately 25% less capacity compared to PR-2.5 beams. The higher ultimate strain in PR-1.5 beams compared to PR-2.5 and 3.5 beams is due to the arch action that developed in these beams. Arch action increases the demand on the longitudinal reinforcement that acts as the tension tie of the arch and provides anchorage to the compressive struts.

Higher strain in the longitudinal reinforcement of deep beams was also observed by Fathifazl et al. (2009) who tested steel reinforced recycled concrete beams without stirrups and different a/d ratios. In their experiment, the authors monitored the strain in the longitudinal steel

reinforcement at a distance d from the support. In case of deep beams with a/d = 1.5, the longitudinal steel yielded at the support due to high tensile stresses sustained by the bars from arch action. The authors found that the resistance of the beams were limited by the tensile capacity of their longitudinal reinforcement rather than the shear capacity of the reinforced recycled concrete beams.

5.8 Effect of Distributed Load on the Behaviour of the Beams

It was shown earlier in this chapter that the slope of the load-strain curve in the bottom longitudinal reinforcement was similar between PR-U and PR-2.5 beams in the post-cracking stage (Figure 5-18). The mid-span deflection results as well as the deflection profiles of the beams also showed that the post- cracking stiffness of the PR-U beams was relatively closer to PR-2.5 beams than PR-3.5 beams. Also, the flexural cracking load and the angle of diagonal web shear cracks near the supports were relatively similar between PR-2.5 and PR-U beams (Table 5-4, Table 5-5).

The PR-U beams had a span length of 1300 mm close to the span length of PR-2.5 beams which was 1394 mm. Applying Kani's analogy (1966) as outlined in Section 2.7 to the PR-U beams provided a corresponding a/d ratio of 2.1 which is very close to 2.5 for PR-2.5 beams. Considering the similarities between PR-U and PR-2.5 beams, it seems the results of this project confirm Kani's argument that a distributed load can be modeled using a four point bending setup with point loads applied at quarter lengths.

While the flexural cracking load was only slightly higher for PR-U beams compared to PR-2.5 beams, the diagonal shear cracking load was 42% higher. Also, the diagonal tension failure in beams tested under four point bending always happened at the diagonal crack near the supports, while the failure location for PR-U beams was slightly closer to the mid-span of the beams.

The ultimate shear capacity of Series 1 PR-U beams that failed in diagonal tension was 63% higher than the shear capacity of PR-2.5 beams with similar failure. The higher load carrying capacity of PR-U beams compared to beams tested under four point bending showed that distributing the load over the span length of the beam allowed it to reach higher loads. Kani (1966) did mention that the beams subjected to distributed load were able to reach fairly higher shear strength compared to beams tested under four point bending. The PR-U beams were expected to reach higher shear capacity than PR-2.5 beams due to lower equivalent a/d according

to Kani (1966). However, the shear capacity of PR-U beams was not expected to be much less if the beams were designed so that the resultant forces from distributed load exactly matched the location of the point loads on PR-2.5 beams. Therefore, it can be concluded that that four point bending provides a conservative estimate of the shear capacity of beams subjected to distributed load.

5.9 Strain Profiles at Mid-span of the Beams

The strain profiles for the beams were plotted based on data from the gauges installed on the concrete at mid-span of the beams. As mentioned before, these gauges included two 200 mm Pi-gauges at 54 mm and 100 mm height from the extreme tension fibre and a gauge on the compression face in the middle of the flange. The gauge used on the flange was a 100 mm Pi-gauge for all the beams tested under four point bending and a concrete strain gauge for all the PR-U beams. The strain profiles are plotted at 100 kN intervals and the ultimate load. For some of the beams one or two of the gauges broke off close to failure, consequently the strain profile at ultimate for those beams is not shown. The principle of plane section remains plane is visible in all the strain profiles as the strain remained linear all the way to failure at the location of the gauges which was the constant bending region (Appendix B). For few of the beams, the gauges did not work properly which in that case their mid-span strain profiles could not be plotted.

The strain in the bottom strands is also shown on the strain profiles for comparison between the strain gauge on the strands and the Pi-gauge at the same level on the concrete. The strain values from the longitudinal reinforcement are sometimes not shown all the way to failure due to strain gauges breaking-off. The strains in the bottom longitudinal reinforcement and the Pi-gauge on the concrete agreed well at lower loads but were significantly different at higher loads passed flexural cracking. It should be noted that unless the strain gauge is directly located at the location of the crack that goes through the Pi-gauge, it would not read the same strain values. This is due to different bond between the concrete and the bar depending on the location of the gauge. The Pi-gauge with a gauge length of 200 mm was crossed by multiple cracks while the strain gauge measured strain over a 2 mm gauge length.

5.10 Estimating the Moment-Curvature of the Beams

The experimental moment-curvature behaviour of the beams at mid-span was plotted based on the same data that was used to plot the strain profiles in Appendix B. The experimental and

theoretical mid-span moment-curvature relationships of the beams were compared to verify the readings from gauges and the estimated effective prestressing in the beams.

Figure 5-20 to Figure 5-23 compare the experimental and theoretical moment-curvature at mid-span for different beam groups. For some of the beams the gauges malfunctioned which explains the anomalies in the experimental results. The moment- curvature relationships could not be plotted for NS2-1.5, S1-1.5 and S2-U due to problem with the gauges.

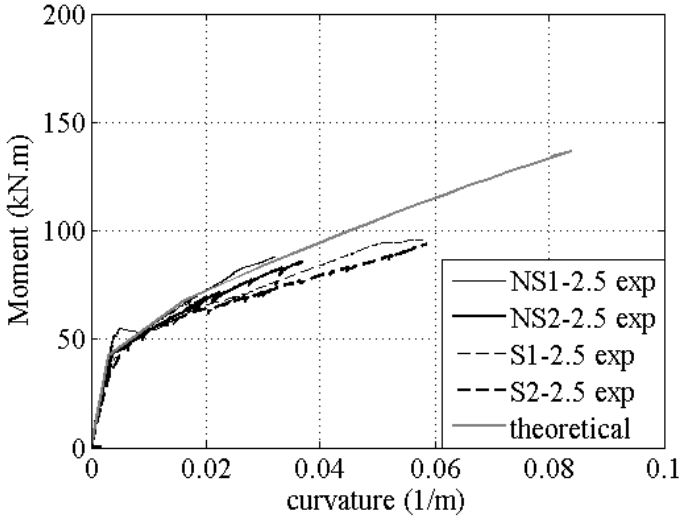

Figure 5- 20: Moment-curvature for PR-2.5 beams

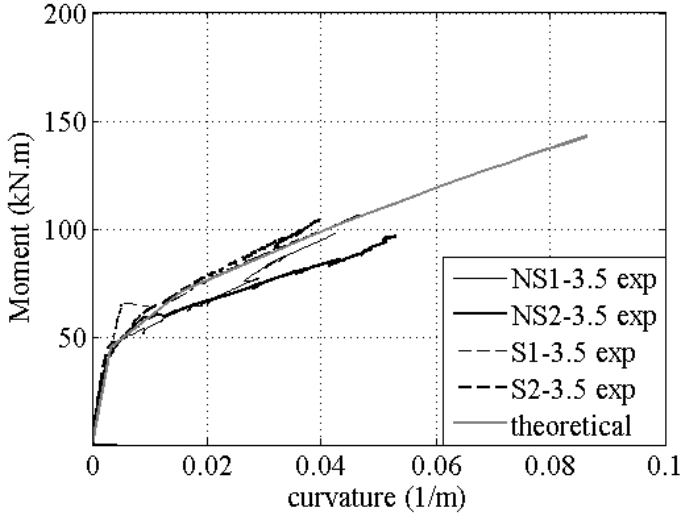

Figure 5- 21: Moment-curvature for PR-3.5 beams

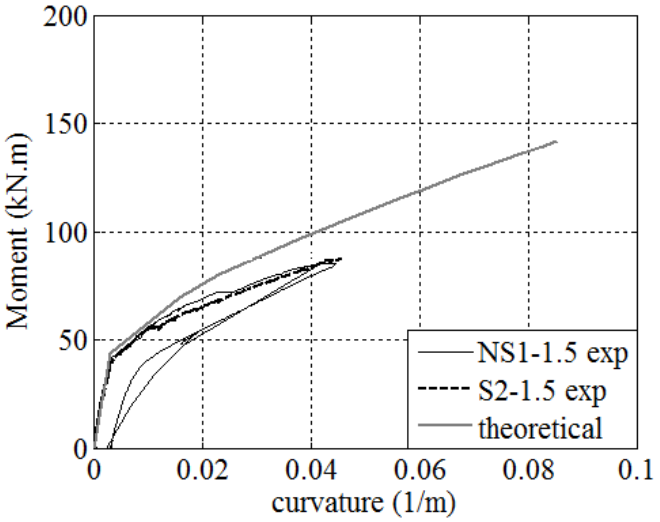

Figure 5- 22: Moment-curvature for PR-1.5 beams

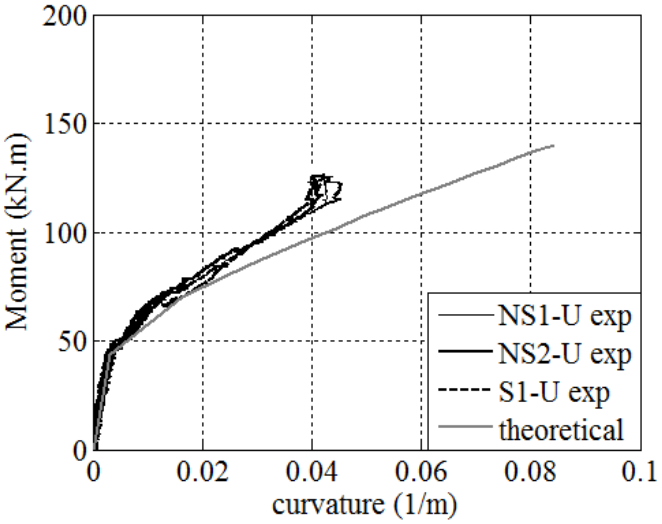

Figure 5- 23: Moment-curvature for PR-U beams

5.10.1 Discussion of the Moment-Curvature Results

Linear elastic behaviour of the beams as well as the cracking moment from experiment perfectly matched the theory for all the specimens, which shows the effective prestressing was estimated correctly. Also, the non-linear behaviour of the beams matched well for at least two specimens in PR-2.5 and PR-3.5 beam groups. For PR-3.5 beams, the experimental results matched the theory perfectly for Series 2 beams, while for PR-2.5 beams the theoretical and experimental results best matched for Series 1 beams.

The estimated theoretical flexural failure of the beams was tension failure as is expected from under reinforced concrete beams. However, since all the beams were designed to fail in shear, the ultimate moment resistance was never reached, except for S1-U and S2-U beams that failed in tension. In Figure 5-23, the ultimate experimental moment resistance of the beams almost matched the experiment, while the ultimate theoretical curvature was significantly off from the experimental results due to malfunction of the gauges. The gauges on S1-U and S2-U beams did not work properly all the way to failure as it can be seen from Figure 5-23 and stopped working at around 135 kN.m which corresponds to 500 kN.

For beam S2-1.5 the ultimate moment resistance of the beam is not reached as it can be seen in Figure 5-22 even though the beam failed in flexural compression. This type of behaviour is expected in these beams due to arch action that develops which relies on a system of compressive struts and a tension tie to carry the load. Although the concrete crushed at mid-span it does not mean that the flexural capacity of the member was reached. The Series 1 PR-1.5 beams failed at approximately 660 kN compared to PR-2.5 and 3.5 beams that failed at 368 KN and 295 kN respectively. The ultimate flexural capacity for PR-1.5 beams was nevertheless higher compared to PR-2.5 and PR-3.5 beams due to much shorter shear span of PR-1.5 beams. Zararis (2003) argued that this type of failure occurs in deep beams without web reinforcement. According to the study, in deep beams without web reinforcement, splitting cracks can extend from the tip of critical diagonal crack to the mid-span and result in concrete crushing between the load points. However, in beams with web reinforcement, the splitting cracks would not occur due to restraining effect of the stirrups and the concrete crushes at the load points resulting in shear compression failure (Zararis 2003).

Although, in this research beam S2-1.5 contained stirrups, only close to minimum amount of stirrups were provided. Looking at the failure profile of beam S2-1.5 in Figure 5-5, splitting cracks can be noticed in the mid-span region of the beam. These cracks are not visible in the other beams in the PR-1.5 group and the reason they occurred in S2-1.5 beam could just be different concrete properties besides strength for this beam compared to the others.

5.11 Principal Strain Values in Shear Spans of PR-1.5, 2.5 and 3.5 Beams

The results in this section show the concrete strains in the shear spans of the beams tested under four point bending. 45^{o} rosette stations of Pi-gauges and LVDTs were installed on the concrete

beams in their shear spans to record the strains in transverse, longitudinal and diagonal direction. The best of the data is presented here with the rest available in Appendix D.

The location of the rosette stations was maintained the same between beams in each group and it was selected to capture all the diagonal cracks for each beam. It should be noted that rosette stations were placed in both north and south shear spans and were placed at the location of the stirrups. The results presented here correspond to the side of the beam that failed. The diagonal, longitudinal and transverse strains were recorded during the experiment and used to calculate the principal tensile strain.

Figure 5-24 shows the orientation of the sensors in each rosette station. θ_1, θ_2 and θ_3 are respectively the directions of the normal strains $\varepsilon(\theta_1)$, $\varepsilon(\theta_2)$ and $\varepsilon(\theta_3)$ with respect to the horizontal x-axis.

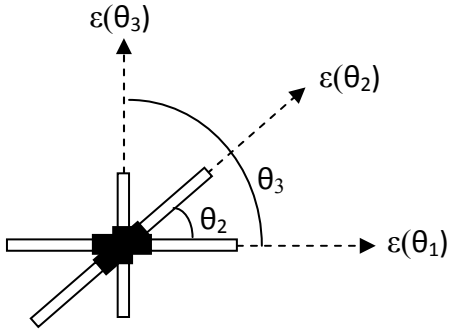

Figure 5- 24: Typical orientation of the rosette stations

Using the following equations, the longitudinal strain (ε_x), the transverse strain (ε_y) and the shear strain (γ_{xy}) can be determined and used to calculate the principal strains. (Lardner and Archer 1994).

$$\varepsilon(\theta_1) = \varepsilon_x \cos^2\theta_1 + \gamma_{xy} \sin\theta_1 \cos\theta_1 + \varepsilon_y \sin^2\theta_1$$
$$\varepsilon(\theta_2) = \varepsilon_x \cos^2\theta_2 + \gamma_{xy} \sin\theta_2 \cos\theta_2 + \varepsilon_y \sin^2\theta_2 \qquad \textbf{Eq.5- 1}$$
$$\varepsilon(\theta_3) = \varepsilon_x \cos^2\theta_3 + \gamma_{xy} \sin\theta_3 \cos\theta_3 + \varepsilon_y \sin^2\theta_3$$

In this experiment the common configuration of $\theta_1 = 0$, $\theta_2 = 45^o$ and $\theta_3 = 90^o$ is adopted which leads to $\varepsilon_x = \varepsilon(0)$, $\varepsilon_y = \varepsilon(90^o)$, and $\gamma_{xy} = 2\varepsilon(45^o) - (\varepsilon_x + \varepsilon_y)$ and the principal strains are determined using Eq.5 -2.

$$\varepsilon_{1,2} = \frac{\varepsilon_x + \varepsilon_y}{2} \pm \sqrt{(\frac{\varepsilon_x - \varepsilon_y}{2})^2 + (\frac{\gamma_{xy}}{2})^2} \qquad \textbf{Eq.5- 2}$$

5.11.1 Discussion of the Concrete Strain Results for PR-1.5, 2.5 and 3.5 beams

As it was discussed in Chapter 3, stirrups do not prevent inclined cracking but rather restrict the opening of the cracks. Once the stirrup is crossed by a diagonal crack, a portion of the shear will be carried by tension through the stirrup which will contribute towards the shear resistance of the beam. In this project, rosette stations were set up to capture the longitudinal, transverse and diagonal strains at the location of one of the stirrups along the shear span of the beams tested under four point bending as discussed in Section 4.9. The gauges measured a combination of crack opening and sliding deformation as well as material strains. Assuming that deformation due to crack sliding and material strains is negligible, the diagonal strains recorded as well as the calculated principal strains can be an indication of the average diagonal crack opening.

In case of PR-1.5 beams, only a diagonal Pi-gauge was installed at the location of the stirrup near the supports to capture the diagonal tensile strains that result in the formation and opening of the diagonal cracks. Due to the short length of the shear span in PR-1.5 beams, rosette stations were not used. The diagonal Pi-gauges were installed for all the beams except NS1-1.5, which had demec points instead. The diagonal concrete strain for NS2-1.5 and S1-1.5 are compared in Figure 5-27. The results from the gauges installed on beams tested under four point bending are plotted with respect to load in Figure 5-25 to Figure 5-27.

In all the figures, the initial linear portion in each curve is a function of the concrete properties and shows the concrete deformations. The load at the end of the linear segment represents the diagonal cracking load. It is evident that between Series 1 and 2 beams in each beam group, the diagonal cracking load was approximately the same.

It can be seen from Figure 5-25 and Figure 5-26, that at any given post-cracking load, the average strain in Series 2 beams was less than Series 1 due to the presence of stirrup at the crack location. However, this trend is not seen in Figure 5-27 that shows the average diagonal strain for PR-1.5 beams. It can be seen from the figure that the average diagonal strain at any post-cracking load is in fact higher for S1-1.5 compared to NS2-1.5, which is probably due to variation in concrete properties between the two beams. It is evident that the stirrups did not contribute to the

shear strength of PR-1.5 beams as they did for PR-2.5 and 3.5 beams. This is also seen for beams NS2-1.5 and S2-1.5 (Figure D-2).

Also, it can be noticed from Figure 5-27, Figure 5-25 (c) and Figure 5-26 (c) that the slope of the ascending branch of the curves decreased as the a/d ratio was increased. Fathifazl et al. (2009) also noticed the same pattern in steel reinforced recycled concrete beams. The authors recorded diagonal deformation across the major diagonal crack in the shear span of the beams and noticed that slope of the ascending part of the load with respect to diagonal deformation line is a function of a/d. The authors believed that the slope of the ascending portion of the curve is higher in deep beams due to higher shear stiffness of these beams. For the same shear force, the ratio of maximum moment to shear will be larger for beams with longer shear span, which results in lower effective moment of inertia in the section post diagonal cracking. Therefore, the stiffness of the beam drops as a/d ratio is increased (Fathifazl et al. 2009). This was also noticed with the load-deflection graphs for this project presented in Section 5.6.

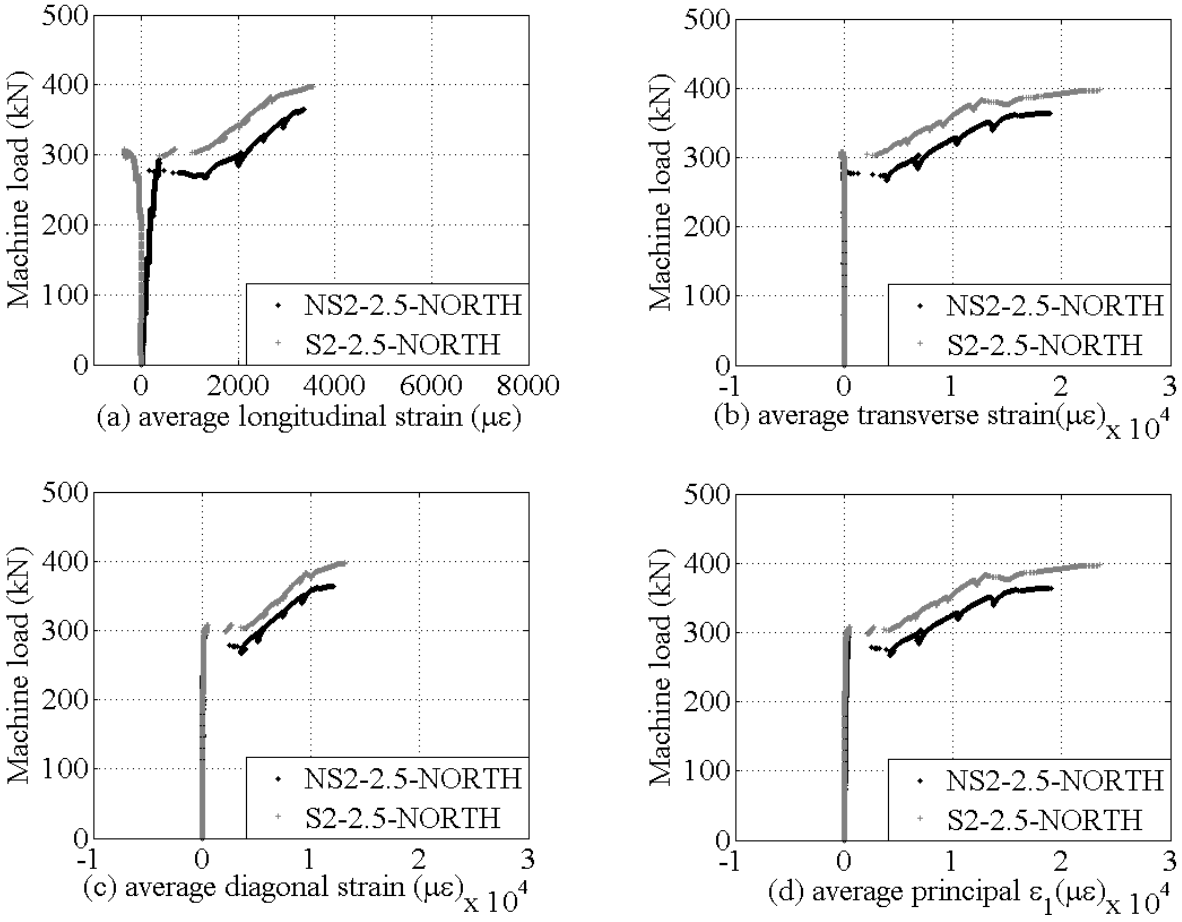

Figure 5- 25: Concrete strains for PR-2.5 beams

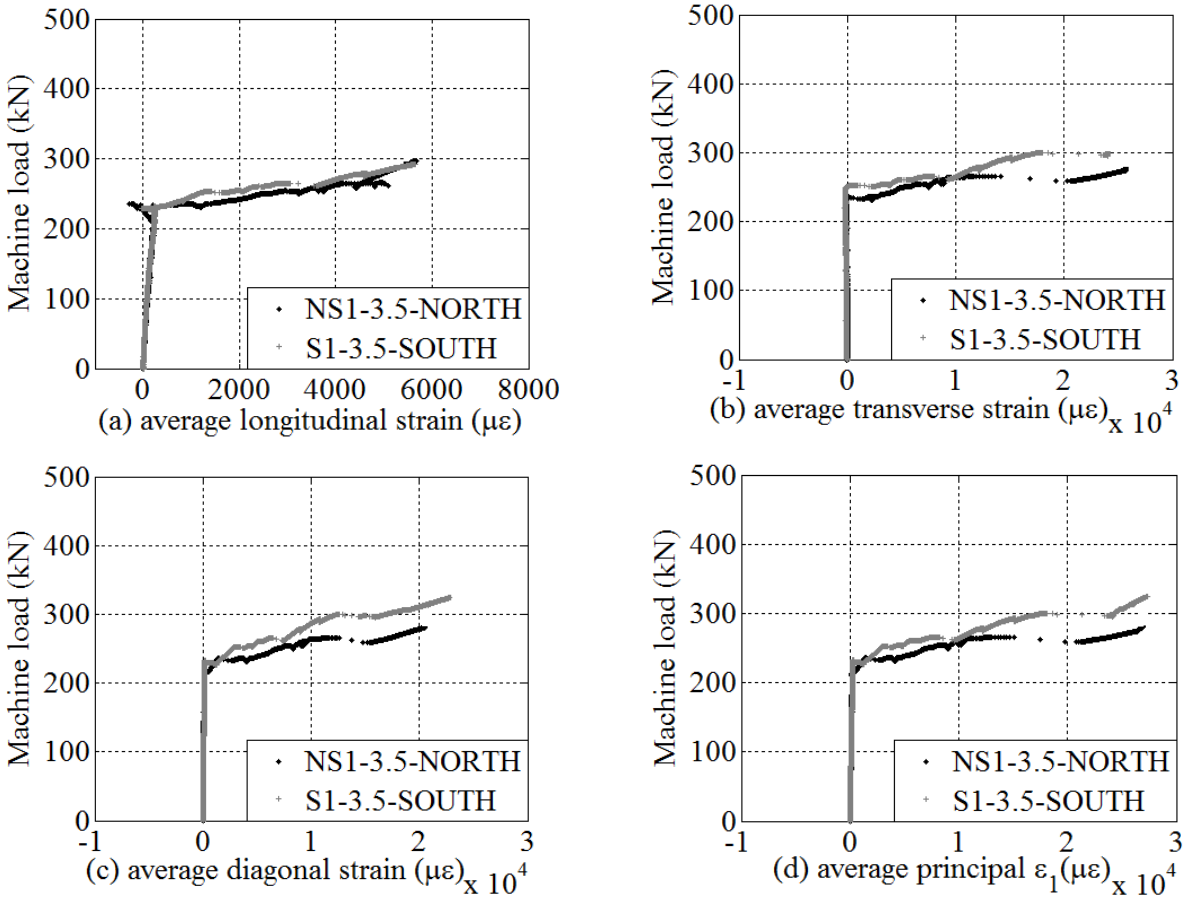

Figure 5- 26: Concrete strains for PR-3.5 beams

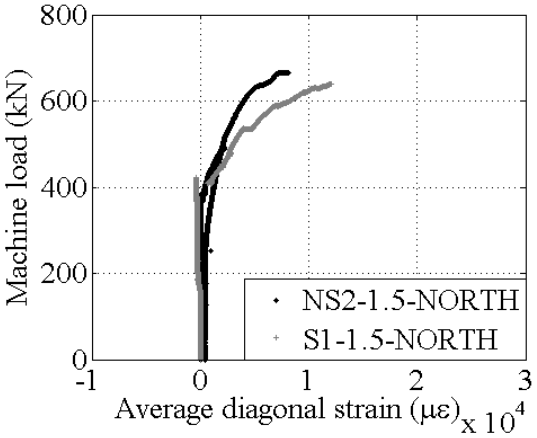

Figure 5- 27: Average diagonal strain for PR-1.5 beams

5.11.2 Discussion of the Concrete Strain Results for PR-U beams

As mentioned before in Chapter 4, the rosette stations for PR-U beams were placed at the same distance from the centre line of the supports as PR-3.5 beams. The purpose was to see if the concrete strains at the same location from the supports would change when a point load is replaced with distributed load. Since the spacing of stirrups were different in PR-U beams compared to PR-3.5 beams, the rosette stations in PR-U beams were 40 mm offset from the centre line of the adjacent stirrup. Therefore, the same analysis that was done for the previous beams can not apply to the PR-U beams, because the gauges were off centred from the stirrup.

Also, PR-U Series 1 and Series 2 beams did not have the same mode of failure as was the case for beams tested under four point bending. While Series 1 beams failed in shear between the mid-span of the beam and the north support, the Series 2 beams failed in tension right at the mid-span. The results from beams NS2 and S2 can be found in Figure 5-28. Results for NS1 and S1 beams can be found in Appendix D. It should be noted that the Pi-gauges did not always work properly all the way to failure, especially the 100 mm gauges measuring transverse strain.

The sudden jumps in the graphs (a) and (c) and subsequently (d) for S2-U in Figure 5-28, is also visible in Figure D-3 plots (b) and (c) for beam NS1-U. These jumps are due to Pi-gauges becoming loose and not recording correct strain values once the cracks occurred.

It can be seen in both Figure 5-28 and Figure D-3 that the cracking load from the graphs which is around 300 kN does not match the 400 kN reported in Table 5-4. The reason for that is that the value for shear cracking load in Table 5-4 refers to load at which the first diagonal web shear crack was observed. However, the rosette stations were placed away from the supports where they were crossed by diagonal cracks that extended from the tip of the flexural cracks. These flexural shear cracks occurred before the diagonal web shear cracks.

It is evident from comparison between Figure 5-26 and Figure 5-28 that the slope of the load-average strain in all 3 directions is higher for PR-U beams compared to PR-3.5 beams. Slope of the load-average diagonal strain for Series 1 PR-U and PR-3.5 beams was calculated based on the experimental results between 80% and 90% of the ultimate shear capacity of the beams. The slope for NS1 and NS2-3.5 beams were 0.00234 and 0.00415 respectively, while the same values for NS1 and NS2-U beams were 0.045 and 0.0144. It is evident that PR-U beams had higher post- cracking stiffness as it was also seen with the deflection results in Section 5.6.

The other thing that can be noticed from looking at load-average strain in the concrete for PR-U beams is the gradual transition from linear to non-linear behaviour. While, in PR-U beams the graph gradually curved from linear to non-linear behaviour, in PR-2.5 and 3.5 beams this transition was not gradual. The reason for that is the fact that the rosette stations on PR-2.5 and 3.5 beams were crossed by diagonal web shear cracks that occurred suddenly in a brittle manner. For PR-U beams as it was discussed earlier, the rosettes were placed in a location that was crossed mainly by flexural shear cracks that are not as brittle as web shear cracks. It should be noted that Series 1 PR-U beams actually failed at the location of one of the rosette stations and not at the diagonal cracks adjacent to the supports.

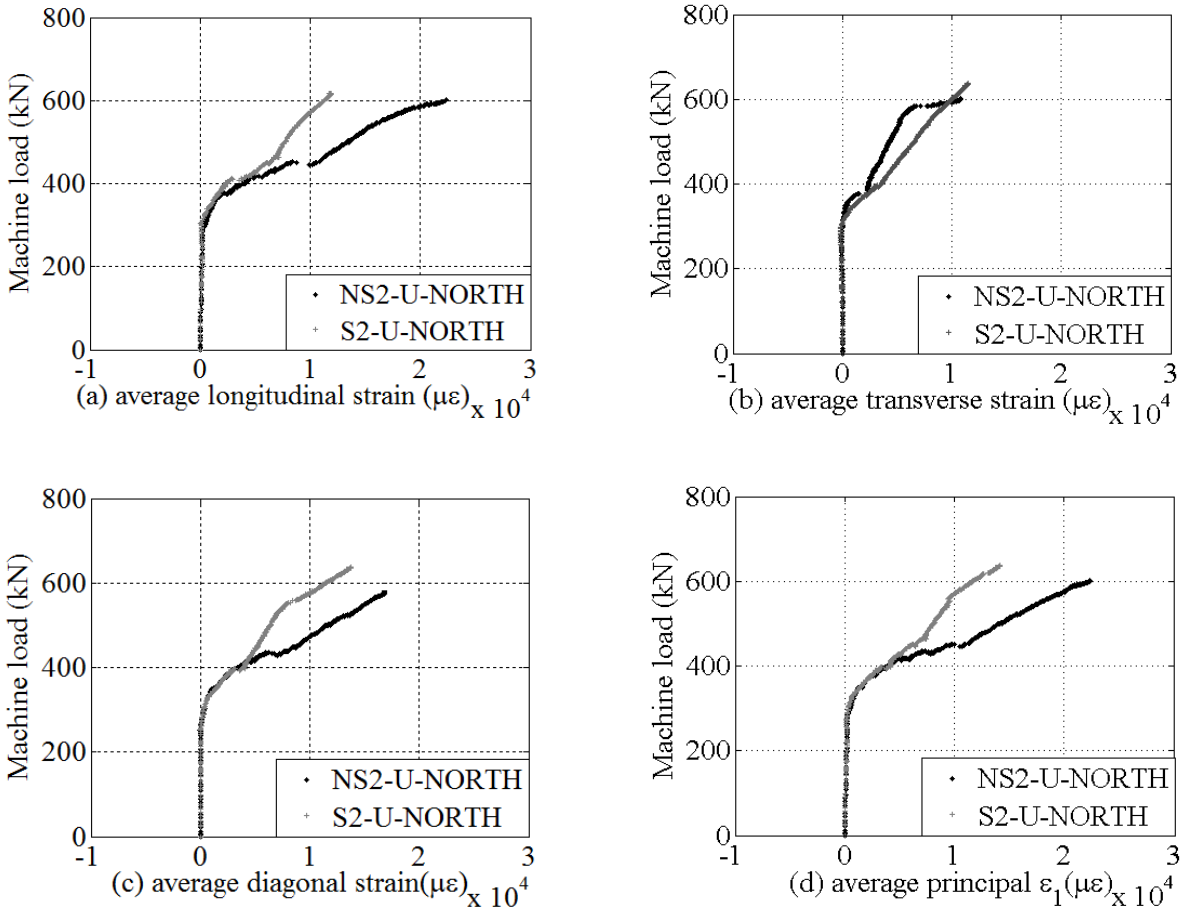

Figure 5- 28: Concrete strains for PR-U beams

5.12 Summary

The results from the experimental program were discussed in this chapter. It was shown that the shear strength of the FRP prestressed concrete T-beams tested in this project increased significantly as the a/d was reduced below 2.5. Also, the results showed that the post-cracking stiffness of the beams was a function of a/d and increased significantly when a/d was reduced to 1.5 from 2.5.

Results from the rosette stations installed within the shear span at the location of one of the stirrups showed that the stirrups restricted diagonal crack opening in PR-2.5 and PR-3.5 beams. The shear capacity of PR-2.5 and PR-3.5 beams increased by an average of 8% when stirrups were provided but the mode of failure did not change. In PR-U beams, the mode of failure of the beams shifted from diagonal tension to tension failure when stirrups were provided as the shear capacity of the beams exceeded their flexural capacity. Providing approximately the minimum required stirrups according to CSA-S6-10 (2010) in the PR-1.5 beams did not enhance their shear capacity or restrict diagonal crack opening at the location of the stirrup.

Based on Kani's formula (1966), the beams tested under distributed load in this project had an equivalent a/d = 2.1 which was close to that of PR-2.5 beams. It was shown that the behaviour of these two beam groups were relatively similar in terms of flexural cracking load, post-cracking stiffness, strain in the longitudinal reinforcement, and angle of diagonal shear cracks near the supports. However, the Series 1 PR-U beams that failed in diagonal tension had approximately 60% higher shear capacity compared to PR-2.5 beams. The equivalent a/d of PR-U beams was of course slightly less than 2.5 which means their capacity was expected to be slightly higher. However, the capacity of these beams would only be somewhat lower if the equivalent a/d for was exactly 2.5. Therefore, as Kani (1966) acknowledged himself four point bending was found to provide a conservative estimate of the shear capacity of beams subjected to distributed load, which is desirable for design related purposes.

6. Evaluation of the North American Shear Design Codes and Guidelines

6.1 General

The experimental values obtained for the shear resistance of the tested beams were compared to estimates from the major North American codes and guidelines for design with FRP. The latest versions of the Canadian Highway Bridge Design Code CSA-S6 (2010) general method and Design and Construction of Building Structures with Fibre Reinforced Polymers CSA-S806 (2012) were evaluated. Also, the guidelines from the America Concrete Institute ACI-440.4R (2004) for design of concrete structures prestressed with FRP were examined.

In case of PR-1.5 beams, the strut and tie models from CSA- A23.3 (2004), CSA-S6 (2010) and ACI-318 (2005) were evaluated as well as models proposed in literature (Tan et al. 2001, Wang et al. 2008). The behaviour of these beams was governed by arch action; therefore, the shear formulas in the codes could not be used to predict their capacity as they are based on beam behaviour. Only CSA-S806 (2012) provides a factor to account for arch action and it is therefore used along with the strut and tie models to predict the capacity of PR-1.5 beams.

It should be noted that the concrete shear resistance (V_c) was obtained based on the shear capacity of beams without stirrups. Also, the shear resistance of beams with stirrups (V_r) was predicted from theory and compared to the ultimate experimental capacity of the Series 2 beams.

In the following sections, the latest shear design formulas from CSA-S806 (2012), CSA-S6 (2010) and ACI-440.4R (2004) and ACI-440.4R (2006) are outlined. The theoretical shear resistance predictions are compared against values from experiment. Also, the performance of the design codes and guidelines are compared between FRP reinforced and prestressed concrete beams.

The Canadian Highway Bridge Design Code (CSA-S6-10) V_c formula from the general method is developed based on the modified compression field theory same as CSA-A23.3 (2004). The V_c formula in CSA-S6 (2010) is shown below (Clause 16.8.7 (a))

$$V_c = 2.5\phi_c \beta f_{cr} b d_v \qquad \text{Eq.6- 1}$$

ϕ_c is the resistance factor for concrete taken as 1.0 for calculations in this project and f_{cr} is the cracking strength of concrete and it is taken as the minimum of $0.4\sqrt{f'_c}$ or 3.2 MPa. For the case of concrete with a compressive strength of less than 65 MPa, f_{cr} will be equal to $0.4\sqrt{f'_c}$ which will make Eq.6-1 exactly the same as V_c formula for CSA-A23.3 (2004). The shear formulas for FRP reinforced concrete beams are essentially the same as those for steel reinforced concrete beams. The stirrup contribution is calculated according to the 45^o truss model. The variable σ_v is added for FRP stirrups to estimate the lower capacity of the FRP stirrups around the bend.

$$V_{FRP} = \frac{\phi_{FRP} A_v \sigma_v d_v \cot\theta}{s} \qquad \textbf{Eq.6- 2}$$

$$\sigma_v = \min\left(\frac{[(0.05r/d_s)+0.3] f_{FRPbend}}{1.5}, E_{vFRP}\varepsilon_v\right) \qquad \textbf{Eq.6- 3}$$

ϕ_{FRP} is the resistance factor for FRP, taken as 1.0 in this project; d_v is the effective shear depth of the longitudinal reinforcement; r is the radius of curvature of the bend of an FRP stirrup; d_s is the diameter of the stirrup; $f_{FRPbend}$ is the specified tensile strength of the straight portion of a bent FRP stirrup; and ε_v is the strain in a FRP stirrup taken as 0.004. The angle θ is calculated according CSA-S6-10 Clause 8.9.3.7.

6.2 Shear Formulas in CSA-S806-12

The current V_c shear formula in CSA-S806 (2012) is an improved version of the formula proposed by Razaqpur et al. (2004). In the proposed formula, the contribution of aggregate interlock and uncracked concrete were separated as the first one is a function of cubic root of the axial stiffness of longitudinal reinforcement, while the latter was found to be a function of $\sqrt{f'_c}$. Also new factors were introduced to account for the interaction of shear and moment at a section in the beam, arch action, size effect, and the longitudinal reinforcement stiffness.

Razaqpur et al. (2011) modified the original formula and among the changes was the addition of the decompression moment multiplied by the ratio of factored shear over factored moment for FRP prestressed concrete beams. The new term considers the effect of prestressing in enhancing the shear resistance of FRP reinforced concrete beams. Also, the square root of f'_c was replaced with cubic root of f'_c.

$$V_r = V_c + V_{FRP} + 0.5V_p + \frac{M_{dc}V_f}{M_f}$$ **Eq.6- 4**

$$V_c = 0.05\phi_c k_m k_r (f_c')^{1/3} b_w d_v$$ **Eq.6- 5**

$$k_m = \sqrt{\frac{V_f d}{M_f}} \leq 1.0$$ **Eq.6- 6**

$$k_r = 1 + (E_f \varphi_f)^{1/3}$$ **Eq.6- 7**

k_m accounts for the effect of the interaction of factored shear and moment at a section of the beam on its shear resistance or the effect of a/d; k_r represents the effect of longitudinal reinforcement rigidity with ρ_f being the longitudinal reinforcement ratio. Eq.6-5 is valid for members with an effective depth of less than 300 mm. For larger members and members with less transverse reinforcement than required, Eq.6-5 is multiplied by the size factor k_s:

$$k_s = \frac{750}{450 + d}$$ **Eq.6- 8**

Also, for sections located within 2.5d from the face of the support when the support reaction causes compression in the beam parallel to the shear force, the following factor is included in the V_c formula:

$$k_a = \frac{2.5}{M_f / V_f d} \qquad [1.0 \leq k_a \leq 2.5]$$ **Eq.6- 9**

This was the case for the PR-1.5 beams in this project. The factor k_a was adopted from Zsutty's equations for steel reinforced concrete beams to account for arch action in deep beams (Zsutty 1968).

The contribution of the FRP transverse reinforcements is calculated as follows:

$$V_{FRP} = \frac{0.4\phi_{FRP} A_{Fv} f_{Fu} d_v}{s} \cot\theta$$ **Eq.6- 10**

$$\theta = 30 + 7000.\varepsilon_x$$ **Eq.6- 11**

ϕ_{FRP} is the material resistance factor for FRP taken as 1.0 in this case; f_{Fu} is the ultimate strength of the FRP shear reinforcement and cannot be greater than $0.005.E_f$. The capacity of the stirrup at

the bend is taken as 40% of the ultimate capacity of the stirrup at the straight portion; ε_x is the longitudinal strain at mid-depth of the section (CSA-S806-12 Clause 8.4.4.9)

6.3 Shear Formulas in ACI-440.1R (2006)

ACI 440.1R-06 guidelines recommend the following formula for design of concrete beams reinforced with FRP:

$$V_c = \frac{2}{5}\sqrt{f_c^{'}}\, b_w c \qquad \textbf{Eq.6- 12}$$

b_w is width of the web; c is neutral axis depth in cracked transformed section; $f_c^{'}$ is compressive strength of concrete.

ACI 440.4R-04 (2004) recommends Eq.6-13 (Clause 5.2) for estimating V_c for prestressing concrete structure with FRP tendons:

$$V_c = 0.17\sqrt{f_c^{'}}\, b_w d_v \qquad \textbf{Eq.6- 13}$$

The ACI 440.4R-04 (2004) uses the V_{cmin} formula for steel prestressed concrete beams based on research by Dowden et al. (1997) who found Eq.6-13 to be the best match for FRP prestressed concrete beams tested by Yonekura et al. (1993). The authors applied several ACI equations to the test results from 10 concrete beams prestressed with CFRP and AFRP tendons with transverse FRP spiral reinforcement. Eq. 6-13 was found to provide the best conservative estimate for the test results with an average ratio of experimental to theoretical nominal shear strength of 1.14.

Eq. 6-13 was not expanded beyond recommendations of Dowden et al. (1997) due to lack of sufficient research and the fact that FRP prestressed concrete beams are likely to develop wider cracks than steel counterparts (ACI 440.4R-04). However, the findings by Dowden et al. (1997) were based on a limited data from Yonekura et al. (1993) and may not always be applicable. This is especially true since Eq. 6- 13 includes no provisions to account for the beneficial effect of prestressing in enhancing the shear capacity of FRP reinforced concrete beams. The contribution of the FRP stirrups is calculated according to 45^o truss model as shown below:

$$V_{fv} = \frac{A_{fv}\, f_{FRPbend}\, d_v}{s} \qquad \textbf{Eq.6- 14}$$

$$f_{FRPbend} = \min(\phi_{bend} f_{Fu}, 0.002E_{vFRP}) \quad \textbf{Eq.6- 15}$$

$$\phi_{bend} = (0.11 + 0.05\frac{r}{d_s}) \quad \textbf{Eq.6- 16}$$

In Equations 6-14 to 6-16, $f_{FRPbend}$ is the stress in the bent stirrup; ϕ_{bend} accounts for the reduction in the strength of the FRP stirrup at the bend and should be $0.25 \leq \phi_{bend} \leq 1.0$; r and d_s are the radius of the bend and diameter of the FRP stirrup respectively.

6.4 Comparison of the Experimental Results with Theoretical Estimates

In this section the experimental shear strength of beam specimens is compared to theoretical estimates from the design codes and guideline listed in Section 6.2 and 6.3. PR-1.5 beams are evaluated separately in Section 6.6, since the behaviour of these beams unlike the other specimens was governed by arch action. As mentioned earlier, the shear formulas listed previously are developed based on beam behaviour and therefore did not apply to PR-1.5 beams except for CSA-S806 (2012) that includes a factor for arch action. Table 6-1 and Table 6-2 compare the average experimental capacity of the slender beams with the theoretical estimates from the design codes. The experimental load in Table 6-1 is equal to the shear force at the support or half the total load applied by the test machine and the estimate from design codes represent the theoretical shear capacity of the beams.

Table 6- 1: Comparison between experimental values and theoretical estimates

Beams	Series 1 Beams with no Stirrups				Series 2 Beams with Stirrups			
	P_{expavg} [kN]	ACI [kN]	CSA-S806 [kN]	CSA-S6 [kN]	P_{expavg} [kN]	ACI [kN]	CSA-S806 [kN]	CSA-S6 [kN]
PR-2.5	184	34	110	97	201	39	117	117
PR-3.5	148	34	88	97	160	39	96	117
PR-U	300	35	190	98	321	41	196	121

For beams S1-U and S2-U, ratio of experimental to theoretical values is not provided in Table 6-2, since these beams did not fail in shear. This could be the reason the average ratio of experimental to theoretical shear capacity for ACI 440.4R-04 (2004) and CSA-S6-10 (2010) is higher for Series 1 compared to Series 2 beams. The experimental load for Series 2 PR-U beams corresponds to the flexural capacity of the beams as they failed in tension, which shows their shear capacity exceeded their flexural capacity as a result of the addition of stirrups. The

predictions from all the design codes for Series 2 PR-U beams is significantly less than the actual failure load for these beams which means theoretically these beam had to fail in shear.

Table 6- 2: Ratio of experimental to theoretical shear capacity

Beam Groups	Ratio of experimental to theoretical shear capacity					
	Series 1 Beams with no Stirrups			Series 2 Beams with Stirrups		
	ACI	CSA-S806	CSA-S6	ACI	CSA-S806	CSA-S6
PR-2.5	5.41	1.67	1.90	5.15	1.72	1.72
PR-3.5	4.35	1.68	1.53	4.10	1.67	1.37
PR-U	8.57	1.58	3.06	-	-	-
Average	6.10	1.64	2.16	4.62	1.69	1.54

The CSA-S806 (2012) code was the least conservative for Series 1 PR-U beams, which shows CSA-S806 (2012) is more adaptable to change in loading scheme from four point bending to distributed loading. The ratio of experimental to theoretical shear capacity remained consistent for CSA-S806 (2012) through all beam groups for Series 1 beams. However, both CSA-S6 (2010) and ACI 440.4R-04 (2004) were significantly more conservative than CSA-S806 (2012) for Series 1 PR-U beams compared to PR-2.5 and PR-3.5 beams. CSA-S6 (2010) was approximately 13% more conservative than CSA-S806 (2012) for PR-2.5 beams and was 9% less conservative for PR-3.5 beams. However, CSA-S6 (2010) was approximately 93% more conservative than CSA-S806 (2012) for Series 1 PR-U beams. ACI 440.4R-04 (2004) was on average approximately 3 times more conservative than CSA-S6 (2010) and almost 4 times more conservative than CSA-S806 (2012) for Series 1 beams.

Also, from Table 6-1, it can be seen that the capacity of the beams increased by providing transverse reinforcement for all the beam groups that were evaluated. For PR-U beams, the failure mode shifted from diagonal shear to flexural tension failure when stirrups were placed along the span of the beams. Comparing the theoretical shear capacity of Series 1 and 2 beams, it is evident that CSA-S6 (2010) had an estimate of approximately 20 kN for the contribution of the stirrups. However, both CSA-S806 (2012) and ACI 440.4R-04 (2004) estimated approximately 6 kN for the stirrups contribution due to their conservative estimate of the strength of the stirrup at the bend. CSA-S6 (2010) provided the highest estimate for capacity of FRP stirrups. The experimental results showed improvement of about 15 kN in the shear capacity of PR-2.5 and

PR-3.5 beams due to addition of the stirrups which corresponded to approximately 8% increase in shear capacity. For Series 2 PR-U beams the full contribution of the stirrups was not utilised since these beams failed in flexure before their ultimate shear capacity was reached. It should be noted that the net improvement in the experimental shear capacity between Series 1 and Series 2 beams is not an indication of the value of V_s. The concrete shear resistance mechanisms such as aggregate interlock are affected by the presence of stirrups and are therefore not the same between beams with and without stirrups.

6.5 Code Estimates for FRP Reinforced and Prestressed Concrete Beams

Results from this project along with a database of FRP reinforced and prestressed concrete beams were used to evaluate the performance of the shear formulas for FRP prestressed concrete beams compared to FRP reinforced beams. Table 6-3 and Table 6-4 list the databases for FRP reinforced and FRP prestressed concrete beams respectively. The results for PR-1.5 beams in this project were not included because the behaviour of these beams was governed by arch action. All the beams included in the analysis failed in shear and did not include transverse reinforcement. It is evident from Table 6-4 that the available data for FRP prestressed concrete beams is very limited, while Table 6-3 is only a portion of data available for FRP reinforced concrete beams.

Table 6- 3: Database of FRP reinforced concrete beams

Reference	a/d	No. Reinforced specimens
Alkhrdaji et al. (2001)	2.6	3
Gross et al. (2004)	6.3	8
Matta et al. (2008)	3.1	3
Mota (2005)	2.8-3.09	4
Nishikawa et al.(1993)	2.57	3
Razaqpur et al. (2004)	2.67-4.5	5
Tureyen et al. (2002)	3.4	4
Whitehead et al. (2005)	3.1	2
Yost et al. (2001)	4.1	6
Zhao et al. (1995)	3	2

Table 6- 4: Database of FRP prestressed concrete beams

Reference	a/d	No. Prestressed specimens	f_{pe} [$\%f_{pu}$]
Nishikawa et al.(1993)	2.57	6	0.3-0.6
Sang et al. (1999)	2.5	2	0.51
Whitehead et al. (2005)	3.1	4	0.4

Figure 6-1 and Figure 6-2 show the results for FRP reinforced and prestressed concrete beams. The experimental load refers to the magnitude of the ultimate shear force at the supports. Both CSA-S806-12 (2012) and CSA-S6-10 (2010) provided reasonable estimates of the experimental results for FRP reinforced concrete beams. The average ratio of experimental to theoretical shear capacity for FRP reinforced concrete beams was 1.18 for CSA-S806-12 (2012) and 1.14 for CSA-S6-10 (2010) (Table 6- 5). ACI 440.1R-06 (2006) was more conservative compared to CSA-S806 (2012) and CSA-S6-10 (2010) for FRP reinforced concrete beams as shown in Figure 6-1. The average ratio of experimental to theoretical shear capacity for FRP reinforced concrete beams was 2.02 for ACI 440.1R-06 (2006) which was almost twice the average ratio of CSA-S6-10 (2010) and CSA-S806-12 (2012).

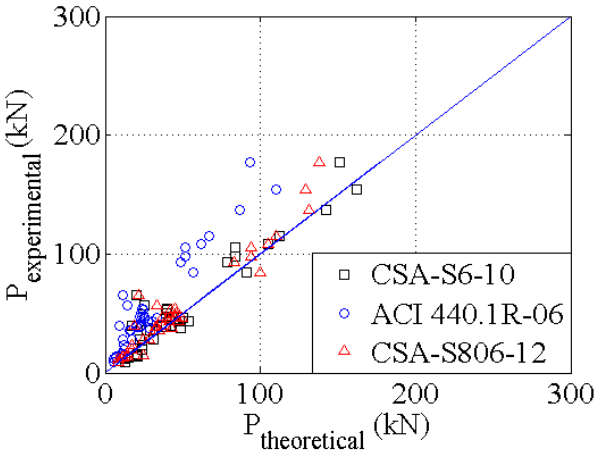

Figure 6- 1: Reinforced concrete database

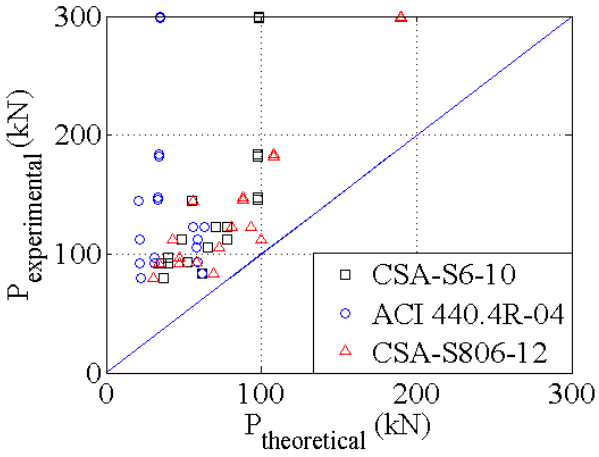

Figure 6- 2: Prestressed concrete database

Table 6- 5: Average ratio of experimental to theoretical loads

Design Codes	Ratio of experimental to theoretical shear capacity					
	Reinforced concrete beams			Prestressed concrete beams		
	CSA-S6	ACI 440.1R	CSA-S806	CSA-S6	ACI 440.4R	CSA-S806
Average	1.14	2.02	1.18	2.04	4.08	1.82
St. Dev.	0.48	0.86	0.38	0.54	2.26	0.50
COV [%]	42	43	32	26	55	29

All the design codes and guidelines that were evaluated were significantly more conservative for FRP prestressed concrete beams compared to reinforced concrete beams (Figure 6-1 and Figure 6-2). ACI 440.4R-04 (2004) was significantly more conservative for prestressed concrete beams than CSA codes since it does not account for the effect of prestressing in enhancing the shear capacity of the beams. The average ratio of experimental to theoretical shear capacity of FRP prestressed concrete beams was 4.08 for ACI 440.4R-04 (2004) compared to 1.82 and 2.04 for CSA-S806 (2012) and CSA-S6 (2010) respectively (Table 6-5). The data points on the top border of Figure 6-2 refer to the results from Series 1 PR-U beams.

Beside PR-U beams that were tested under distributed load, the other beams included in the analysis were all tested under four or three point bending. However, the beams varied in longitudinal reinforcement ratio, a/d, compressive strength of concrete, level of prestressing, size and type of FRP longitudinal reinforcement. The beam designs also varied in width of the web and effective depth of the longitudinal reinforcement. Considering these variations the COV can be an indication of the versatility of the shear design formulas. It can be seen in Table 6-5 that for FRP prestressed concrete beams, the COV is 29% and 26% for CSA-S806 (2012) and CSA-S6 (2010) respectively but 55% for ACI 440.4R-04 (2004). This shows that CSA-S806 (2012) and CSA-S6 (2010) have relatively wider range of applicability compared to ACI 440.4R-04 (2004) for FRP prestressed concrete beams.

6.6 Strut and Tie Models for Estimating the Capacity of PR-1.5 Beams

The strut and tie models outlined in Section 3.6 were used to evaluate the capacity of PR-1.5 beams. As mentioned earlier, arch action was the governing behaviour for PR-1.5 beams but it also developed to a lesser extent in PR-2.5 beams. However, using the strut and tie models for

these beams resulted in significantly over estimating their capacity which is expected considering their behaviour was governed by beam action.

The strut and tie models that were evaluated, varied in their estimates of the capacity of the compressive strut and tension tie as well as the nodal capacities. The overall modelling of the beam and the location of the tension tie and compressive struts remained the same among all models. The method shown in the CPCI design handbook was followed to calculate the capacity of the beams based on CSA and ACI methods (CPCI handbook 2007). For Tan et al. (2001) and Wang et al. (2008) models, the procedure outlined by the authors was followed. For Tan et al. (2001) model, the changes proposed later to the model for reinforced concrete beams were incorporated in to the model for prestressed concrete beams (Tan et al. 2001). The detailing of the strut and tie model for PR-1.5 beams is outlined in Appendix E along with the procedure for determining the shear strength of the beams using the modified Tan et al. (2001) model. The results based on the original model over estimated the capacity of PR-1.5 beams, however incorporating the changes added a slight level of conservatism.

All the strut and tie models that were used here were developed for steel reinforced concrete beams. However, since the beams tested in this project did not have any non-prestressed reinforcement, the relative term that requires value for the yield stress of steel (f_{py}) was omitted. Also, arch action is governed by the a/d ratio and concrete compressive strength and in case of concrete crushing; it is independent of the longitudinal reinforcement properties. Therefore, the aforementioned strut and tie models are applicable to structures utilising FRP, provided proper anchorage is provided for the compressive struts to avoid failure of the flexural tension reinforcement (Razaqpur et al. 2004).

The results of the comparison between the different strut and tie models that were analysed can be found in Table 6-6. Since approximately minimum required stirrups were provided and no contribution from the stirrups was observed, their effect was ignored in the analysis for S1-1.5 and S2-1.5 beams. Apart from beam S2-1.5, all the beams failed by concrete crushing at the load points as discussed earlier. Nevertheless, the results from S1-1.5 and S2-1.5 beams were included in the average experimental load. Including S2-1.5 lowered the average experimental load by only 5 kN.

Table 6- 6: Results from strut and tie models

Experimental results		Strut and Tie Models					
Beams	Pexp [kN]	CSA-A23.3 [kN]	CSA-S6 [kN]	ACI-318 [kN]	Modified Tan model [kN]	CSA-S806 [kN]	Wang model [kN]
NS1-1.5	328	184	180	129	312	207	344
S1-1.5	320						
NS2-1.5	333						
S2-1.5	307						
P_{expavg} / Model		1.75	1.79	2.49	1.03	1.55	0.93

As it can be seen from Table 6-6, the ACI.318 (2005) strut and tie model gave the most conservative estimate when compared to the average experimental load. The CSA-S806 (2012) V_c formula provided a reasonable estimate for capacity of PR-1.5 beams and was 13% less conservative than CSA A23.3 (2004) strut and tie model. The strut and tie model proposed by CSA-S806 (2012) is similar to CSA A23.3 (2004) model and therefore was not evaluated here. Modified Tan et al. (2001) and Wang et al. (2008) models provided the best predictions of the experimental results; however the Wang et al. (2008) model was unconservative. The Tan et al. (2001) model provided the best estimate after the changes to the model for reinforced concrete deep beams (Zhang et al. 2007) were incorporated into the Tan et al. (2001) model for prestressed concrete deep beams.

6.7 Variability of the Code Predictions with a/d Ratio

This project showed that the strength of FRP prestressed concrete beams varies with the a/d ratio which indicates the effect of moment and shear interaction on the beam's shear capacity. However, from the design codes evaluated here, only CSA-S806 (2012) considers the effect of a/d ratio on shear resistance of concrete beams. In this section, the variability of the design code predictions with a/d ratio is examined using the data from the Series 1 beams tested under four point bending. The capacity of PR-1.5 beams was estimated based on the analysis outlined in Section 6.6. Figure 6-3 shows the variation in code predictions and experimental shear resistance of the beams with respect to a/d ratio.

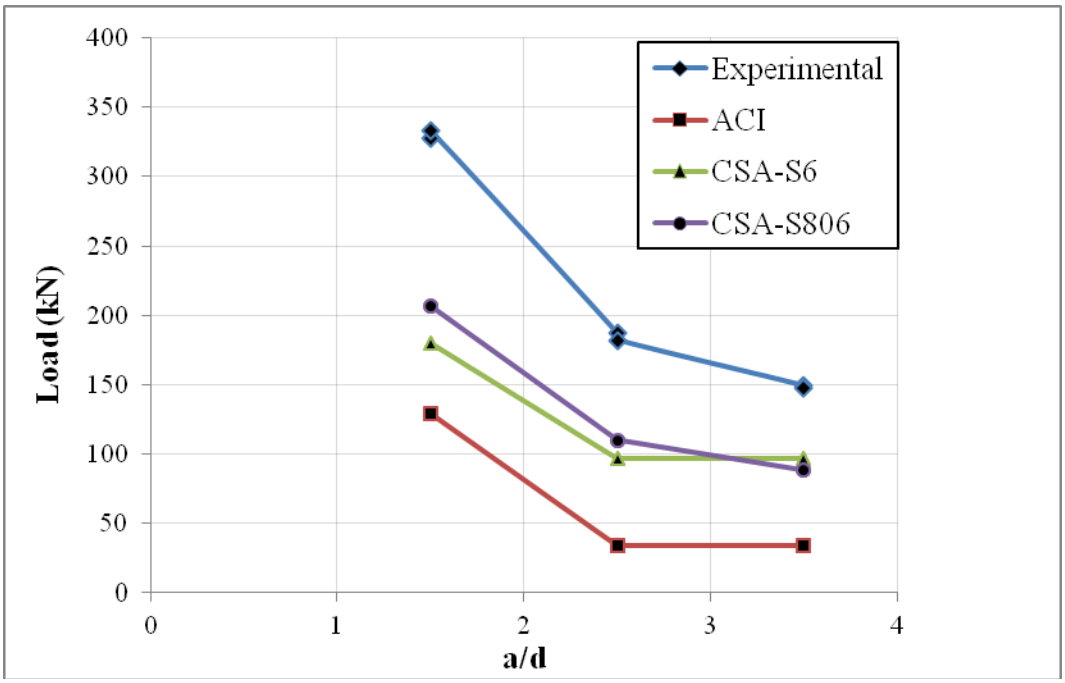

Figure 6- 3: Variability of the code predictions with a/d ratio

As it can be seen from Figure 6-3, the data points were connected with straight lines to see the trend in data as the a/d changed. A trend line was not passed through the data points since no data was available beyond a/d = 3.5. The figure shows that as the a/d was reduced below 2.5, the strength of the beams increased significantly due to the contribution of arch action. The increase in shear resistance was much less when the a/d was reduced from 3.5 to 2.5. Wang et al. (2011) also noticed a similar trend for CFRP prestressed concrete beams without transverse

reinforcement. The study showed that the shear capacity of the beams increased by 72% as the a/d ratio was reduced from 2.14 to 1.43.

Looking at the code estimates of the shear capacity of the beams with respect to the a/d ratio, it can be seen that CSA-S806 (2012) provides the best match for the trend seen with the experimental results. For both CSA-S6 (2010) and ACI 440.4R-04 (2004), the V_c shear formula showed no variation in strength as the a/d was varied from 2.5 to 3.5. While, the graph for CSA-S806 (2012) sloped down between 2.5 and 3.5 ratio, the other codes showed a flat line. It can also be seen from the figure that the CSA-S6 (2010) prediction of the capacity of the beams was close to that of CSA-S806 (2012), while ACI guidelines were much more conservative.

6.8 Summary

In this chapter, the shear capacity of the beams tested in this project were compared to estimates from the shear formulas in the current North American design codes. It was shown that CSA-S6-10 (2010) provided the highest estimate for the capacity of the GFRP stirrups. The variation in shear strength with a/d ratio that was noticed in the experimental results was only matched by CSA-S806-12 (2012) that includes a factor to account for the effect of a/d ratio. Also, the V_c formula from CSA-S806-12 (2012) maintained the same level of conservatism through all the beam groups. However, CSA-S6-10 (2010) and ACI-440.4R-04 (2004) were significantly more conservative for Series 1 PR-U beams compared to PR-2.5 and PR-3.5 beams.

The shear formulas from the design codes and guidelines were also compared for FRP reinforced and FRP prestressed concrete beams based on data available in literature and results from this project. ACI guidelines were found to be significantly more conservative for both FRP reinforced and FRP prestressed concrete beams compared to the CSA codes. The CSA codes were both reasonably conservative for FRP reinforced concrete beams, while CSA-S806-12 (2012) provided the best estimate for FRP prestressed concrete beams. Evaluating the available strut and tie models also showed that the modified model by Tan et al. (2001) provided the best estimate of the shear capacity of PR-1.5 beams.

7. Conclusions and Recommendations

7.1 General

This project investigated the effect of shear span to depth ratio (a/d) on shear behaviour of concrete beams prestressed with CFRP cables. The variation in the behaviour of the beams was analysed from perspective of deflection, strength, crack pattern, failure mode and concrete strains in the shear critical regions. Also, the contribution of FRP stirrups in slender and deep concrete beams was studied.

The shear behaviour of the beams was also investigated for beams subjected to distributed load and four point bending which is the conventional shear testing method for concrete beams. The results showed that distributing the load over the span as opposed to applying two point loads allows the beams to reach higher shear capacity.

The CSA (CSA-S806-12, CSA-S6-10), and ACI (ACI-440.1R-06 and ACI-440.4R-04) shear formulas were investigated for FRP reinforced and prestressed concrete beams based on results collected from literature and this project. Also, various strut and tie models were evaluated for estimating the capacity of the FRP prestressed deep beams tested in this project.

7.2 Variation in Shear Behaviour of the Beams with a/d Ratio

[1] The inclined cracking load of the beams increased by 39% as the a/d was reduced below 2.5, while the ultimate shear capacity of the beams increased by 80% due to contribution of arch action.

[2] The deformability of the beams decreased significantly when the a/d was reduced below 2.5, while the post-cracking stiffness of the beams increased. The increase in stiffness was minimal when a/d was reduced to 2.5 from 3.5.

[3] Behaviour of beams with a/d of 2.5 and 3.5 was governed by beam action and the beams failed in diagonal tension shortly after diagonal cracking. However, beams with a/d of 1.5 were able to carry significant additional shear load beyond diagonal cracking due to arch action and failed in shear compression at the load points or the concrete crushed in between the load points.

[4] Approximately minimum required stirrups were provided in 2 out of 4 beams in each of the four beam groups. The shear capacity of beams with a/d = 2.5, 3.5 approximately increased by 8% when transverse reinforcement was added; however no increase in strength was observed for beams with a/d = 1.5. For beams tested under distributed load, the mode of failure shifted from diagonal tension to flexural tension failure when stirrups were provided. However, the full contribution of the stirrups was not utilised because the shear capacity of these beams exceeded their flexural capacity.

[5] The angle of the diagonal web shear cracks increased with decrease in the a/d ratio as the distance between the load points and the supports was reduced.

[6] The strain in the longitudinal reinforcement at ultimate was approximately 40% higher for beams with a/d = 1.5, compared to beams with a/d = 2.5, 3.5. This was due to arch action that developed in beams with a/d = 1.5, which relied heavily on the longitudinal reinforcements as tension tie of the arch.

[7] Results from rosette stations in the shear critical regions of the beams showed that the stirrups restricted the diagonal crack opening in beams with a/d = 2.5,3.5. Also, the slope of the ascending branch of the load with respect to measured average diagonal tensile strain decreased as the a/d ratio was increased.

7.3 Behaviour of the Beams under Distributed Load

[1] Applying Kani's (1966) analogy to beams tested under distributed load in this project, provided a corresponding a/d = 2.1 which was close to that of beams tested under four point bending with a/d = 2.5. The flexural cracking load, post-cracking stiffness, angle of diagonal web shear cracks near the supports and strain in the longitudinal reinforcement were relatively similar between the two beam groups. The results seemed to confirm Kani's argument that distributed load is best approximated with a four point bending setup with two load point at quarter spans.

[2] The diagonal shear cracking load was 42% higher for beams tested under distributed load, while the ultimate shear capacity of the beams was 63% higher compared to beams tested with a/d = 2.5. Somewhat higher shear capacity was expected for PR-U beams compared to PR-2.5 beams since the equivalent a/d for PR-U beams using Kani's analogy (1966) was slightly less than 2.5. However, the shear capacity of PR-U beams is not expected to be

much less if the PR-U beams were designed with an equivalent a/d of exactly 2.5. Therefore, it is evident that a four point bending test provides a more conservative estimate of the shear capacity of beams subjected to distributed load which is desirable for design purposes.

[3] The beams without stirrups that were subjected to distributed load failed in diagonal tension similar to PR-2.5 and PR-3.5 beams; however, the location of failure changed. Beams tested under four point bending failed at the diagonal crack adjacent to the support that extended from the load point to the support. However, the beams subjected to distributed load did not fail at the diagonal cracks near the support and the location of failure was slightly closer to mid-span of the beams.

[4] The slope of the load-strain curves in longitudinal, diagonal and transverse directions increased for beams tested under distributed load compared to beams tested under four point bending with a/d = 3.5 at the same distance from the centre of the supports. This was due to higher post-cracking stiffness of PR-U beams compared to PR-3.5 beams.

7.4 Evaluation of North American Design Codes and Guidelines

[1] Evaluation of the latest versions of CSA-S806-12 (2012), CSA-S6-10 (2010) and ACI 440-1R-06 (2006), and ACI 440-4R-04 (2004) shear design formulas for FRP reinforced and prestressed concrete beams proved that all the design codes are more conservative for FRP prestressed concrete beams compared to FRP reinforced concrete beams.

[2] ACI guidelines were found to be the most conservative especially for FRP prestressed concrete beams. ACI 440-4R-04 (2004) shear formula for calculating V_c for FRP prestressed concrete has no provisions to account for beneficial effect of prestressing in enhancing the shear capacity of FRP reinforced concrete beams.

[3] CSA-S806-12 (2012) and CSA-S6-10 (2010) approximately provided the same level of conservatism for FRP reinforced concrete beams, while CSA-S806-12 (2012) was on average 12% less conservative than CSA-S6-10 (2010) for FRP prestressed concrete beams. The beams evaluated in the study included both results from this project and data from literature.

[4] Both CSA-S6-10 (2010) and ACI 440-4R-04 (2004) were significantly more conservative for beams tested under distributed load compared to beams tested under four point bending, while CSA-S806-12 (2012) maintained a consistent level of conservatism through all beam groups.

[5] Both CSA-S806-12 (2012) and CSA-S6-10 (2010) were found to be more versatile with respect to variation in a/d, size of the beams, longitudinal reinforcement ratio and type of loading compared to ACI guidelines.

[6] CSA-S6-10 (2010) provided the highest estimate for the shear capacity of the GFRP stirrups.

[7] A modified strut and tie model proposed by Tan et al. (2001) was found to provide the best estimate for the shear capacity of beams tested with a/d = 1.5. The changes proposed by Zhang and Tan (2007) for reinforced concrete deep beams were incorporated into Tan et al. (2001) model for prestressed deep beams. The strut and tie model proposed by ACI-318 (2005) was found to be the most conservative.

7.5 Recommendations

[1] This research showed that minimum required FRP stirrups are ineffective in FRP reinforced concrete deep beams with a/d = 1.5. However, it is possible that sufficient amount of FRP stirrups would actually make a difference. Therefore, it will be beneficial to further study the effect of stirrups on the shear capacity of FRP reinforced and prestressed concrete deep beams for different ratios of web reinforcement.

[2] The effect of different factors such as size of the beam, level of prestressing and ratio of longitudinal reinforcement on the shear behaviour of beams subjected to distributed load should be studied.

[3] The current North American shear design codes are more conservative for FRP prestressed concrete beams compared to FRP reinforced concrete beams. The limited database that was compiled in this project included other variables beside level of prestressing such as longitudinal reinforcement ratio, FRP material and size of the beams It will be useful to study the effect of each of these variables separately on the shear behaviour of FRP prestressed beams and see how they affect the level of conservatism of the shear formulas.

Appendix A

Strain in Concrete and Bottom Longitudinal Reinforcement at Mid-span

Compressive strains in the flange

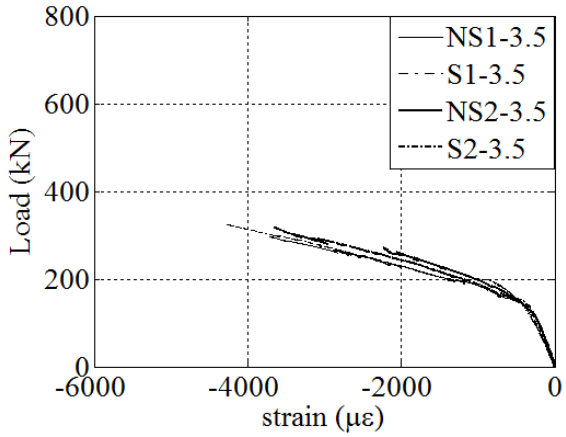

Figure A- 1: Concrete compressive strain (PR-3.5 beams)

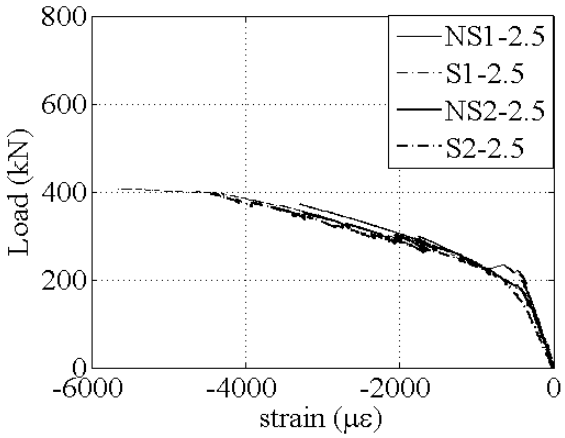

Figure A- 2: Concrete compressive strain (PR-2.5 beams)

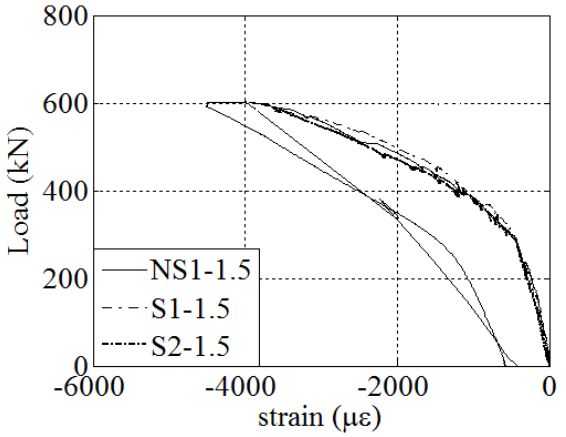

Figure A- 3: Concrete compressive strain (PR-1.5 beams)

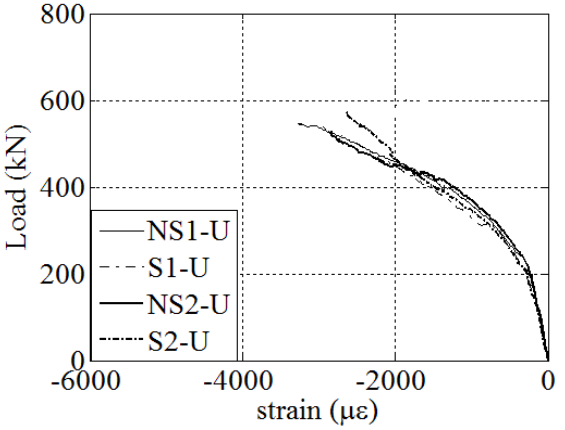

Figure A- 4: Concrete compressive strain (PR-U beams)

Strain in Bottom Longitudinal Reinforcement

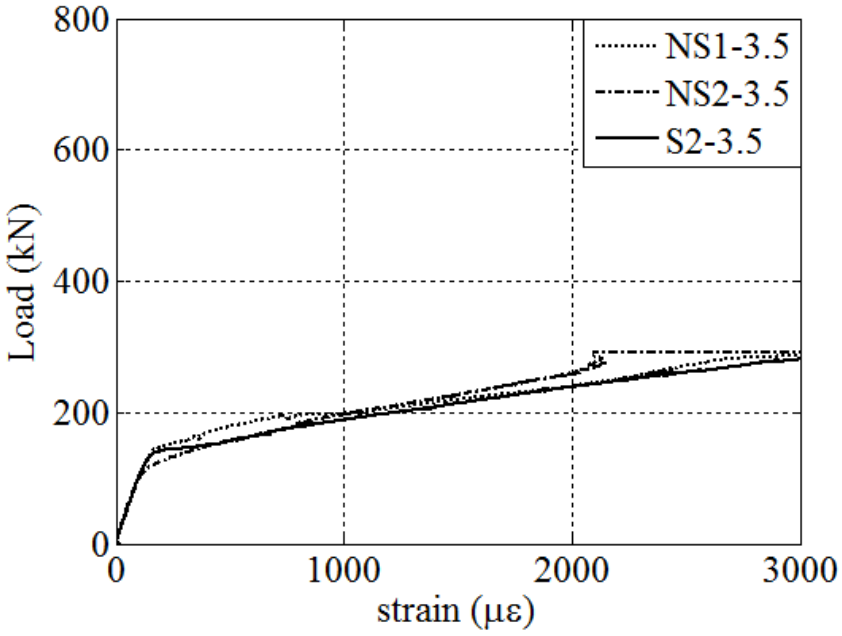

Figure A- 5: Bottom strand strain for PR-3.5 beams

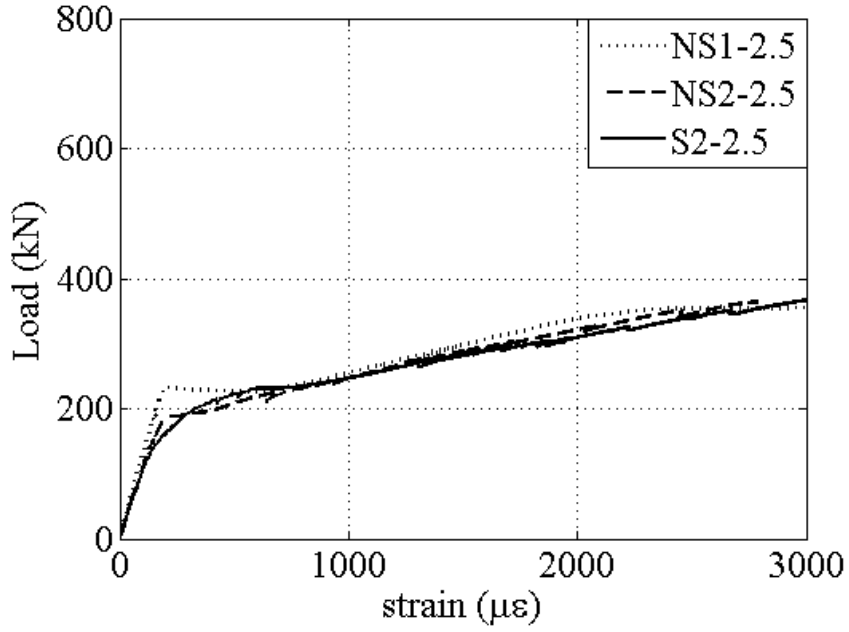

Figure A- 6: Bottom strand strain for PR-2.5 beams

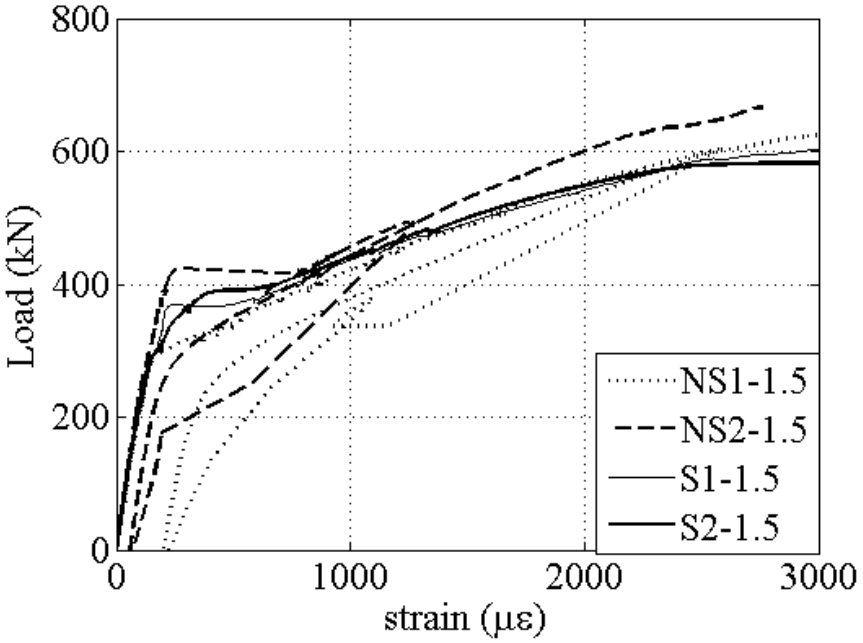

Figure A- 7: Bottom strand strain for PR-1.5 beams

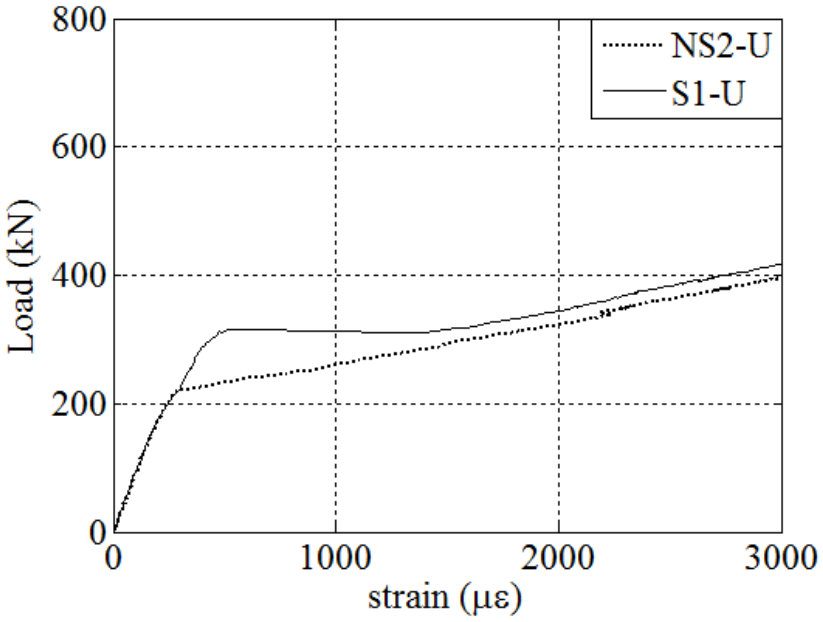

Figure A- 8: Bottom strand strain for PR-U beams

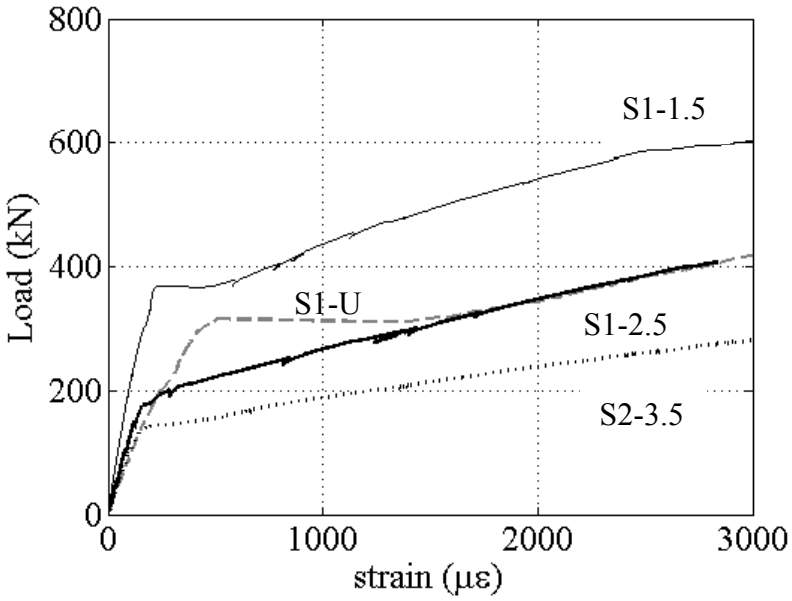

Figure A- 9: Load-strain behaviour in the bottom strands for Series 2 beams

Strain in Concrete at the Level of Bottom Reinforcement

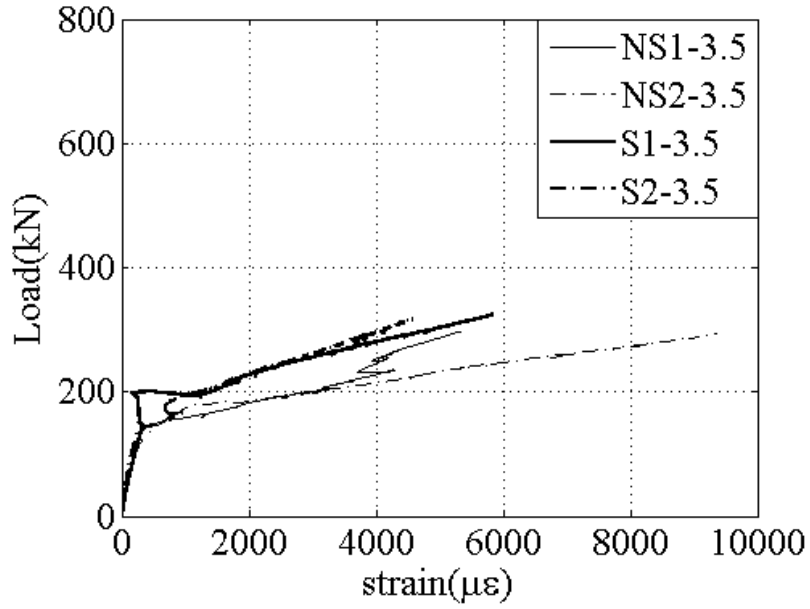

Figure A- 10: Concrete strain at level of bottom reinforcement for PR-3.5 beams

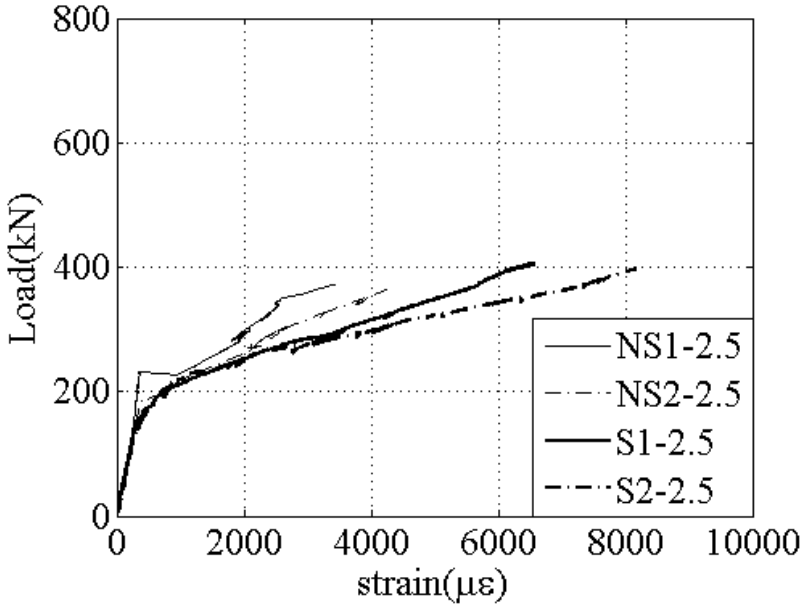

Figure A- 11: Concrete strain at level of bottom reinforcement for PR-2.5 beams

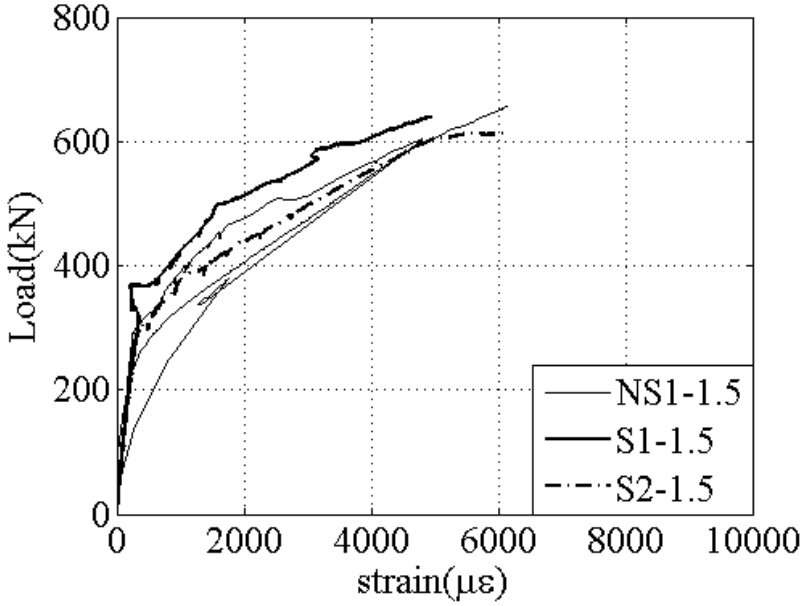

Figure A- 12: Concrete strain at level of bottom reinforcement for PR-1.5 beams

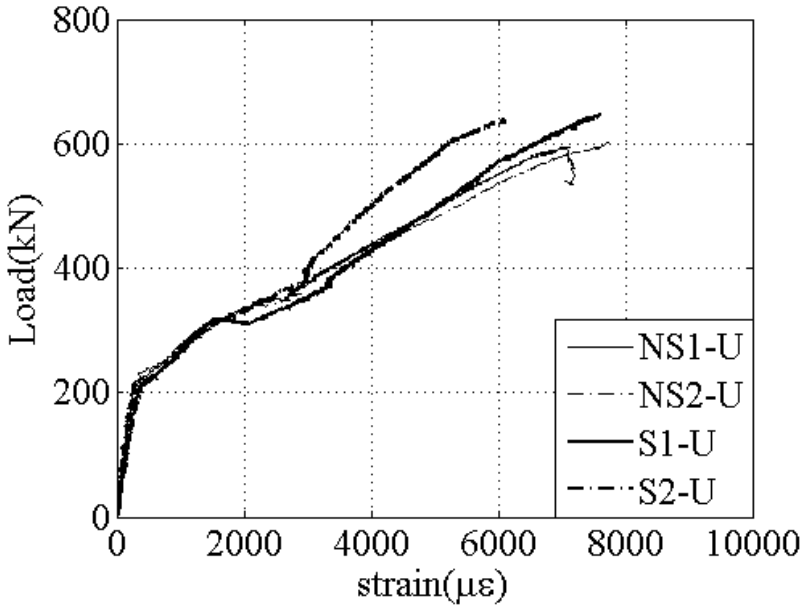

Figure A- 13: Concrete strain at level of bottom reinforcement for PR-U beams

Strain in Concrete at 100mm height in the web from extreme tension fibre

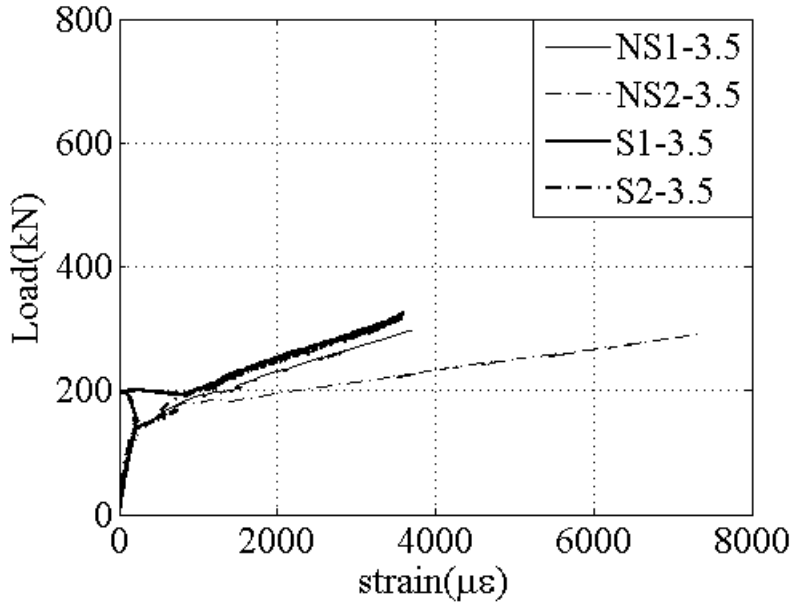

Figure A- 14: Concrete strain at 100mm from the bottom of the web for PR-3.5 beams

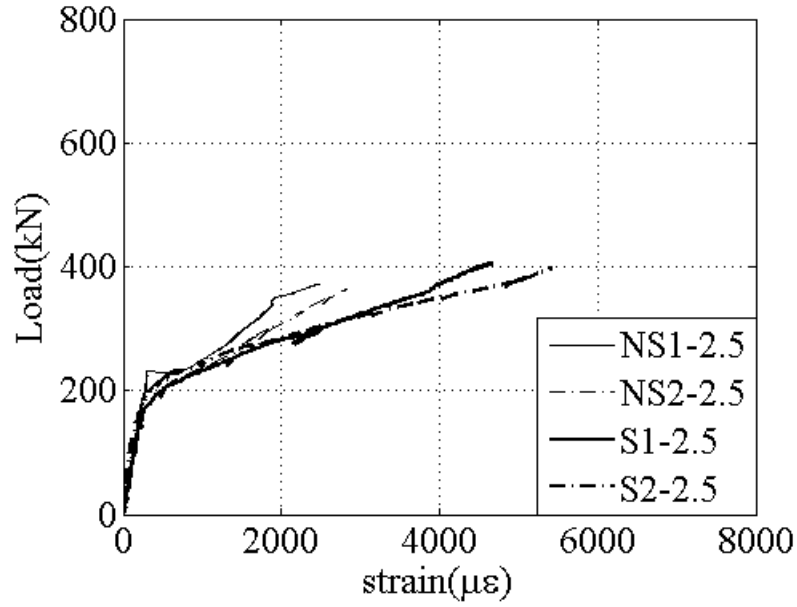

Figure A- 15: Concrete strain at 100mm from the bottom of the web for PR-2.5 beams

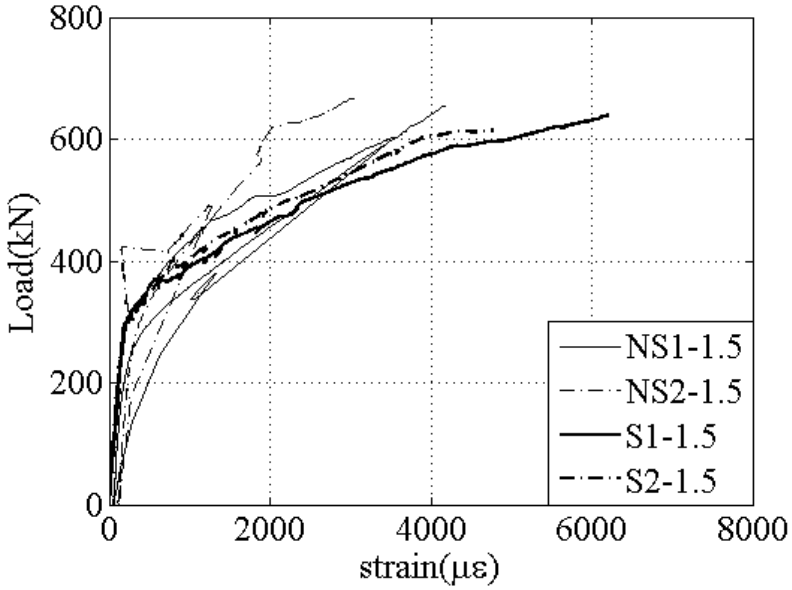

Figure A- 16: Concrete strain at 100mm from the bottom of the web for PR-1.5 beams

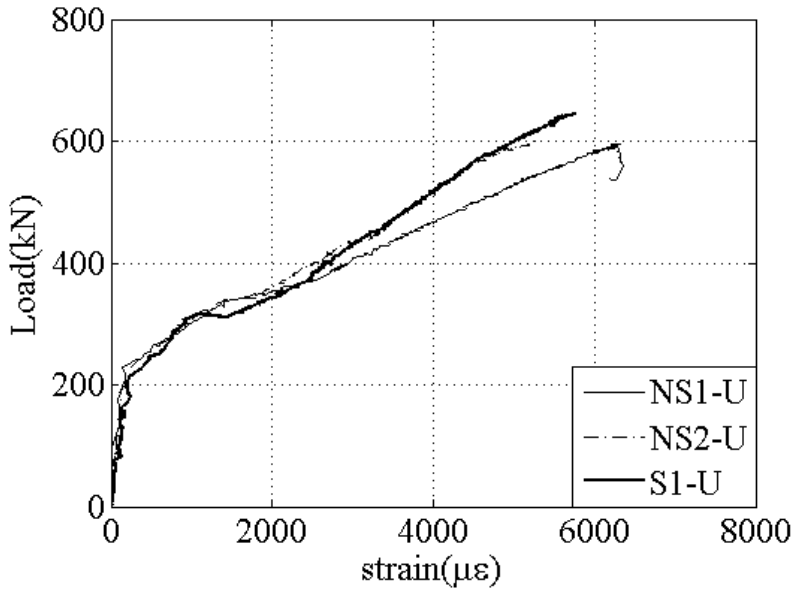

Figure A- 17: Concrete strain at 100mm from the bottom of the web for PR-U beams

Appendix B

Strain Profiles at mid-span

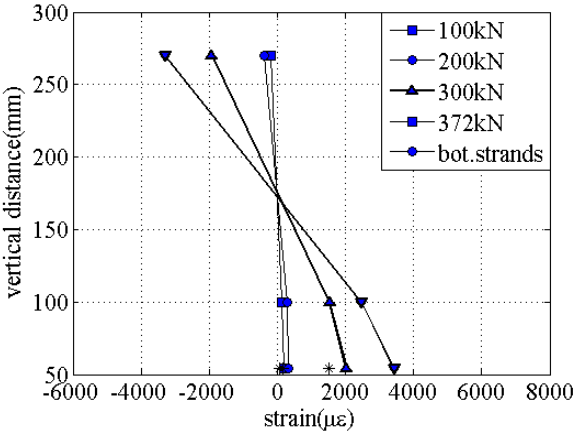

a) NS1-2.5

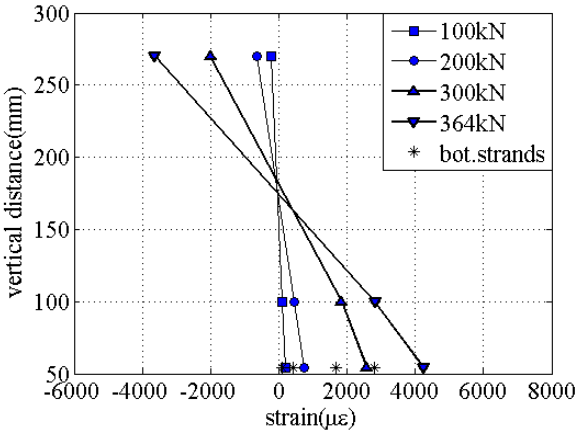

b) NS2-2.5

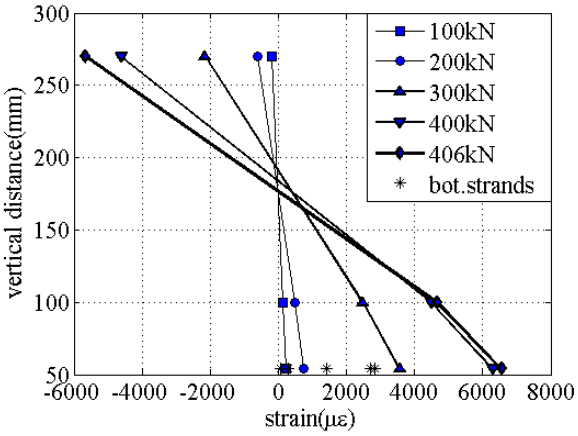

c) S1-2.5

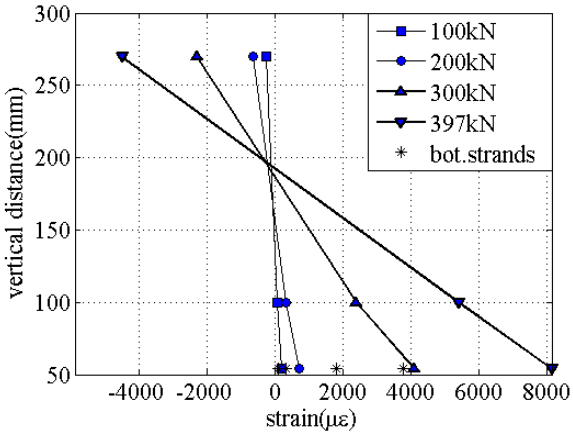

d) S2-2.5

Figure B- 1: Strain profiles at mid-span for PR-2.5 beams

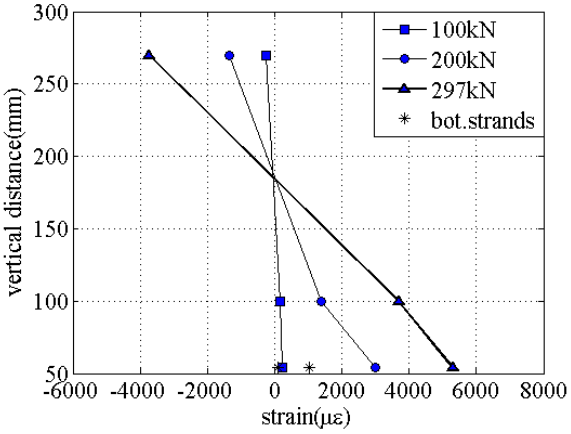

a) NS1-3.5

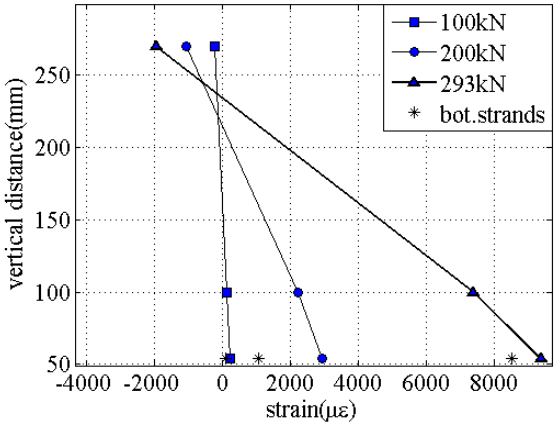

b) NS2-3.5

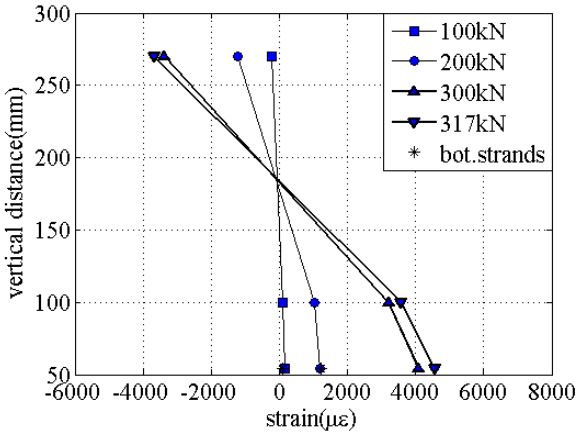

c) S2-3.5

Figure B- 2: Strain profiles at mid-span for PR-3.5 beams

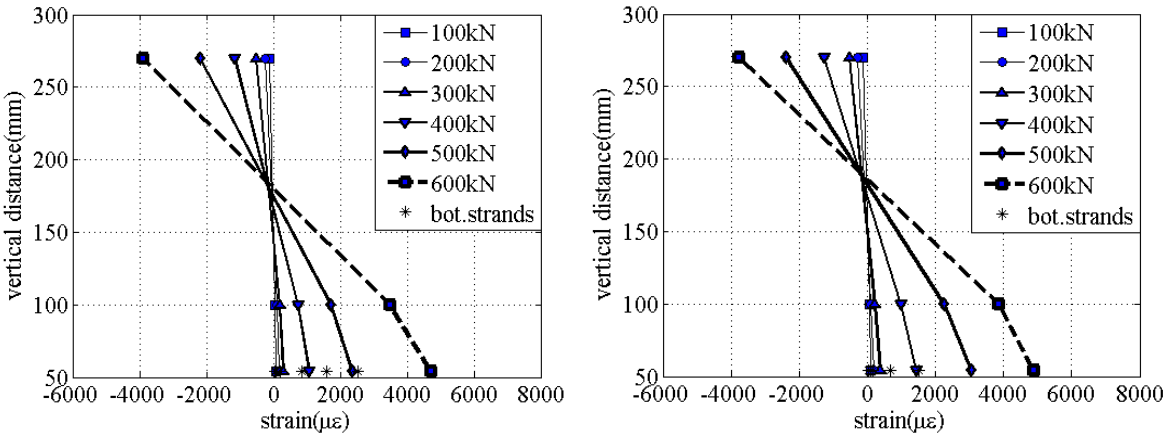

a) NS1-1.5

b) S2-1.5

Figure B- 3: Strain profiles at mid-span for PR-1.5 beams

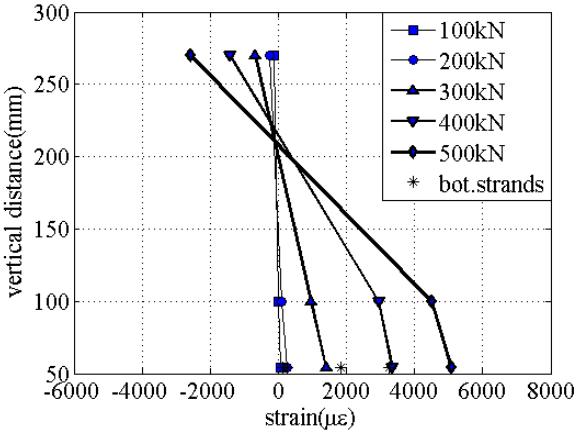

b) NS1-U

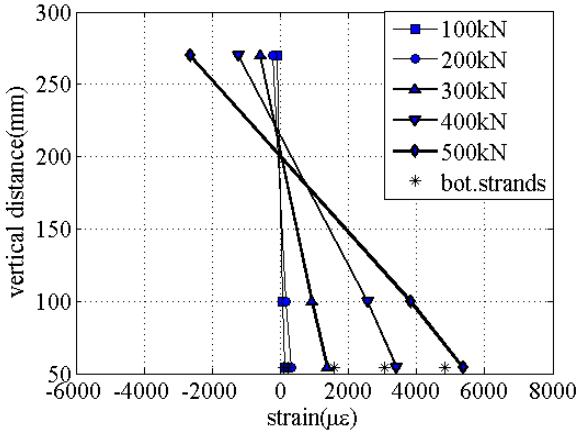

a) NS2-U

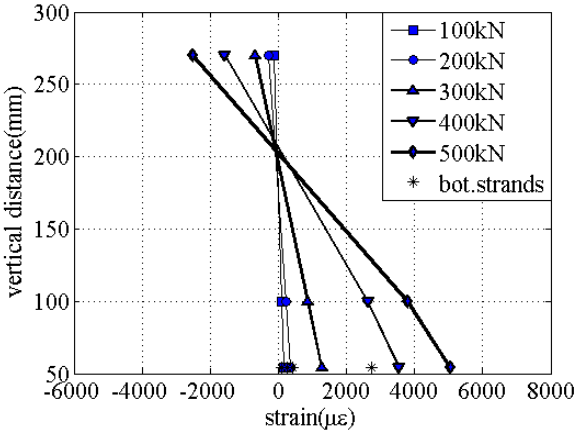

c) S1-U

Figure B- 4: Strain profiles at mid-span for PR-U beams

Appendix C

Deflection Figures

Load - Mid-span deflection

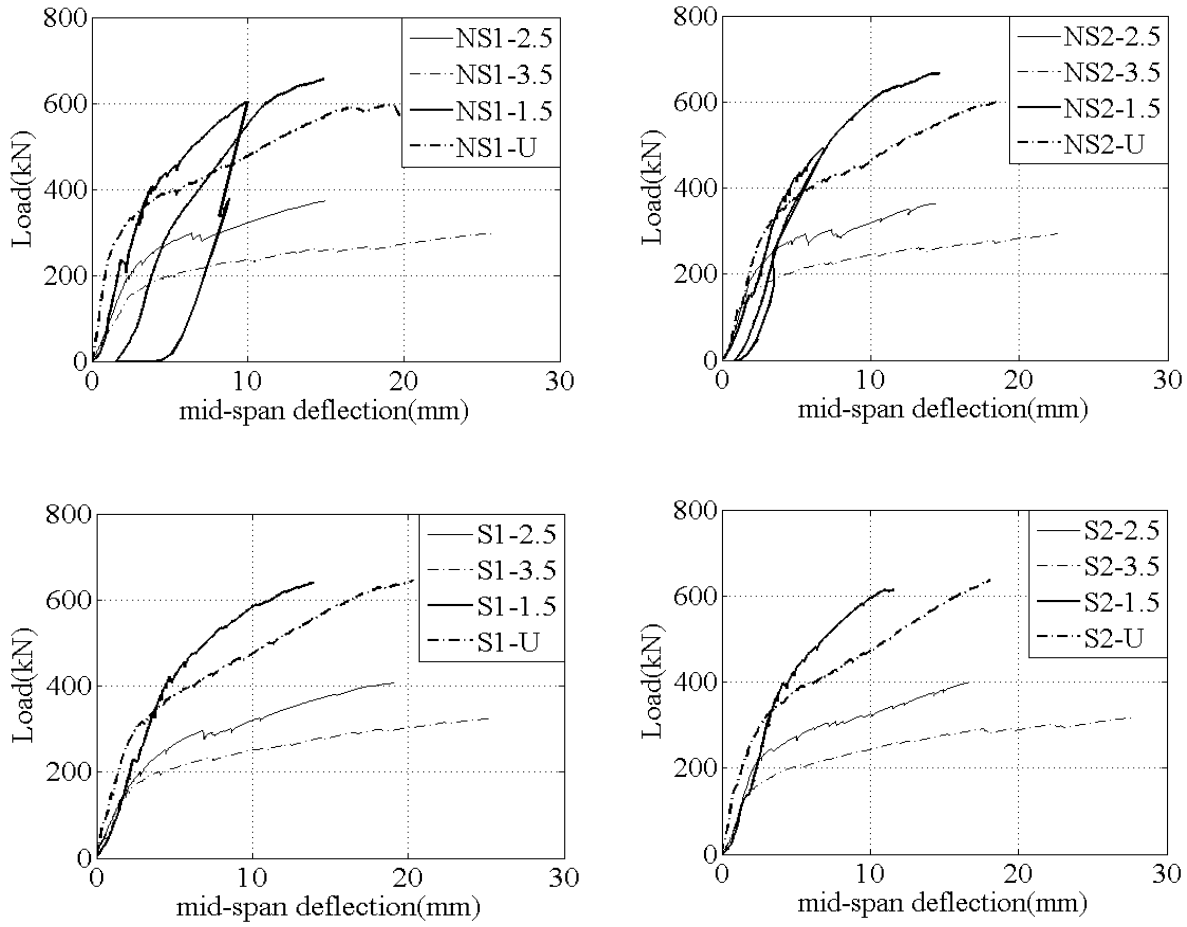

Figure C- 1: Load - mid-span deflection for beams with different a/d ratio

Normalised load - mid-span deflection figures

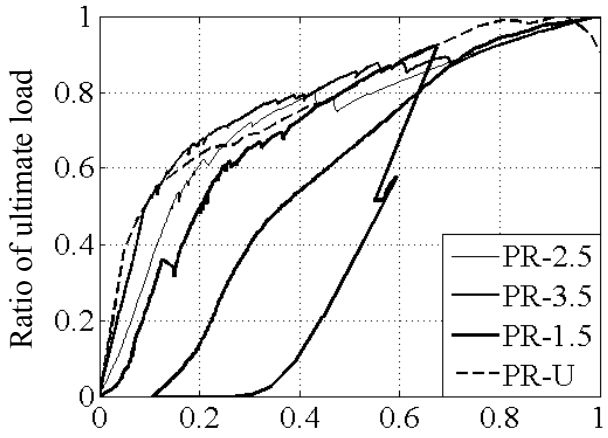

b) NS1 beams

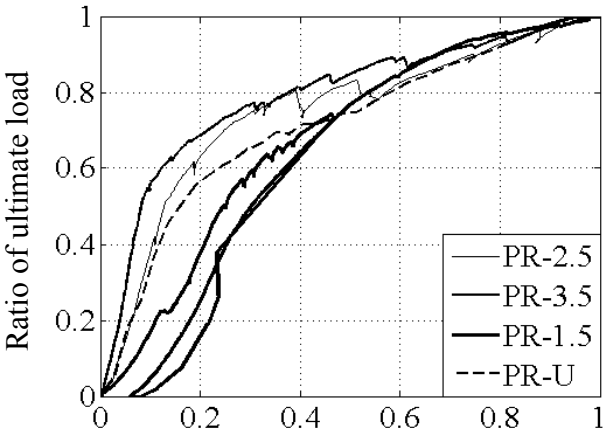

a) NS2 beams

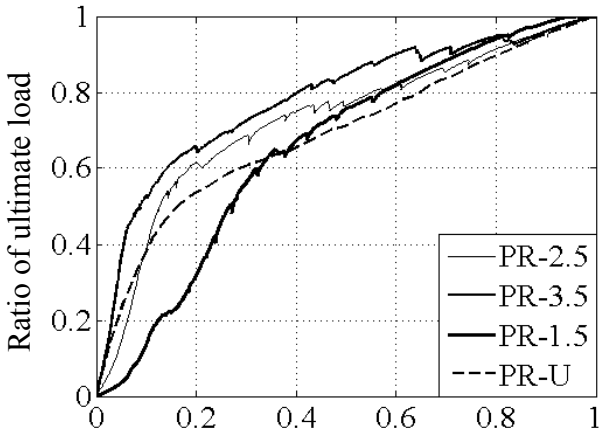

c) S2 beams

Figure C- 2: Normalised load - mid-span deflection graphs

Deflection profile of beam specimens

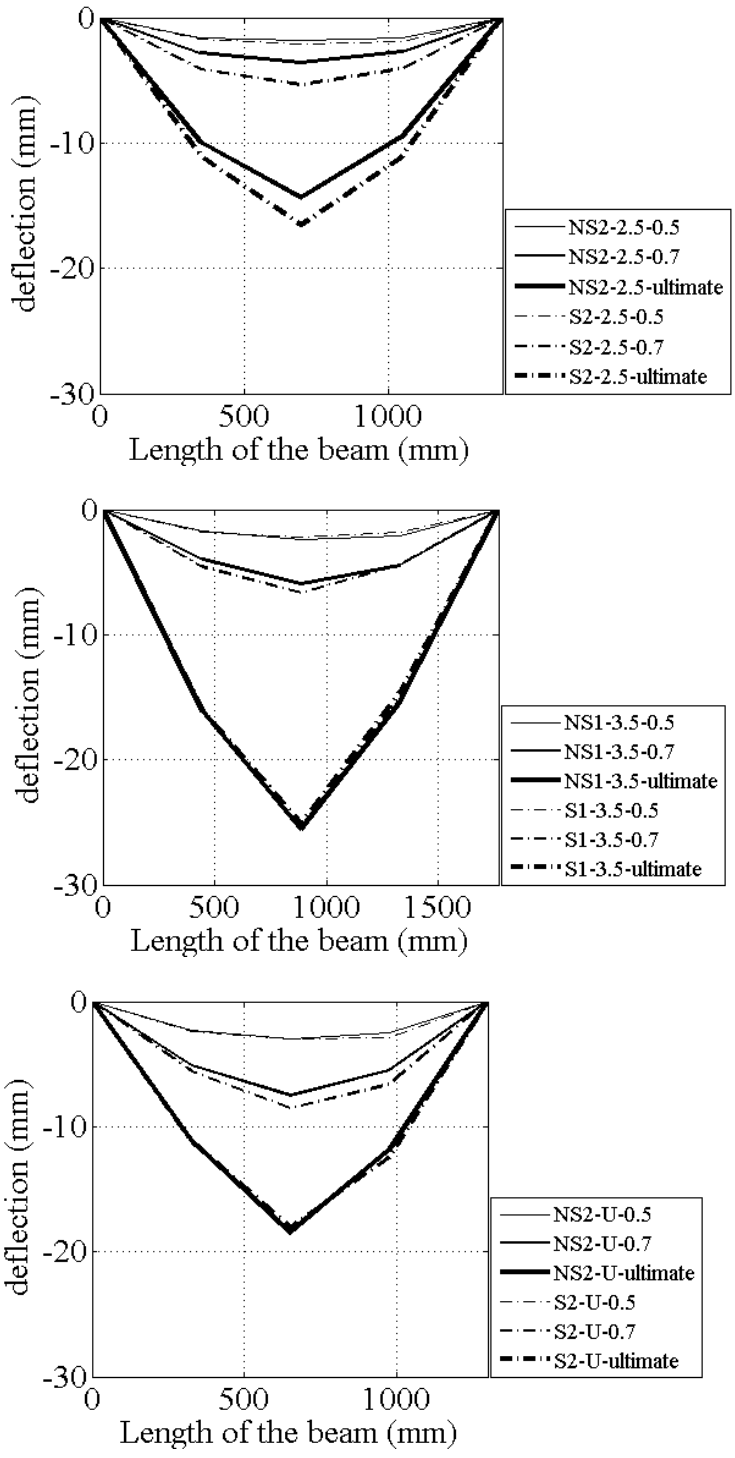

Figure C- 3: Deflection profile of the beams

Appendix D

Concrete Strains from the Rosette Stations

Concrete strains for PR-3.5 beams

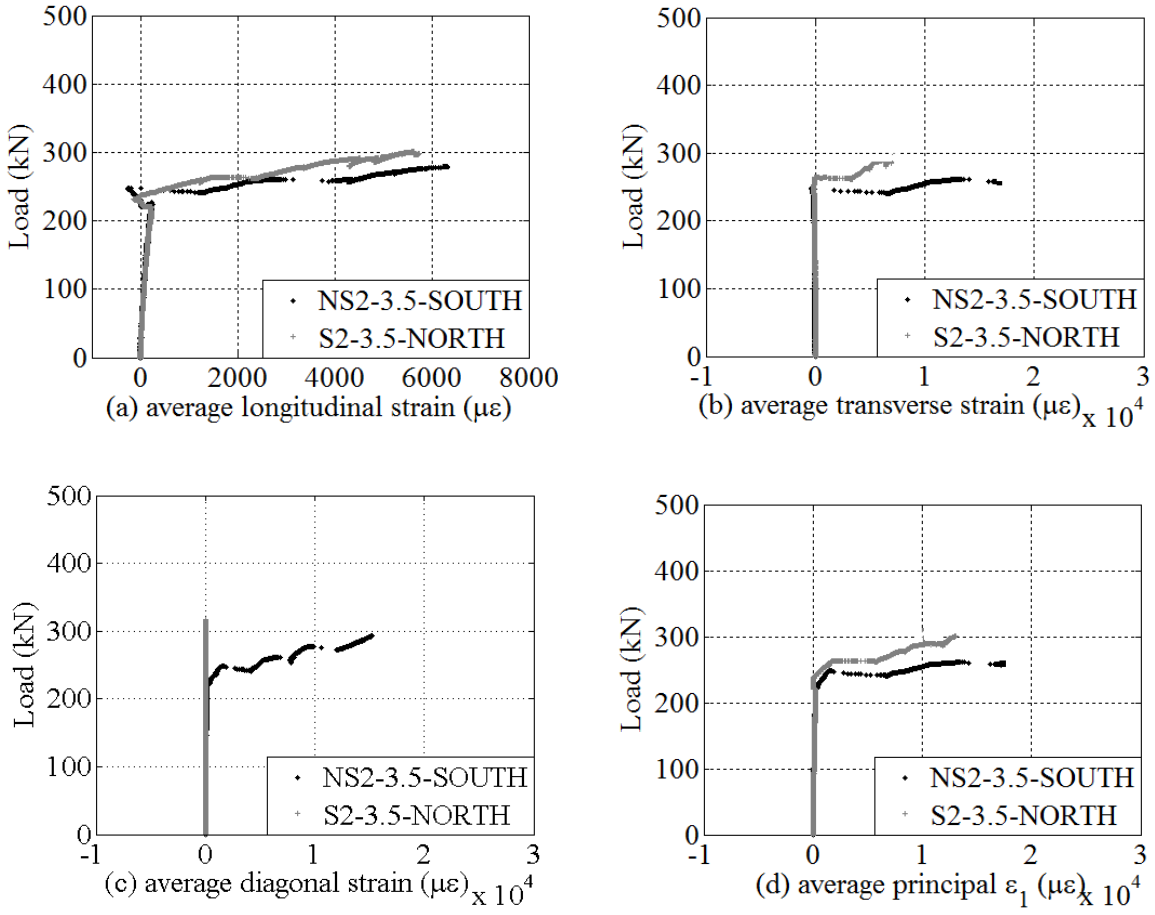

Figure D- 1: Concrete strains for PR-3.5 beams

Concrete strains for PR-1.5 beams

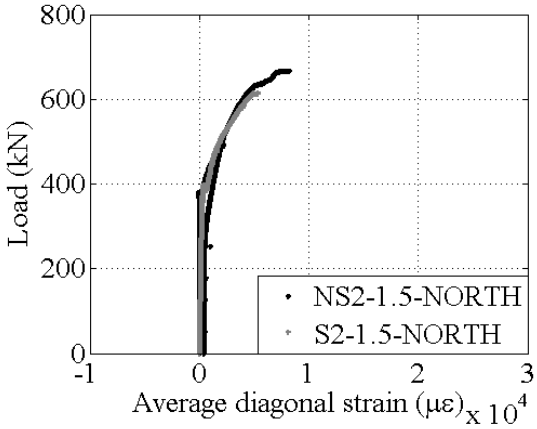

Figure D- 2: Average diagonal strain for PR-1.5 beams

Concrete strains for PR-U beams

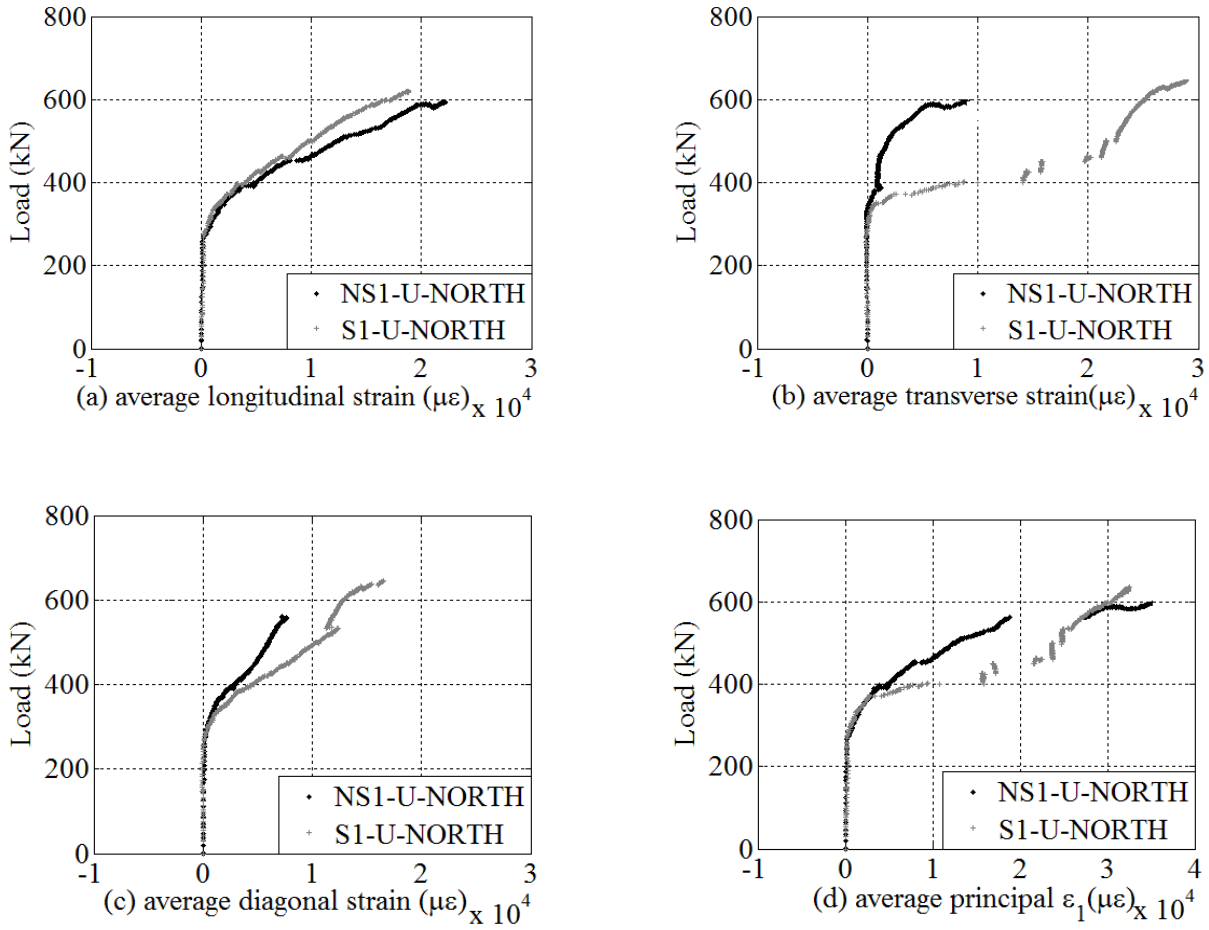

Figure D- 3: Concrete strains for PR-U beams

Appendix E

Strut and Tie Model Detailing

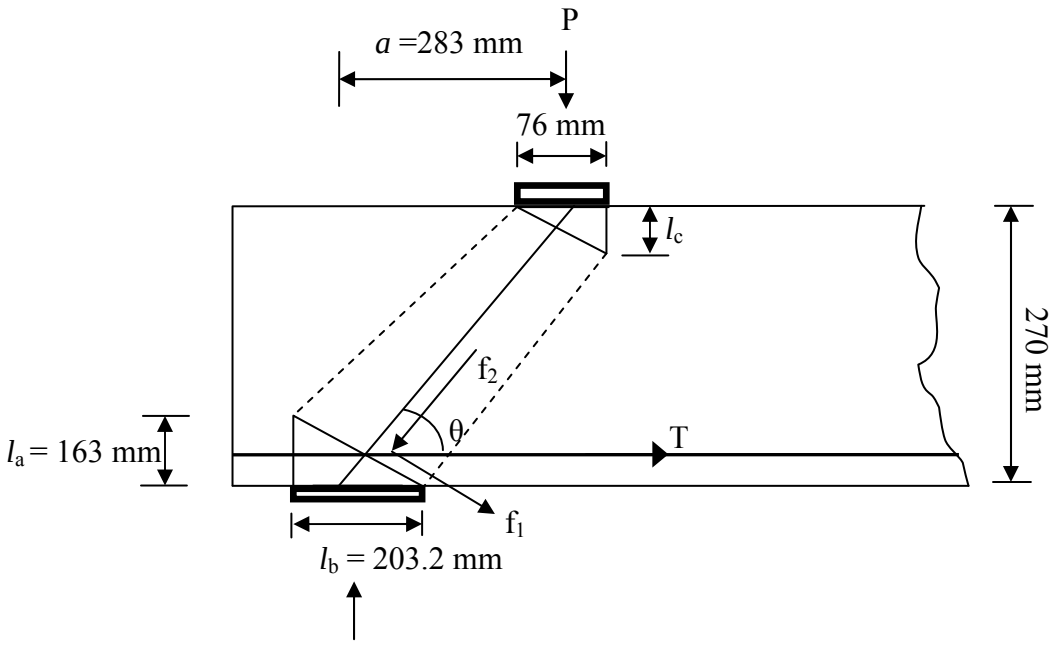

Tan et al. (2001) Model for Prestressed Deep Beams

The formulas outlined here have been simplified for deep beams with straight prestressed tendons, no non-prestressed reinforcement and no transverse reinforcement.

$$\frac{f_1}{f_t} + \frac{f_2}{f_c'} = 1.0$$

$$f_1 = \frac{2T\sin\theta}{A_c/\sin\theta} - \frac{2F_{pe}\sin\theta}{A_c/\sin\theta} \qquad k = 2$$

$$f_2 = \frac{V_n}{\sin\theta A_{cs}}$$

$$f_t = \frac{2(F_{pu} - F_{pe})\sin\theta}{A_c/\sin\theta} + f_{ct}$$

$$T = \frac{V_n}{\tan\theta}$$

$$F_c = \frac{V_n}{\sin\theta}$$

Zhang and Tan Modified Model for Reinforced Deep Beams (2007)

$$f_1 = \frac{4T\sin\theta}{A_c/\sin\theta} \qquad k = 4$$

$$f_2 = \frac{F_c - T\cos\theta}{A_{cs}}$$

$$f_t = f_{st} + f_{ct}$$

$$f_{ct} = 0.31\sqrt{f_c'}\left(\frac{\varepsilon_{cr}}{\varepsilon_1}\right)^{0.4}$$

$$f_{st} = \frac{4A_s f_y \sin\theta}{A_c/\sin\theta}$$

Modified Tan et al. (2001) Model based on modifications listed above

$$f_1 = \frac{4T\sin\theta}{A_c/\sin\theta} - \frac{4F_{pe}\sin\theta}{A_c/\sin\theta}$$

$$f_2 = \frac{F_c - T\cos\theta}{A_{cs}}$$

$$f_t = \frac{4(F_{pu} - F_{pe})\sin\theta}{A_c/\sin\theta} + f_{ct}$$

$$f_{ct} = 0.31\sqrt{f_c'}\left(\frac{\varepsilon_{cr}}{\varepsilon_1}\right)^{0.4}$$

Determining the Shear Capacity of PR-1.5 beams using Tan et al. Model

1. Assume l_c and calculate θ

$$\tan\theta = \frac{270 - l_a/2 - l_c/2}{a}$$

$$A_{cs} = b_w(l_a\cos\theta + l_b\sin\theta)$$

2. Assume the nominal shear capacity (V_n)

3. Calculate ε_s and ε_1

$$\varepsilon_s = \frac{T}{A_p E} \qquad A_p = 4*76 = 304 \text{ mm}^2, \text{ E} = 136 \text{ GPa}$$

$$\varepsilon_1 = \varepsilon_s + (\varepsilon_s + 0.002)\cot^2\theta$$

4. Calculate f_{ct}, f_t, f_1 and f_2.

5. Back calculate l_c from formula below:

$$l_{c2} = \frac{V_n}{f_c' b_w \tan\theta}$$

6. Check the condition below:

$$\frac{f_1}{f_t} + \frac{f_2}{f_c'} = 1.0$$

7. Adjust l_c based on the value of l_{c2} and repeat calculations until $l_c = l_{c2}$ and the condition above is satisfied.

References

[1] (ACI), A. C. (2005). *318-05: Building Code Requirements for Structural Concrete and Commentary.* Farmington Hills, Michigan: American Concrete Institute.

[2] (ACI), A. C. (2006). *ACI Committee 440 Report(ACI-440.1R-06): Guide for the Design and Construction of Structural Concrete Reinforced with FRP Bars.* Farmington Hills, Michigan, USA: American Concrete Institute.

[3] (ACI), A. C. (2004). *ACI Committee 440 Report-ACI 440-4R-04: Prestressing Concrete Structures with FRP Tendons.* Farmington Hills,Michigan, USA: American Concrete Institute.

[4] (CSA), C. S. (2004). *CAN/CSA-A23.3-04-Design of Concrete Structures.* Toronto, Ontario: Canadian Standards Association.

[5] (CSA), C. S. (2012). *CAN/CSA-S806-12- Design and Construction of Building Structures with Fibre-Reinforced Polymers.* Canadian Standards Association.

[6] A.Ghani, R., & Isgor, O. B. (2006). Proposed Shear Design Method for FRP-Reinforced Concrete Members without Stirrups. *ACI Structural Journal* , 93-101.

[7] Alkhrdaji, T., Wideman, M., Belarbi, A., & Nanni, A. (2001). Shear Strength of GFRP RC Beams and Slabs. *Proceedings of the International Conference on Composites in Construction (CCC)*, (pp. 409-414). Porto, Portugal.

[8] Association, C. S. (2010). *CAN/CSA-S6-10-Canadian Highway Bridge Design Code.* Mississauga, Ontario: Canadian Standards Association.

[9] Belarbi, A., & Hsu, T. (1994). Constitutive Laws of Concrete in Tension and Reinforcing Bars Stiffened by Concrete. *ACI Structural Journal* , 465-474.

[10] Bentz, E. C., & Collins, M. P. (2006). Development of the 2004 Canadian Standards Association (CSA) A23.3 Shear Provisions for Reinforced Concrete. *Canadian Journal of Civil Engineering* , 521-534.

[11] Bentz, E. C., Vecchio, F. J., & Collins, M. P. (2006). Simplified Modified Compression Field Theory for Calculating Shear Strength of Reinforced Concrete Elements. *ACI Structural Journal* , 614-624.

[12] Canadian Precast/ Prestressed Concrete Institute. (2007). *Design Manual Precast and Prestressed Concrete.* Ottawa, Ontario: Canadian Precast/ Prestressed Concrete Institute.

[13] China, N. S. (2002). *Code for Design of Concrete Structures (GB50010-2002).* Beijing: China Architectural Industry Press.

[14] Collins, M. P., & Mitchell, D. (1997). *Prestressed Concrete Structures.* Ontario: Response Publications.

[15] Cucchiara, C., La Mendola, L., & Papia, M. (2004). Effectiveness of Stirrups and Steel Fibres as Shear Reinforcement. *Cement and Concrete Composites* , 777-786.

[16] Dowden, D., & Dolan, C. (1997). Comparison of Experimental Shear Data with Code Predictions for FRP Prestressed Beams. *Proceedings of the Third International Symposium on Non-Metallic (FRP) Reinforcement for Concrete Structures*, (pp. 687-694).

[17] El-Hacha, R. (2005). Prestressing Concrete Structures with FRP Tendons (ACI 440.4R-04). *Structures Congress 2005: Metropolis and Beyond*, (pp. 1-8). New York.

[18] El-Sayed, A. K., & Soudki, K. (2011). Evaluation of Shear Design Equations of Concrete Beams with FRP Reinforcement. *Journal of Composites for Construction* , 9-20.

[19] Fathifazl, G., Razaqpur, A., Isgor, O. B., Abbas, A., Fournier, B., & Foo, S. (2009). Shear Strength of Reinforced Recycled Concrete Beams without Stirrups. *Magazine of Concrete Research* , 477-490.

[20] Gross, S., Dinehart, D., & Yost, J. (2004). Experimental Tests of High-Strength Concrete Beams Reinforced with CFRP Bars. *4th International Conference on Advance Composite Materials in Bridges and Structures (ACMBS).* Calgary.

[21] Guadagnini, M., Pilakoutas, K., & Waldron, P. (2006). Shear Resistance of FRP RC Beams: Experimental Study. *Journal of Composites for Construction* , 464-473.

[22] Kani, G. (1966). Basic Facts Concerning Shear Failure. *Journal of the American Concrete Institute* , 675-689.

[23] Khaldoun, N., & Collins, M. P. (1999). Background to the General Method of Shear Design in the 1994 CSA-A23.3 Standard. *Canadian Journal of Civil Engineering* , 827-839.

[24] Khuntia, M., & Stojadinovic, B. (2001). Shear Strength of Reinforced Concrete Beams without Transverse Reinforcement. *ACI Structural Journal* , 648-656.

[25] Kupfer, H., & Gerstle, K. (1999). Behavior of Concrete Under Biaxial Stress. *Proc ASCE J Eng Mech Div 1973* , 853-866.

[26] Lardner, T., & Archer, R. (1994). *Mechanics of Solids an Introduction.* Hightstown, NJ: McGraw-Hill.

[27] MacGregor, J. G., & Bartlett, F. (2000). *Reinforced Concrete Mechanics and Design.* Scarborough, Ontario: Prentice-Hall Canada Inc.

[28] Matta, F., Nanni, A., Hernandez, T., & Benmokrane, B. (2008). Scaling of Strength of FRP Reinforced Concrete Beams without Shear Reinforcement. *4th International Conference on FRP Composites in Civil Engineering (CICE).* Zurich.

[29] Nishikawa, K., Kanda, M., & Kenichi, U. (1993). *Structural Behavior of Prestressed Concrete Beams Using FRP Tendons.* Japan: Public Works Research Institute, Ministry of Construction.

[30] Oh, J.-K., & Shin, S.-W. (2001). Shear Strength of Reinforced High-Strength Concrete Deep Beams. *ACI Structural Journal* , 164-172.

[31] Park, R., & Paulay, T. (1975). *Reinforced Concrete Structures.* A Wiley-interscience publication.

[32] Park, S. Y., & Naaman, A. E. (1999). Shear Behavior of Concrete Beams Prestressed with FRP Tendons. *PCI Journal* , 74-84.

[33] Razaqpur, A., Isgor, B. O., Greenaway, S., & Selley, A. (2004). Concrete Contribution to the Shear Resistance of Fiber Reinforced Polymer Reinforced Concrete Members. *Journal of Composites For Construction* , 452-460.

[34] Russo, G., Somma, G., & Mitri, D. (2005). Shear Strength Analysis and Prediction for Reinforced Concrete Beams without Stirrups. *Journal of Structural Engineering* , 66-74.

[35] Shehata, E., Morphy, R., & Rizkalla, S. (2000). Fibre Reinforced Polymer Shear Reinforcement for Concrete Members: Behaviour and Design Guidelines. *canadian Journal of Civil Engineering* , 859-871.

[36] Tan, K., Tang, C., & Tong, K. (2003). A Direct Method for Deep Beams with Web Reinforcement. *Magazine of Concrete Research* , 53-63.

[37] Tan, K., Tong, K., & Tang, C. (2001). Direct Strut-and-Tie Model for Prestressed Deep Beams. *Journal of Structural Engineering* , 1076-1084.

[38] Vecchio, F., & Collins, M. (1982). *The Response of Reinforced Concrete to In-Plane Shear and Normal Stresses.* Toronto, Ontario: Department of Civil Engineering, University of Toronto.

[39] Wagner, H. (1929). Ebene Blechwandtrager mit sehr dunnem Stegblech. *Zeitschrift fur Flugtechnik und Motorluftschiffahr* , 8-12.

[40] Wang, G.-L., & Meng, S.-P. (2008). Modified Strut-and-Tie Model for Prestressed Concrete Deep Beams. *Engineering Structures* , 3489-3496.

[41] Wang, Z., Du, X., & Liu, J. (2011). Shear Behavior of CFRP Prestressed Concrete Beams without Stirrups. *Advanced Materials Research* , 126-129.

[42] Whitehead, P. A., & Ibell, T. J. (2005). Novel Shear Reinforcement for Fiber-Reinforced Polymer-Reinforced and Prestressed Concrete. *ACI Structural Journal* , 286-294.

[43] Yonekura, A., Tazawa, E., & Nakayama, H. (1993). *Flexural and Shear Behavior of Prestressed Concrete Beams Using FRP Rods as Prestressing Tendons.* Detroit, Michigan: Nanni and Dolan,eds.ACI.

[44] Zararis, P. D. (2003). Shear Compression Failure in Reinforced Concrete Deep Beams. *Journal of Structural Engineering* , 544-553.

[45] Zhang, N., & Tan, K. (2007). Direct Strut-and-Tie Model for Single Span and Continuous Deep Beams. *Engineering Structures* , 2987-3001.

[46] Zsutty, T. C. (1968). Beam Shear Strength Prediction by Analysis of Existing Data. *ACI Journal* , 943-951.